AD-A094 438 ARMY MISSILE COMMAND REDSTONE ARSENAL AL SYSTEMS SI--ETC F/G 12/1
TURBULENCE MODEL COMPARISONS FOR SHEAR LAYERS AND AXISYMMETRIC --ETC(U)
OCT 79 B J WALKER
UNCLASSIFIED DRSMI/RD-80-1-TR SBIE-AD-E950 074 NL

1 of 2
AD
A094438

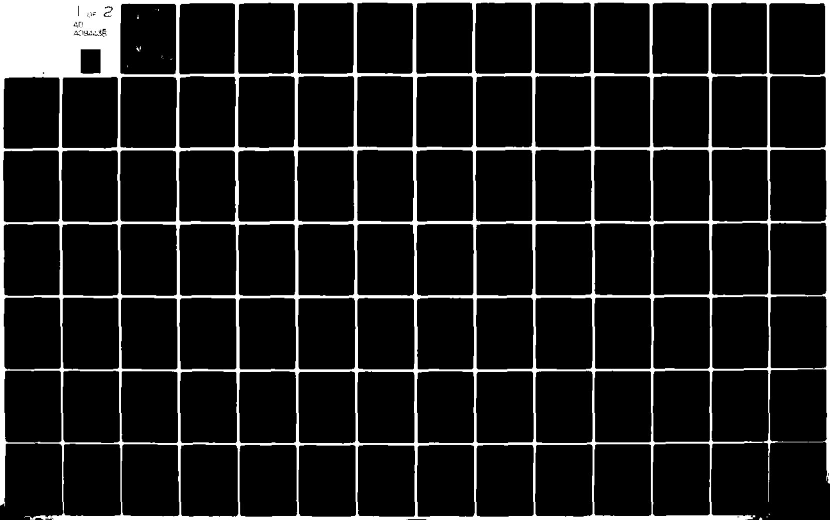

AD-E950074

(14) LEVEL III

AD A094438

TECHNICAL REPORT RD-80-1

TURBULENCE MODEL COMPARISONS FOR SHEAR LAYERS AND AXISYMMETRIC JETS

B.J. Walker
Systems Simulation and Development Directorate
US Army Missile Laboratory

October 1979

U.S. ARMY MISSILE COMMAND
Redstone Arsenal, Alabama 35809

Approved for public release; distribution unlimited.

SMI FORM 1021, 1 JUL 79 PREVIOUS EDITION IS OBSOLETE

81 2 02 165

DISPOSITION INSTRUCTIONS

DESTROY THIS REPORT WHEN IT IS NO LONGER NEEDED. DO NOT RETURN IT TO THE ORIGINATOR.

DISCLAIMER

THE FINDINGS IN THIS REPORT ARE NOT TO BE CONSTRUED AS AN OFFICIAL DEPARTMENT OF THE ARMY POSITION UNLESS SO DESIGNATED BY OTHER AUTHORIZED DOCUMENTS.

TRADE NAMES

USE OF TRADE NAMES OR MANUFACTURERS IN THIS REPORT DOES NOT CONSTITUTE AN OFFICIAL INDORSEMENT OR APPROVAL OF THE USE OF SUCH COMMERCIAL HARDWARE OR SOFTWARE.

Unclassified

SECURITY CLASSIFICATION OF THIS PAGE (When Data Entered)

REPORT DOCUMENTATION PAGE

READ INSTRUCTIONS BEFORE COMPLETING FORM

1. REPORT NUMBER: RD-80-1 / 2. GOVT ACCESSION NO.: AD-A094 138	3. RECIPIENT'S CATALOG NUMBER
4. TITLE (and Subtitle): Turbulence Model Comparisons for Shear Layers and Axisymmetric Jets	5. TYPE OF REPORT & PERIOD COVERED: Technical Report
	6. PERFORMING ORG. REPORT NUMBER
7. AUTHOR(s): B.J. Walker	8. CONTRACT OR GRANT NUMBER(s)
9. PERFORMING ORGANIZATION NAME AND ADDRESS: Commander, US Army Missile Command, ATTN: DRSMI-RDK, Redstone Arsenal, Alabama 35809	10. PROGRAM ELEMENT, PROJECT, TASK AREA & WORK UNIT NUMBERS
11. CONTROLLING OFFICE NAME AND ADDRESS: Commander, US Army Missile Command, ATTN: DRSMI-RPT, Redstone Arsenal, Alabama 35809	12. REPORT DATE: October 1979
	13. NUMBER OF PAGES: 133
14. MONITORING AGENCY NAME & ADDRESS (if different from Controlling Office)	15. SECURITY CLASS. (of this report): Unclassified
	15a. DECLASSIFICATION/DOWNGRADING SCHEDULE

16. DISTRIBUTION STATEMENT (of this Report)

Approved for public release; distribution unlimited.

17. DISTRIBUTION STATEMENT (of the abstract entered in Block 20, if different from Report)

18. SUPPLEMENTARY NOTES

19. KEY WORDS (Continue on reverse side if necessary and identify by block number)

Rocket Exhaust Plume
Pseudo-Vorticity
Vortex Interactions
Energy Dissipation
Shear Flow

20. ABSTRACT (Continue on reverse side if necessary and identify by block number)

Comparisons were made between experiment and theory to assess the capability of turbulent mixing models to predict the fluid flow-properties in the mixing region of both shear layers and jets. Jets exiting into both moving and quiescent streams were investigated. Both chemically non-reacting and reacting shear layers were investigated. Attention was centered on two turbulence models: (i) $k\varepsilon 2$ and (ii) $k\omega'$. The same numerical flow field code was utilized with both turbulence models thus allowing a direct comparison of the

DD FORM 1 JAN 73 1473 EDITION OF 1 NOV 65 IS OBSOLETE

Unclassified

SECURITY CLASSIFICATION OF THIS PAGE (When Data Entered)

20.
turbulence models without fear of differences in the numerics masking the results.

Results showed that significant errors can be made when utilizing these models for prediction of shear flows of interest. The flow structure for these shear flows is in no way accounted for by the models and hence poor predictions result. It is felt that the basic vortex structure will have to be modeled before significant improvements in the modeling will occur.

Accession For
NTIS GRA&I
DTIC TAB
Unannounced
Justification
By
Distribution/
Availability Codes

Dist	Avail and/or Special
A	

CONTENTS

ILLUSTRATIONS

ILLUSTRATIONS (Continued)

ILLUSTRATIONS (Continued)

ILLUSTRATIONS (Concluded)

TABLES

I. INTRODUCTION

In the development of a predictive tool for the fluid flow field due to the interaction of the rocket exhaust plume with its environment, the mixing region analysis is critical. The manner in which these streams interact and the accurate prediction of this interaction is paramount to several missile systems applications. Missile signature and vehicle design are two of the most important of these applications. In order to properly simulate the mixing region, the numerical calculational procedure must be accurate and the turbulence model must be physically correct. Having a physically correct turbulence model is certainly the most demanding of these two requirements.

Turbulence has been investigated for many years now and is usually characterized by its randomness and disorderliness. Despite the randomness and disorderliness however, statistically distinct average values are obtainable for the velocity, temperature, and density for example. The randomness and disorderliness is characterized by scale size. Not only is the fine scale characterized by vortex interactions but likewise for the large scale. This large scale motion has been studied intensively over the last several years by scientists at the California Institute of Technology and offers a better understanding of the physical phenomenology of turbulence.

II. MATHEMATICAL FLOW MODEL

The mathematical flow model utilized in this investigation consists of the axisymmetric jet mixing equations for a reacting gas mixture. This set of coupled partial differential equations is solved utilizing a mixed implicit/explicit finite difference procedure. The governing equations are parabolic and are solved in streamline coordinates using a marching scheme. This technology was essentially developed by the Joint Army, Navy, NASA and Air Force (JANNAF) Plume Technology Working Group in 1972 with the development of the Low-Altitude Plume Program (LAPP). Technology developments since that time have occurred and are being incorporated in the JANNAF Standardized Plume Flowfield (SPF) Program. The improvements to the mixing portion of this program include the employment of a discretized shear layer which grows due to the mixing of the jet and the external streams. This allows a more optimum placement of the grid points in the flowfield. Hence, this procedure of retaining the (x, ψ) computational grid and discretizing the shear layer has led to a much more efficient handling of the numerical procedures used to solve the problem. Other improvements such as the formulation of the energy equation in terms of total enthalpy rather than temperature leads to more accurate solutions in higher energy rocket propellants. In addition a mass flow check has been added to insure that mass flow is truly being conserved. This model has been formulated by Aeronautical Research Associates of Princeton (ARAP) and constitutes a vital working portion of the SPF program being developed by them for the JANNAF Plume Technology Subcommittee. This code has been called BOAT in previous references in the literature [9]. Detailed derivations of the governing fluid dynamic equations utilized in this investigation can be found in the literature [9 - 12] and will only briefly be presented here. The governing equations are

Global Continuity

$$\frac{\partial}{\partial x}(\rho u) + \frac{1}{r}\frac{\partial}{\partial r}(\rho v r) = 0 \tag{1}$$

Species Diffusion

$$\rho u \frac{\partial F_i}{\partial x} + \rho v \frac{\partial F_i}{\partial r} = \frac{1}{r}\frac{\partial}{\partial r}\left(\frac{Le}{Pr}\mu r \frac{\partial F_i}{\partial r}\right) + \dot{w}_i \tag{2}$$

Axial Momentum

$$\rho u \frac{\partial u}{\partial x} + \rho v \frac{\partial u}{\partial r} = -\frac{\partial p}{\partial x} + \frac{1}{r}\frac{\partial}{\partial r}\left(\mu r \frac{\partial u}{\partial r}\right) \tag{3}$$

Energy

$$\begin{aligned} \rho u \frac{\partial H}{\partial x} + \rho v \frac{\partial H}{\partial r} &= \frac{1}{r}\frac{\partial}{\partial r}\left\{\frac{\mu r}{Pr}\frac{\partial H}{\partial r}\right\} + \\ \frac{1}{r}\frac{\partial}{\partial r}\left\{\mu\left[1 - \frac{1}{Pr}\right] r u \frac{\partial u}{\partial r}\right\} &+ \frac{1}{r}\frac{\partial}{\partial r}\left\{\frac{\mu}{Pr}(Le - 1) \sum_i \left(h_i - h_i^0\right) r \frac{\partial F_i}{\partial r}\right\} \end{aligned} \tag{4}$$

State

$$\rho = \frac{p MW}{\bar{R} T} \tag{5}$$

These equations are then transformed from the (x,r) to the (x, ψ) coordinate system with the transformation

$$
\begin{aligned}
\psi \quad \frac{\partial \psi}{\partial r} &= \rho u r \\
\psi \quad \frac{\partial \psi}{\partial x} &= - \rho v r
\end{aligned}
\tag{6}
$$

Utilizing the transformation in (6), the governing equations become

Axial Momentum

$$
\frac{\partial u}{\partial x} = - \frac{1}{\rho u} \frac{\partial p}{\partial x} + \frac{1}{\psi} \frac{\partial}{\partial \psi} \left(A \frac{\partial u}{\partial \psi} \right) \tag{7}
$$

where $A \equiv \mu_t \dfrac{\rho u r^2}{\psi}$

Energy

$$
\begin{aligned}
\frac{\partial H}{\partial x} = {} & \frac{1}{\psi} \frac{\partial}{\partial \psi} \left\{ \frac{A}{Pr} \frac{\partial H}{\partial \psi} \right\} + \frac{1}{\psi} \frac{\partial}{\partial \psi} \left[A \left\{ 1 - \frac{1}{Pr} \right\} u \frac{\partial u}{\partial \psi} \right] \\
& + \frac{1}{\psi} \frac{\partial}{\partial \psi} \left\{ \frac{A}{Pr} (Le - 1) \sum_i \left(h_i - h_i^0 \right) \frac{\partial F_i}{\partial \psi} \right\}
\end{aligned}
\tag{8}
$$

Species Continuity

$$
\frac{\partial F_i}{\partial x} = \frac{1}{\psi} \frac{\partial}{\partial \psi} \left(\frac{Le}{Pr} A \frac{\partial F_i}{\partial \psi} \right) + \frac{\dot{w}_i}{\rho u} \tag{9}
$$

Two turbulence kinetic energy (TKE) models were used to determine the turbulent viscosity that appears in the governing equations. The first was the $K\epsilon 2$ model developed by Spalding and co-workers, and the second was the $k\omega'$ model developed by Saffman and co-workers. A detailed derivation of the latter model development for this investigation is given in Section IV of this report. Details of the $K\epsilon 2$ model can be found in other references [12].

The governing turbulence equations for the $k\epsilon 2$ model are given by

$$\rho \frac{Dk}{Dt} = \frac{1}{r}\frac{\partial}{\partial r}\left\{ \frac{r\mu_t}{\sigma_k} \frac{\partial k}{\partial r} \right\} + \mu_t \left\{ \frac{\partial u}{\partial r} \right\}^2 - \rho\varepsilon \qquad \text{TKE} \qquad (10)$$

$$\rho \frac{D\varepsilon}{Dt} = \frac{1}{r}\frac{\partial}{\partial r}\left\{ \frac{r\mu_t}{\sigma_\varepsilon} \frac{\partial \varepsilon}{\partial r} \right\} + C_{\varepsilon 1} \frac{\varepsilon}{k} \mu_t \left(\frac{\partial u}{\partial r} \right)^2 - C_{\varepsilon 2}\, \rho \frac{\varepsilon^2}{k} \qquad (11)$$

ENERGY
DISSIPATION
RATE

where

$$\mu_t = \frac{C_\mu \rho k^2}{\varepsilon} \qquad (12)$$

Note that this model utilizes five empirical constants — C_μ, $C_{\epsilon 1}$, $C_{\epsilon 2}$, σ_k, σ_ϵ.

For axisymmetric flows --

$$C_\mu = C_\mu \left\{ \left.\frac{du}{dx}\right|_{\mathbb{C}_L}, \Delta u, \delta \right\} \qquad (13)$$

$$C_{\varepsilon 2} = C_{\varepsilon 2} \left\{ \left.\frac{du}{dx}\right|_{\mathbb{C}_L}, \Delta u, \delta \right\} \qquad (14)$$

When these corrections are made to the constants, the model is known in the literature as the $k\epsilon 1$ turbulence model.

It was determined by exercising the model that the $k\epsilon 1$ model could not accurately predict weak shear flow, i.e., flow in which the two streams interacted at nearly the same velocities. Therefore a correction was made for weak shear flows by altering the constant C_μ as follows

For weak shear flows --

$$C_\mu = 0.09\ G\ (\overline{P/\varepsilon}) - 0.0534F \qquad (15)$$

NOTE: ϵ, ε: These symbols are the same throughout report.

where

$$F = F\left(\frac{du}{dx}\bigg|_{\mathbb{C}},\ \Delta u,\ \delta\right)$$

$$\overline{P/\varepsilon} = fn\ (k)$$

The resulting changes in the kε1 model were then known as the kε2 turbulence model and is utilized as such in this investigation.

In addition, the kε2 model does not contain any terms to handle compressibility effects. Hence, a compressibility correction was introduced into the model when large velocity differences between the mixing streams became important. The compressibility correction that was used resulted from an empirical formulation due to Dash [11]. The compressibility correction factor $\bar{k}$ is multiplied by the constant C_μ and (12) becomes

$$\mu_t = \bar{k}\,\frac{C_\mu \rho k^2}{\varepsilon} \tag{16}$$

where $\bar{k}$ is a function of the maximum turbulence Mach number

$$M_{\tau_{max}} \equiv \frac{\bar{k}_{max}^{\frac{1}{2}}}{a} \tag{17}$$

The functional form of $\bar{k}$ is shown in *Figure 1.*

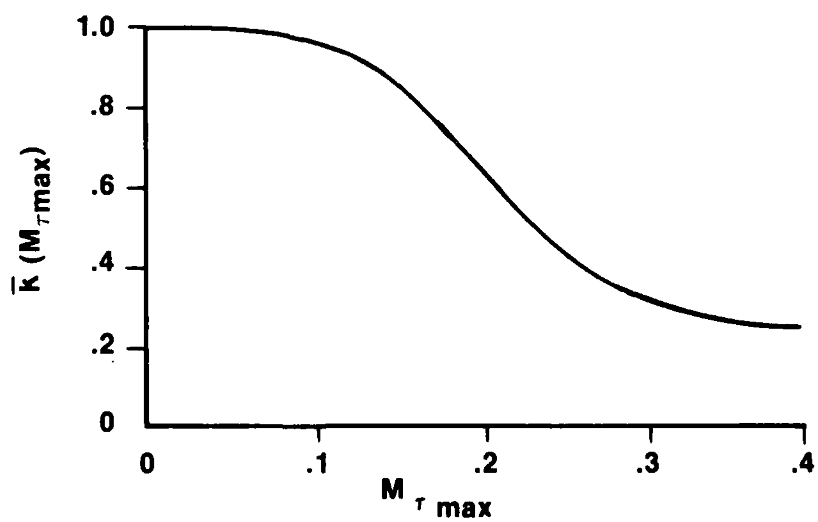

Figure 1. Compressibility correction factor for kε2 turbulence model.

The $k\omega'$ turbulence model was also utilized in this investigation. The governing equations for this model are developed in detail in Section IV, and are as follows

$$\rho \frac{Dk}{Dt} = \frac{1}{2r} \frac{\partial}{\partial r} \left\{ r\mu_t \frac{\partial k}{\partial r} \right\} + C_{k1} \omega\mu_t \left| \frac{\partial u}{\partial r} \right| - \rho k\omega \qquad \text{TKE} \qquad (18)$$

$$\rho \frac{D\omega^2}{Dt} = \frac{1}{2r} \frac{\partial}{\partial r} \left\{ r\mu_t \frac{\partial \omega^2}{\partial r} \right\} + C_{\omega 2} \rho\omega^2 \left| \frac{\partial u}{\partial r} \right|$$

$$+ C_{\omega 3} \frac{\omega}{\rho} \left(\frac{\partial \rho}{\partial r} \right) \frac{\partial}{\partial r} (\rho k) + C_{\omega 4} \rho\omega^3 \qquad \text{PSEUDO-VORTICITY} \qquad (19)$$

where

$$\mu_t = \frac{C_{\omega 5} \rho k}{\omega} \qquad (20)$$

This model also uses five constants, C_{k1}, $C_{\omega 2}$, $C_{\omega 3}$, $C_{\omega 4}$, $C_{\omega 5}$, and when compressibility effects are important, an additional term is included in the turbulence kinetic energy equation

$$\frac{C_{k6} \rho}{MW_e C_{pe} p_e} k\mu_t \left(\frac{\partial u}{\partial r} \right)^2 \qquad (21)$$

These equations were transformed to the (x, ψ) coordinate system utilizing (6) and the following equations result from the transformation of (10) and (11).

For the $k\epsilon 2$ model

Turbulence Kinetic Energy (TKE)

$$\frac{\partial k}{\partial x} = \frac{1}{\psi} \frac{\partial}{\partial \psi} \left(\frac{A}{\sigma_k} \frac{\partial k}{\partial \psi} \right) + \frac{1}{u} (P - \epsilon) \qquad (22)$$

Turbulence Dissipation

$$\frac{\partial \varepsilon}{\partial x} = \frac{1}{\psi}\frac{\partial}{\partial \psi}\left(\frac{A}{\sigma_\varepsilon}\frac{\partial \varepsilon}{\partial \psi}\right) + \frac{\varepsilon}{uk}\left(C_1 P - C_2 \varepsilon\right) \qquad (23)$$

where

$$A = \mu_t \frac{\rho u r^2}{\psi} \qquad (24)$$

$$P = \frac{Au}{\psi}\left(\frac{\partial u}{\partial \psi}\right)^2 \qquad (25)$$

Similarly for the $k\omega'$ model (18) and (19) we transformed to the (x, ψ) coordinate system with the result that

Turbulence Kinetic Energy (TKE)

$$\frac{\partial k}{\partial x} = \frac{1}{2\psi}\frac{\partial}{\partial \psi}\left\{A\frac{\partial k}{\partial \psi}\right\} + C_1 \mu_t \omega \left|\frac{r}{\psi}\frac{\partial u}{\partial \psi}\right| - \frac{k\omega}{u} - \frac{C_{k6}\rho k A}{MW_e C_{p_e} P_e \psi}\left(\frac{\partial u}{\partial \psi}\right)^2 \qquad (26)$$

Turbulence Pseudo Vorticity

$$\frac{\partial \omega^2}{\partial x} = \frac{1}{2\psi}\left\{A\frac{\partial \omega^2}{\partial \psi}\right\} + \frac{C_{\omega 2}\,\omega^2}{u}\left|\frac{\rho u r}{\psi}\frac{\partial u}{\partial \psi}\right| + C_{\omega 3}\frac{ur^2}{\psi^2}\left(\frac{\partial \mu}{\partial \psi}\right)\frac{\partial}{\partial \psi}\left(\rho k\right) + C_{\omega 4}\frac{\omega^3}{u} \qquad (27)$$

where A is defined in (24).

When compressibility effects are not important, C_{k6} is taken equal to zero. Hence, the compressibility term is built into the TKE equation.

III. STARTLINE CONDITIONS

Three methods were utilized to define the startline conditions which are used to initiate the finite difference calculational procedure. The three methods are:

- Boundary Layer Initial Profile
- Shear Layer Initial Profile
- Generalized Specific Profile

The first two methods employ calculational procedures to generate the initial profile. The third simply specifies the value of all the variables at some initial downstream location. Each of these methods was utilized to calculate the shear layer flowfield for the two dimensional He N_2 case run experimentally by Brown and Roshko [1] for a density ratio of ^{1} - and a velocity ratio of 7. This corresponds to the experimental data given in *Figure 13a* of reference [1].

A. Boundary Layer Initial Profile Description

The displacement effect of the jet and external boundary layers is calculated by utilizing a velocity profile that is derived from the combination of the "Law of the Wall" and the "Law of the Wake." *Figure 2* shows the applicable geometric configuration.

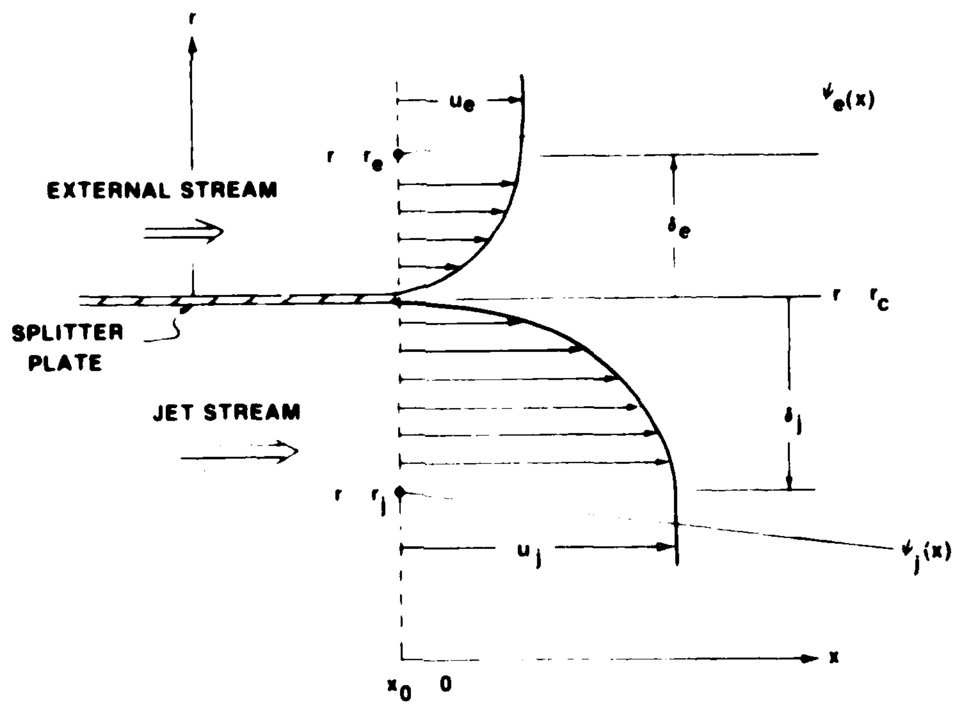

Figure 2. Boundary layer initial profile.

Note that the shear layer starts growing at $x = 0$ from $r_e = r_c + \delta_e$ on the external stream side and $r_j = r_c - \delta_j$ on the jet stream side. The profiles utilized to calculate these initial radii are computed from the velocity profiles

$$\frac{u_j - u}{u_{\tau_j}} = -2.5 \ln \xi - 1.38 \; [2 - w(\xi)] \tag{28}$$

and

$$\frac{u_e - u}{u_{\tau_e}} = -2.5 \ln \xi - 1.38 \; [2 - w(\xi)]$$

where $w(\xi)$ is Cole's universal wave function

$$w(\xi) = 1 + \sin \left\{\frac{2\xi - 1}{2}\right\} \pi \tag{29}$$

and ξ is the non-dimensional radius

$$\xi = \frac{|r - r_c|}{\delta_j} \tag{30}$$

or

$$\xi = \frac{|r - r_c|}{\delta_e}$$

In addition, the frictional velocities

$$u_{\tau_e} = \sqrt{\frac{\tau_{w_e}}{\rho_e}} \tag{31}$$

or

$$u_{\tau_j} = \sqrt{\frac{\tau_{w_j}}{\rho_j}}$$

Now if the displacement thickness is known, then the definition of this quantity

$$\delta_j^* = \frac{1}{r_j} \int_{r_j}^{r_j + \delta_j} \left\{1 - \frac{(u)\,(MW)\,(T_j)}{(u_j)\,(MW_j)\,(T)}\right\} rdr \tag{32}$$

can be inverted to find δ_i provided U_T is also known. Similarly δ_c can be found and then r_i and r_c can be evaluated. Knowing these values, the initial distribution is determined.

B. Shear Layer Initial Profile Description

For this method, a fully developed shear layer profile is assumed to exist at the initial streamwise location. The initial shear layer width is calculated from the incompressible relation [12]

$$r_e - r_j = 0.27 \left\{ \frac{u_j - u_e}{u_j + u_e} \right\} x_o \tag{33}$$

Figure 3 illustrates this notation

Upon establishment of the shear layer upper and lower boundaries utilizing (33), the properties are distributed across the shear layer according to the simple cubic relations

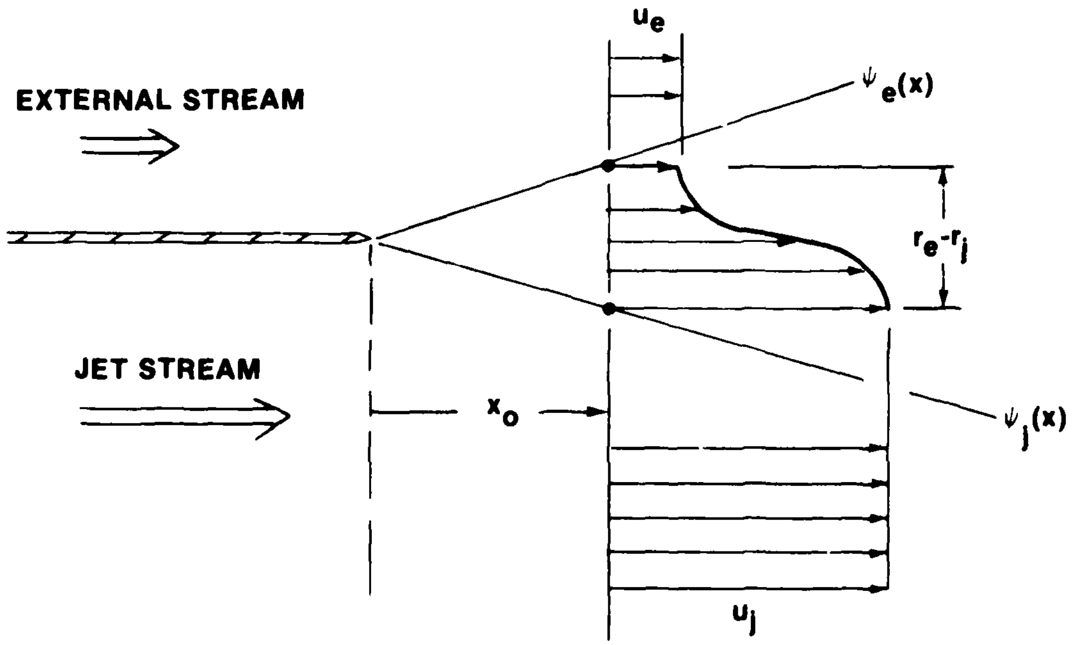

Figure 3. Shear layer initial profile.

$$\frac{u - u_j}{u_e - u_j} = \frac{T - T_j}{T_e - T_j} = \frac{F_i - F_{i_j}}{F_{i_e} - F_{i_j}} = 3\eta^2 \left\{1 - \frac{2\eta}{3}\right\} \quad (34)$$

where

$$\eta = \frac{r - r_j}{r_e - r_j}$$

The shear layer grid points are spaced evenly across it in increments of $\Delta\psi = \frac{\psi_e - \psi_j}{N - 1}$

C. Generalized Specific Profile Description

This method of inputting startline conditions does not rely on any calculations but merely uses the specified profile. *Figure 4* illustrates this case where u(r), T(r), and x(r) are input directly at the startline location $x = x_o$. This method can only be used in rare cases when a significant amount of experimental data is available.

In addition to these fluid dynamic initial conditions, an initial turbulence level must be supplied at the initial axial station x_o. In the absence of known profiles for k and ϵ or ω', the Prandtl mixing length model is used to define the turbulent shear stress in terms of the local velocity gradient utilizing the following relation

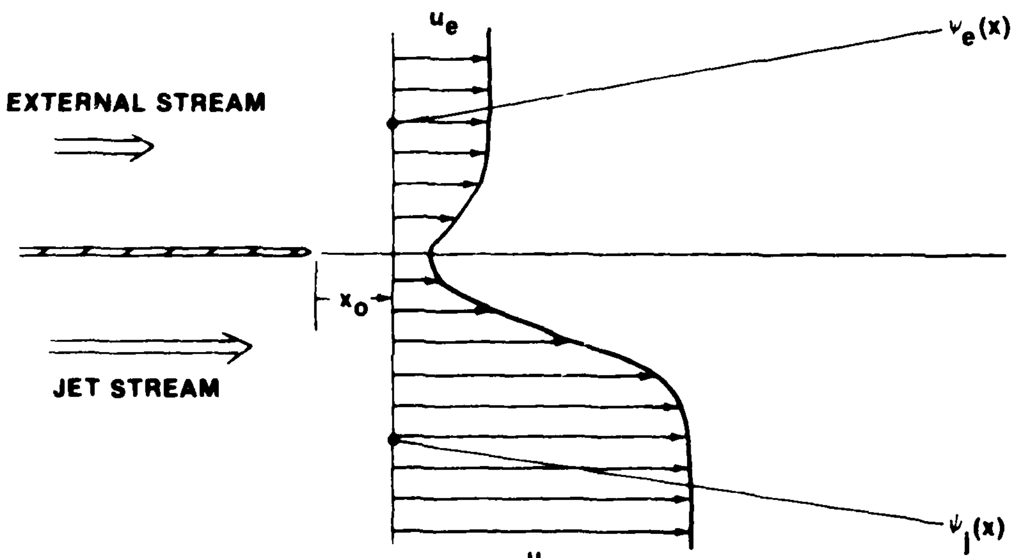

Figure 4. Generalized specific profile.

$$\rho\ \overline{u'v'} = \rho \ell^2 \left(\frac{\partial u}{\partial r}\right) \left|\frac{\partial u}{\partial r}\right| \tag{35}$$

and the relation between the shear stress and the turbulent energy [7]

$$k = \frac{\overline{u'v'}}{0.3} \tag{36}$$

D. Boundary Layer Initial Profile Results

For the He N_2 shear layer of Brown & Roshko, the initial conditions should not affect the resulting similar profile far downstream of the initial station. This was examined by looking at the different methods of specifying the initial profile.

The use of the boundary layer initial profile was examined for the He/N_2 shear layer of Brown and Roshko for which the experimental velocity and density profiles are shown in *Figures 16 and 17.*

δ^* was determined from θ calculated by Brown and Roshko and the relation between these quantities for a flat plate, i.e.

$$\frac{\delta^*}{\theta} = \frac{1.7208\ Re^{\frac{1}{2}}}{0.664\ Re^{\frac{1}{2}}} = 2.592$$

Since the momentum thickness was found to be 0.001 inches and the splitter plate thickness was 0.002 inches, the displacement thickness utilized for this option was

$$\delta^* = \frac{(0.002)(2.592)}{12} = 4.318 \times 10^{-4} \text{ft.}$$

The Re difference between the He and N_2 was not accounted for and the boundary layer displacement thickness was taken as the same for both the jet and the external stream, i.e.

$$\delta^*_j = \delta^*_e = 4.32 \times 10^{-4} \text{ft.}$$

The resulting mixing profiles of the density and the velocity for the two dimensional shear layer are shown in *Figure 6*. These results are given at a distance downstream of x = 1.69 inches.

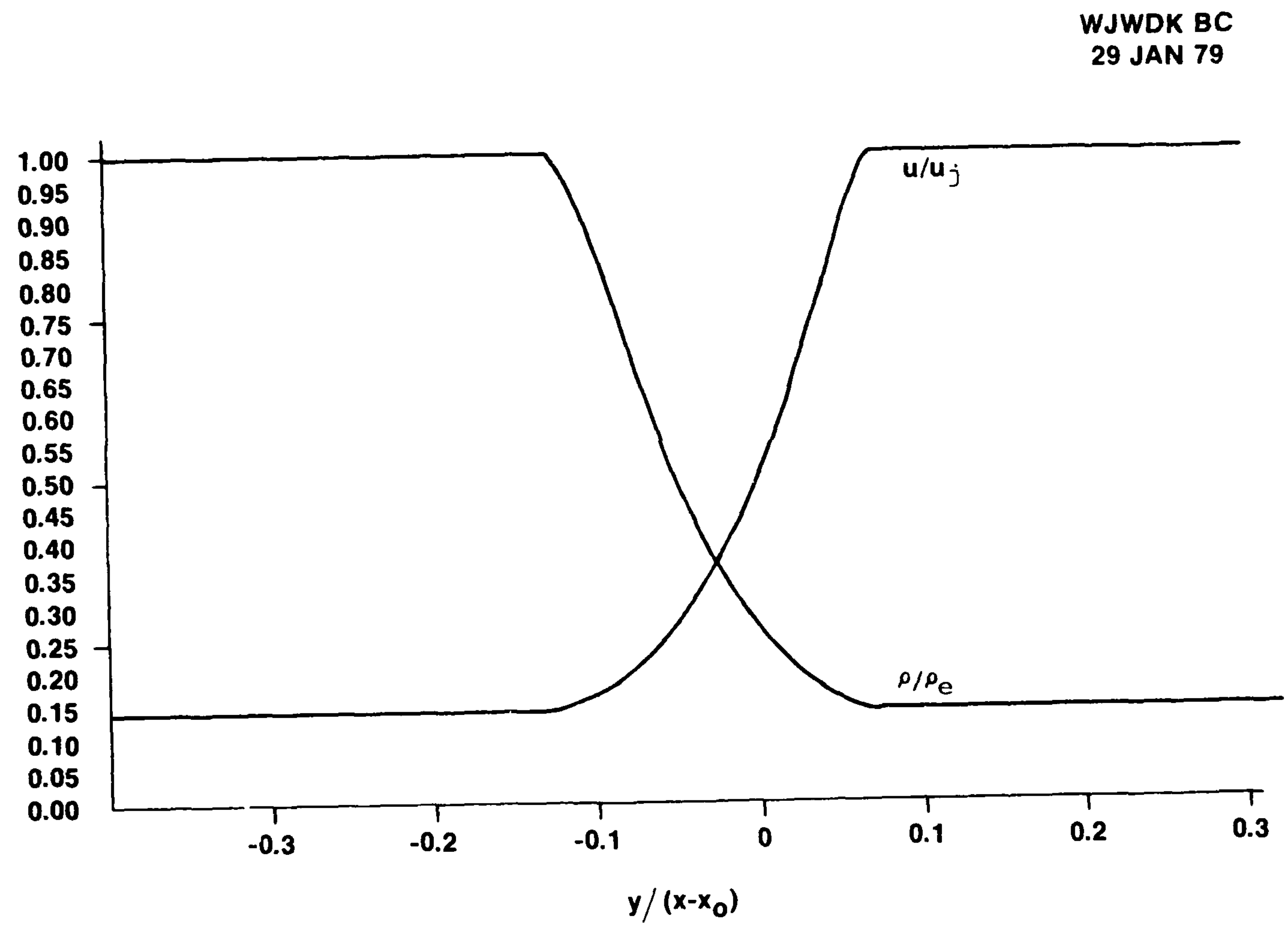

Figure 5. Results for boundary layer initial profile.

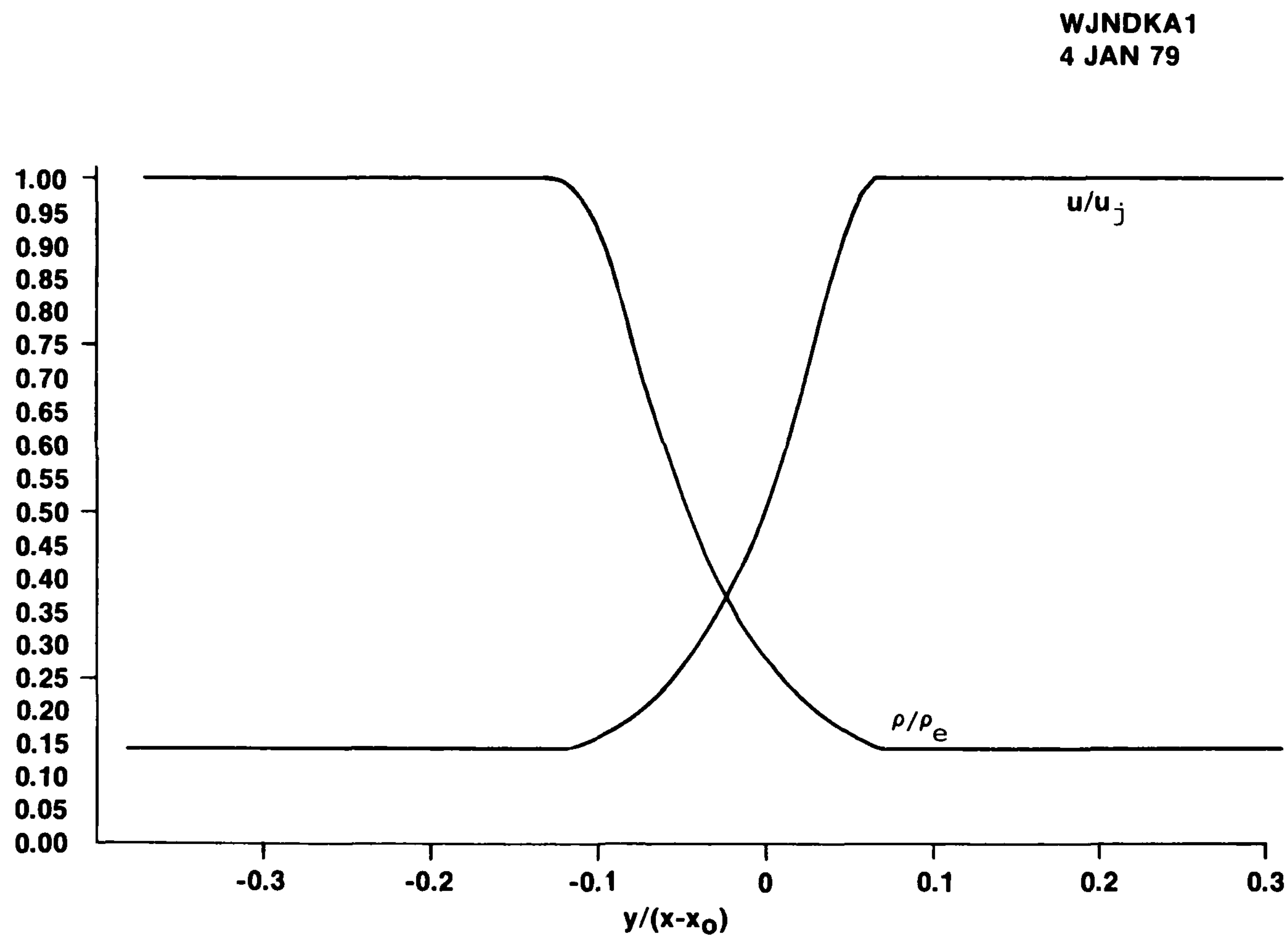

Figure 6. Results for shear layer initial profile.

E. Shear Layer Initial Profiles Results

This method was used to calculate the initial profile from which the finite difference solution was started and the results from this method are shown in *Figure 7*. The initial shear layer based on the cubic profile was calculated at x = .01 feet (8.33×10^{-4} inches) and calculations were started from that point. The kϵ2 turbulence model was used in this calculation just as it was on the boundary layer initialization results given in Section D above. Note that these results are given for a position slightly further downstream x = 1.81 inches. This makes very little difference however, since the profiles have already achieved self-similarity.

F. Generalized Specific Profile Results

This method was also used to specify the initial profile to determine what differences in results occurred because of differences in the initial startline. For this option, the mean profile for the density and velocity were taken at x = 0 directly from the boundary layer initialization scheme described above. However, the turbulence kinetic energy profile at x = 0 was taken from experimental data rather than being calculated using the mixing length turbulence option described above.

The turbulence kinetic energy profile was taken from experimental data for flow over a flat plate. This data was taken from *Figure 5* of Klebanoff [3] and has been tabularized in *Table 1* as a function of y/δ where δ is the shear layer width.

TABLE 1. EXPERIMENTAL TURBULENT KINETIC ENERGY PROFILE

y/δ	u'/U_∞	v'/U_∞	w'/U_∞	$\frac{u'^2+v'^2+w'^2}{U_\infty^2}$	$\frac{1}{2}\left\{\frac{u'^2+v'^2+w'^2}{U_\infty^2}\right\}$
0	.087	.032	.065	1.2818x10-2	6.409x10-3
0.1	.071	.040	.052	9.345x10-3	4.673x10-3
0.2	.066	.040	.050	8.456x10-3	4.228x10-3
0.3	.060	.038	.048	7.348x10-3	3.674x10-3
0.4	.056	.036	.046	6.548x10-3	3.274x10-3
0.5	.051	.033	.041	5.371x10-3	2.686x10-3
0.6	.042	.029	.035	3.830x10-3	1.915x10-3
0.7	034	.022	.029	2.481x10-3	1.241x10-3
0.8	.021	.018	.021	1.206x10-3	6.030x10-4
0.9	.012	.012	.012	4.320x10-4	2.160x10-4
1.0	.007	.007	.007	1.470x10-4	7.350x10-5

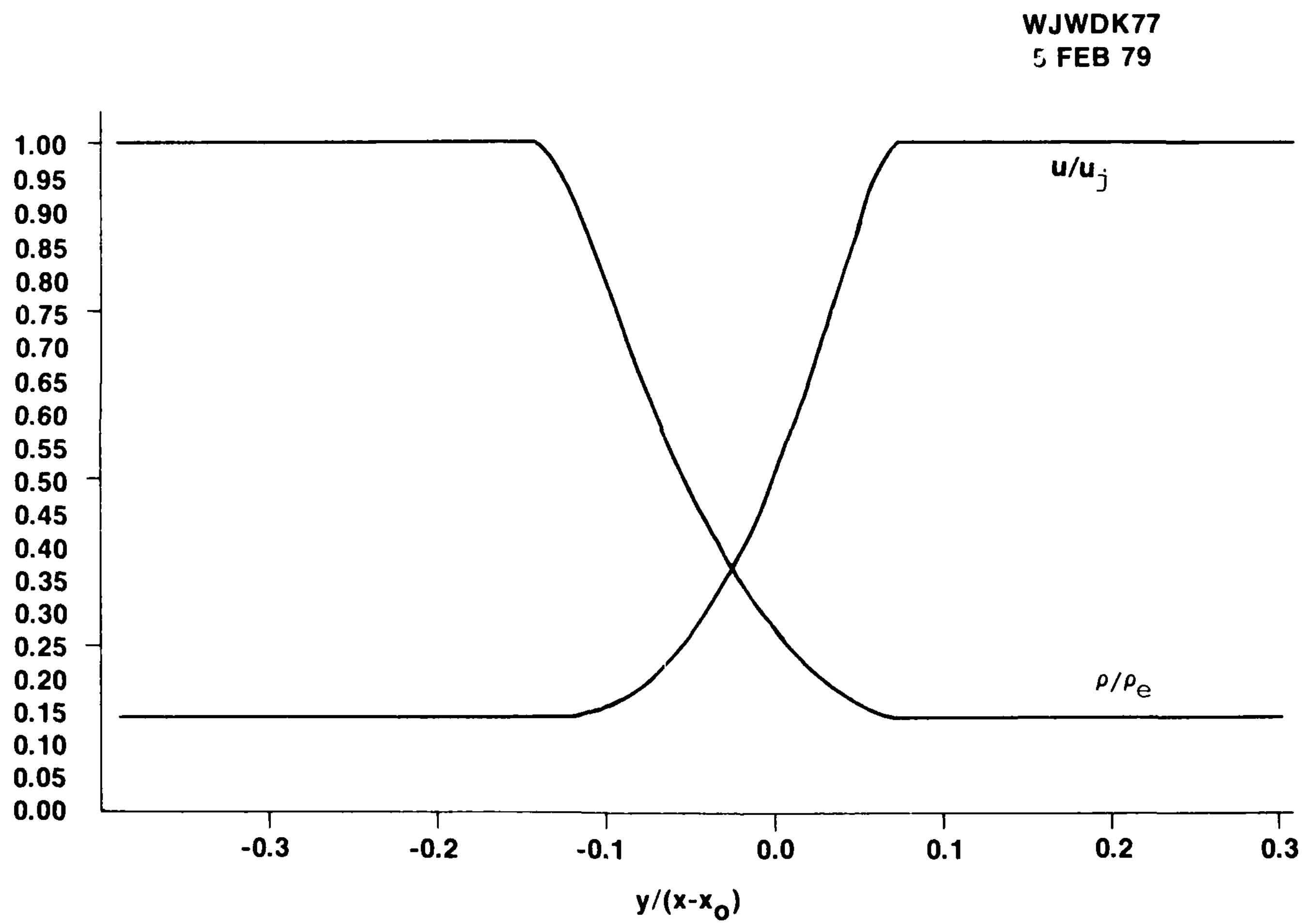

Figure 7. Results for generalized specific profile.

Next, the velocity profile that was generated at $x = 0$ using the boundary layer initialization scheme above is interpolated to obtain velocities at each y/δ location. This was done for both the jet boundary and the external boundary. These results are shown in *Table 2*. Also note that the initial shear layer thickness δ is taken from the boundary layer initialization scheme. The combination of the data for both the external and jet streams provide the specific shear layer profile data used to calculate the mixing layer. This is given in *Table 3*.

This is compared with the initial turbulence data which was calculated utilizing the mixing length model as described above. This initial profile expanded to 50 points across the shear layer is shown for the boundary layer initialization method in *Table 4* and for the specific profile method in *Table 5*.

Comparing *Table 4* with *Table 5* shows large differences in the turbulence kinetic energies for the calculated and input initialization schemes. Note that for the calculated scheme of *Table 4*, $0 \leq k \leq 792.6$ while the data based on experiment is in the range $0.079 \leq k \leq 5.657$. Hence, the turbulent intensity is down two orders of magnitude. Similarly, there are large changes noted in length scale parameter ϵ. However, when these shear layers have been calculated out to a distance of 1.69 inches, *Figure (7)* shows that the initial profile differences have washed out and the density and velocity profiles are virtually the same. *Figure (8)* was obtained from *Figures (5-7)*.

Therefore it has been shown that this calculational scheme is not sensitive to initial conditions when the behavior of the shear layer is examined far enough downstream where the flow becomes self similar. Hence, any of the initial profile methods may be used with confidence.

IV. kω' TURBULENCE MODEL FORMULATION

In order to make meaningful comparisons of various turbulence models for use in rocket exhaust plumes, an investigation of several models was made. The following turbulence models were investigated:

- Prandtl mixing length
- Donaldson-Gray eddy viscosity

TABLE 2. CALCULATION OF TURBULENCE KINETIC ENERGY ACROSS JET AND EXTERNAL BOUNDARIES USING EXPERIMENTAL DATA FROM TABLE 1

JET BOUNDARY

y/δ	k/U_∞^2	U_∞	y†	k	u†	T
0.0	6.409x10-3	32.81	10.00000	6.8992	0.0	300
0.1	4.673x10-3	32.81	9.999847	5.0305	25.84	300
0.2	4.228x10-3	32.81	9.999694	4.5514	27.462	300
0.3	3.674x10-3	32.81	9.999541	3.9550	28.541	300
0.4	3.274x10-3	32.81	9.999388	3.5244	29.449	300
0.5	2.686x10-3	32.81	9.999235	2.8914	30.255	300
0.6	1.915x10-3	32.81	9.999082	2.0615	30.980	300
0.7	1.241x10-3	32.81	9.998929	1.3359	31.610	300
0.8	6.030x10-4	32.81	9.998776	0.6491	32.136	300
0.9	2.160x10-4	32.81	9.993623	0.2325	32.536	300
1.0	7.350x10-5	32.81	9.99847	0.0791	32.810	300

EXTERNAL BOUNDARY

y/δ	k/U_∞^2	U_∞	y	k	u†	T
0.0	6.409x10-3	4.69	10.00000	0.14097	0.0	300
0.1	4.673x10-3	4.69	10.00015	0.10279	3.6915	300
0.2	4.228x10-3	4.69	10.00030	0.09300	3.9241	300
0.3	3.674x10-3	4.69	10.00045	0.08081	4.0800	300
0.4	3.274x10-3	4.69	10.00060	0.07202	4.2094	300
0.5	2.686x10-3	4.69	10.00075	0.05908	4.3247	300
0.6	1.915x10-3	4.69	10.00090	0.04212	4.4283	300
0.7	1.241x10-3	4.69	10.00105	0.02730	4.5186	300
0.8	6.030x10-4	4.69	10.00120	0.01326	4.5933	300
0.9	2.160x10-4	4.69	10.00135	0.00475	4.6508	300
1.0	7.350x10-5	4.69	10.00150	0.00162	4.6900	300

†From the He/N_2 B.L. initialization ouput-

δ_{JET} = 10.0000 - 9.9985 = 1.5×10^{-3}ft (0.018 inches)

δ_{EXT} = 10.0020 - 10.0000 = 2.0×10^{-3}ft (0.024 inches)

UNITS: y – in.; U – ft/sec; k – ft^2/sec^2; T – °K.

TABLE 3. SHEAR LAYER INPUT PROFILE DATA FOR BROWN AND ROSHKO He/N_2 EXPERIMENTAL RUN (FIGURE 16)

PT.	y	u	T	k	α_{He}	α_{N_2}
1	9.998470	32.810	300.00	0.0791	1.0	0.0
2	9.998623	32.536	300.00	0.2325	1.0	0.0
3	9.993776	32.136	300.00	0.6491	1.0	0.0
4	9.993929	31.610	300.00	1.3359	1.0	0.0
5	9.999082	30.980	300.00	2.0615	1.0	0.0
6	9.999235	30.255	300.00	2.8914	1.0	0.0
7	9.999388	29.449	300.00	3.5244	1.0	0.0
8	9.999541	28.541	300.00	3.9550	1.0	0.0
9	9.999694	27.462	300.00	4.5514	1.0	0.0
10	9.999847	25.840	300.00	5.0305	1.0	0.0
11	10.000000	0.000	300.00	6.8992	0.5	0.5
12	10.000150	4.6900	300.00	0.10279	0.0	1.0
13	10.000300	4.6508	300.00	0.09300	0.0	1.0
14	10.000450	4.5933	300.00	0.08081	0.0	1.0
15	10.000600	4.5186	300.00	0.07020	0.0	1.0
16	10.000750	4.4283	300.00	0.05908	0.0	1.0
17	10.000900	4.3247	300.00	0.04212	0.0	1.0
18	10.001050	4.2094	300.00	0.02730	0.0	1.0
19	10.001200	4.0800	300.00	0.01326	0.0	1.0
20	10.001350	3.9241	300.00	0.00475	0.0	1.0
21	10.001500	3.6915	300.00	0.00162	0.0	1.0

UNITS: y – in.; U – ft/sec; k – ft^2/sec^2; T – ^oK.

TABLE 4. INITIAL PROFILE FOR BROWN AND ROSHKO He/N_2 SHEAR LAYER (FIGURE 16) — BOUNDARY LAYER INITIALIZATION

XF= 0.   FEET   ******BROWN/ROSHKO HE/N2 SHEAR FLOW DATA - BL INITIALIZATION ***

X/R	DELTA X FEET	PRESS(ATM)
0.	.1251?1E-04	.100000E+01

FRAR	CFL	C1	C2	DFRCT	FFNCT
0.	.500000E-01	.140000E+01	.194000E+01	.100000E+01	0.

NI	Y/R	VELOCITY FEET/SEC	TEMPERATURE R	DENSITY GM/CC	MACH NO.	ENIF-TKE (FT/S)**2	VISCOSITY LB/FT/S
1	.9998	[illegible]	[illegible]	.113601E-02	.961397E-02	0.	0.
2	.9999	[illegible]	[illegible]	.113601E-02	.961692E-02	.521484E-01	.118007
3	.9999	[illegible]	[illegible]	.113601E-02	.961564E-02	.129822E+00	.139994
4	.9999	[illegible]	.300000E+03	.113601E-02	.962308E-02	.173412E+00	.161880
5	.9999	.323895E+02	[illegible]	.113601E-02	.960222E-02	.222255E+00	.183519
6	.9999	.322153E+02	.300000E+03	.113600E-02	.959606E-02	.277559E+00	.204734
7	.9999	.320435E+02	.300000E+03	.113600E-02	.956470E-02	.335140E+00	.225367
8	.9999	.318848E+02	.300011E+03	.113600E-02	.952815E-02	.390310E+00	.245340
9	.9999	.316424E+02	[illegible]	.113600E-02	.946652E-02	.462987E+00	.264511
10	.9999	[illegible]	[illegible]	.113600E-02	.939990E-02	.529210E+00	.282802
11	.9999	.311808E+02	[illegible]	.113600E-02	.932843E-02	.592291E+00	.300191
12	.9999	.309319E+02	[illegible]	.113600E-02	.925220E-02	.663712E+00	.316707
13	.9999	[illegible]	[illegible]	.113600E-02	.917132E-02	.731393E+00	.332463
14	.9999	.303757E+02	.300001E+03	.113600E-02	.908582E-02	.799845E+00	.347683
15	.9999	.300744E+02	.300002E+03	.113600E-02	.899560E-02	.870742E+00	.362754
16	.9999	.297570E+02	.300002E+03	.113600E-02	.890073E-02	.946930E+00	.376291
17	.9999	.294222E+02	.300002E+03	.113600E-02	.880081E-02	.103379E+01	.395260
18	.9999	.290678E+02	[illegible]	.113600E-02	.869459E-02	.114080E+01	.415177
19	1.0000	.286695E+02	[illegible]	.113600E-02	.858144E-02	.120392E+01	.440489
20	1.0000	[illegible]	[illegible]	.113600E-02	.845899E-02	.149515E+01	.475344
21	1.0000	.278273E+02	[illegible]	.113600E-02	.832352E-02	.184029E+01	.527362
22	1.0000	.273080E+02	.300003E+03	.113600E-02	.816619E-02	.240103E+01	.612324
23	1.0000	.266776E+02	.300003E+03	.113059E-02	.797945E-02	.392329E+01	.769999
24	1.0000	.258273E+02	.300004E+03	.113059E-02	.772529E-02	.609549E+01	.114633
25	1.0000	.244001E+02	.300004E+03	.113059E-02	.729830E-02	.792610E+03	.109444
26	1.0000	.261739E+01	.300012E+03	.796420E-02	.243271E-02	.420104E+03	.557339
27	1.0000	.365912E+01	.300000E+03	.796420E-02	.315951E-02	.141614E+01	.300464
28	1.0000	[illegible]	[illegible]	.796426E-02	.327257E-02	.621655E-01	.743010
29	1.0000	[illegible]	.300000E+03	.796426E-02	.335483E-02	.503138E-01	.581425
30	1.0000	.396272E+01	[illegible]	.796426E-02	.342106E-02	.365905E-01	.495831
31	1.0000	.402568E+01	[illegible]	.796426E-02	.347940E-02	.293570E-01	.444126
32	1.0000	[illegible]	.300000E+03	.796426E-02	.353147E-02	.250103E-01	.409930
33	1.0000	.414553E+01	.300000E+03	.796426E-02	.357934E-02	.220666E-01	.385051
34	1.0001	.419706E+01	.300000E+03	.796427E-02	.362401E-02	.190773E-01	.365451
35	1.0001	.424580E+01	[illegible]	.796427E-02	.366609E-02	.181610E-01	.349317
36	1.0001	.429199E+01	[illegible]	.796427E-02	.370597E-02	.166949E-01	.334921
37	1.0001	[illegible]	[illegible]	.796427E-02	.374383E-02	.153405E-01	.321048
38	1.0001	.437742E+01	[illegible]	.796427E-02	.377974E-02	.140388E-01	.307125
39	1.0001	.441878E+01	[illegible]	.796427E-02	.381373E-02	.127596E-01	.292798
40	1.0001	.445591E+01	.300000E+03	.796427E-02	.384579E-02	.114908E-01	.277659
41	1.0001	.448877E+01	.300000E+03	.796427E-02	.387589E-02	.102321E-01	.262201
42	1.0001	.452131E+01	.300000E+03	.796427E-02	.390390E-02	.899090E-02	.245783
43	1.0001	.455145E+01	.300000E+03	.796427E-02	.393004E-02	.769433E-02	.227371
44	1.0001	[illegible]	[illegible]	.796427E-02	.395375E-02	.640436E-02	.207438
45	1.0001	.460378E+01	[illegible]	.796427E-02	.397516E-02	.525604E-02	.187959
46	1.0001	[illegible]	[illegible]	.796427E-02	.399443E-02	.423257E-02	.168637
47	1.0001	[illegible]	.300000E+03	.796427E-02	.401149E-02	.330398E-02	.148994
48	1.0001	.466306E+01	.300000E+03	.796427E-02	.402636E-02	.248266E-02	.129154
49	1.0001	.467778E+01	.300000E+03	.796427E-02	.403909E-02	.177609E-02	.109240
50	1.0001	[illegible]	.300000E+03	.796427E-02	.404964E-02	0.	0.

USL	YSL	U10	Y10	SPRD	DEL
[illegible]	[illegible]	.750200E+01	.999999E+00	-.700652E-04	-.10741

DELTAAVG
.900800E+00

PRECEDING PAGE BLANK-NOT FILMED

O He/N_2
LAYER

* [illegible] ******   WJWDKBC
29 JAN 7[illegible]

	U2	[illegible]	PENCT
...01	.194000E+01	[illegible]	0.

	MACH NO.	[illegible]	VISCOSITY LB/FT/SEC	PSI	PH-XE	UNORM
...-02	.961397E-02	0.	0.	.269169E+01	0.	1.000
...-02	.970692E-02	[illegible]	.118007E-05	.269170E+01	.46[illegible]26E+02	.997
...-02	.975064E-02	.12[illegible]E+00	.139994E-05	.269172E+01	.766371E+02	.993
...-02	.972302E-02	.173[illegible]2E+00	.161686E-05	.269173E+01	.11[illegible]16E+03	.989
...-02	.968222E-02	[illegible]	.183519E-05	.269175E+01	.173096E+03	.984
...-02	.963060E-02	[illegible]94E+00	.204734E-05	.269176E+01	.240335E+03	.979
...-02	.956470E-02	.33[illegible]E+00	.225367E-05	.269178E+01	.320652E+03	.973
...-02	.952615E-02	.39[illegible]E+00	.245340E-05	.269179E+01	.413614E+03	.966
...-02	.946652E-02	.46[illegible]E+00	.264511E-05	.269181E+01	.516297E+03	.959
...-02	.939990E-02	[illegible]	.282802E-05	.269182E+01	.633425E+03	.951
...-02	.93264[illegible]E-02	[illegible]	.300191E-05	.269184E+01	.757602E+03	.942
...-02	.925220E-02	[illegible]12E+00	.316707E-05	.269185E+01	.869658E+03	.933
...-02	.917132E-02	.75139[illegible]E+00	.332463E-05	.269187E+01	.102915E+04	.924
...-02	.908582E-02	.79[illegible]E+00	.347083E-05	.269188E+01	.117707E+04	.913
...-02	.899588E-02	.870742E+00	.362754E-05	.269190E+01	.133686E+04	.903
...-02	.890073E-02	.946930E+00	.376291E-05	.269191E+01	.151611E+04	.891
...-02	.880081E-02	.103379E+01	.395260E-05	.269193E+01	.172942E+04	.880
...-02	.869459E-02	.114[illegible]0E+01	.415177E-05	.269194E+01	.200426E+04	.867
...-02	.856144E-02	.126392E+01	.440489E-05	.269196E+01	.239364E+04	.853
...-02	.845699E-02	.149515E+01	.475344E-05	.269197E+01	.300602E+04	.839
...-02	.832352E-02	.184[illegible]9E+01	.527362E-05	.269199E+01	.410754E+04	.823
...-02	.816819E-02	.240103E+01	.612324E-05	.269200E+01	.642965E+04	.804
...-02	.797945E-02	.392329E+01	.769999E-05	.269201E+01	.127658E+05	.782
...-02	.772529E-02	.809549E+01	.114633E-04	.269203E+01	.421685E+05	.752
...-02	.729830E-02	.792810E+03	.109444E-03	.269204E+01	.367149E+08	.701
...-02	.243271E-02	.420104E+03	.557339E-03	.269206E+01	.141673E+08	-.067
...-02	.315951E-02	.141614E+01	.300464E-04	.269207E+01	.290875E+04	-.037
...-02	.327257E-02	.621655E-01	.743010E-05	.269209E+01	.406517E+02	-.032
...-02	.335463E-02	.503136E-01	.581425E-05	.269210E+01	.194794E+02	-.029
...-02	.342166E-02	.359905E-01	.495831E-05	.269212E+01	.120608E+02	-.026
...-02	.347940E-02	.293570E-01	.444126E-05	.269213E+01	.868166E+01	-.023
...-02	.353147E-02	.250183E-01	.409930E-05	.269215E+01	.682668E+01	-.021
...-02	.357934E-02	.220865E-01	.385051E-05	.269216E+01	.565781E+01	-.019
...-02	.362401E-02	.190773E-01	.365451E-05	.269218E+01	.483706E+01	-.018
...-02	.366092E-02	.181610E-01	.349317E-05	.269219E+01	.422430E+01	-.016
...-02	.370597E-02	.166449E-01	.334921E-05	.269221E+01	.372324E+01	-.014
...-02	.374383E-02	.153405E-01	.321048E-05	.269222E+01	.327946E+01	-.013
...-02	.377974E-02	.140368E-01	.307125E-05	.269224E+01	.287104E+01	-.011
...-02	.381373E-02	.127596E-01	.292798E-05	.269225E+01	.248771E+01	-.010
...-02	.384579E-02	.114908E-01	.277859E-05	.269227E+01	.212603E+01	-.008
...-02	.387569E-02	.102321E-01	.262201E-05	.269228E+01	.178647E+01	-.007
...-02	.390390E-02	.899090E-02	.245783E-05	.269230E+01	.147146E+01	-.006
...-02	.393004E-02	.769433E-02	.227371E-05	.269231E+01	.116493E+01	-.005
...-02	.395537E-02	.640436E-02	.207436E-05	.269233E+01	.884623E+00	-.004
...-02	.397516E-02	.525604E-02	.187959E-05	.269234E+01	.658063E+00	-.003
...-02	.399443E-02	.423257E-02	.166637E-05	.269236E+01	.475261E+00	-.002
...-02	.401149E-02	.330398E-02	.146994E-05	.269237E+01	.327795E+00	-.002
...-02	.402630E-02	.248266E-02	.129154E-05	.269239E+01	.213511E+00	-.001
...-02	.403909E-02	.177609E-02	.109240E-05	.269240E+01	.129194E+00	-.000
...-02	.404964E-02	0.	0.	.269242E+01	0.	0.000

	Y10	SPHU	DELW	DEL*PRIME	DUDYM	JM
...01	.999999E+00	-.700052E-04	-.107410E-03	.257783E-01	-.261801E+06	26

TABLE 5. INITIAL PROFILE FOR BROWN AND ROSHKO He/N$_2$ SHEAR LAYER (FIGURE 16) — SPECIFIED PROFILE INITIALIZATION

X= 0. FEET [illegible] He/N2 SHEAR FLOW DATA [illegible]

X/H	DELTA * FEET	PRESS(ATM)
0.	.567573E-04	.700000E+01

RLAM	CMU	C1	C2	GFNCT	FFNCT
0.	.900000E-01	.140000E+01	.194000E+01	.100000E+01	0.

PT	Y/H	VELOCITY FEET/SEC	TEMPERATURE R	DENSITY GM/CC	MACH NO.	ENTH-TKE C/0-(F/S)**2	VISCOSITY LB/FT/S
1	.999846E+00	.326100E+02	.300000E+03	.113681E-02	.981597E-02	.791000E-01	0.
2	.999853E+00	.327133E+02	.300000E+03	.113681E-02	.976508E-02	.133215E+00	.156
3	.999859E+00	.326167E+02	.300000E+03	.113681E-02	.975615E-02	.187330E+00	.214
4	.999864E+00	.325124E+02	.300000E+03	.113681E-02	.972490E-02	.257040E+00	.240
5	.999870E+00	.323699E+02	.300000E+03	.113681E-02	.968232E-02	.405544E+00	.330
6	.999875E+00	.322273E+02	.300000E+03	.113681E-02	.963967E-02	.554041E+00	.427
7	.999880E+00	.320875E+02	.300000E+03	.113681E-02	.959189E-02	.738475E+00	.494
8	.999886E+00	.316773E+02	.300000E+03	.113681E-02	.953500E-02	.976840E+00	.611
9	.999892E+00	.312871E+02	.300000E+03	.113681E-02	.947610E-02	.123521E+01	.723
10	.999897E+00	.314720E+02	.300000E+03	.113681E-02	.941377E-02	.149479E+01	.796
11	.999903E+00	.312400E+02	.300000E+03	.113681E-02	.934430E-02	.176204E+01	.913
12	.999908E+00	.310080E+02	.300000E+03	.113681E-02	.927490E-02	.202928E+01	.964
13	.999914E+00	.307400E+02	.300000E+03	.113681E-02	.919480E-02	.233625E+01	.105
14	.999920E+00	.304670E+02	.300000E+03	.113681E-02	.911316E-02	.264867E+01	.117
15	.999926E+00	.301850E+02	.300000E+03	.113681E-02	.902897E-02	.294592E+01	.123
16	.999932E+00	.298744E+02	.300000E+03	.113681E-02	.893580E-02	.319033E+01	.129
17	.999937E+00	.295632E+02	.300000E+03	.113681E-02	.884200E-02	.343473E+01	.133
18	.999943E+00	.292205E+02	.300000E+03	.113681E-02	.874029E-02	.363277E+01	.132
19	.999950E+00	.288595E+02	.300000E+03	.113681E-02	.863233E-02	.380394E+01	.135
20	.999956E+00	.284808E+02	.300000E+03	.113681E-02	.852144E-02	.396305E+01	.129
21	.999962E+00	.280447E+02	.300000E+03	.113681E-02	.840059E-02	.422934E+01	.127
22	.999968E+00	.276005E+02	.300000E+03	.113681E-02	.825574E-02	.447483E+01	.114
23	.999975E+00	.264793E+02	.300000E+03	.113681E-02	.809992E-02	.469398E+01	.989
24	.999981E+00	.222776E+02	.300000E+03	.113681E-02	.780010E-02	.490118E+01	.143
25	.999987E+00	.171756E+02	.300000E+03	.220294E-02	.742048E-02	.565708E+01	.979
26	.999996E+00	.100000E+01	.300000E+03	.534362E-02	.669580E-03	.532162E+01	.297
27	.100001E+01	.371754E+01	.300000E+03	.796427E-02	.320137E-02	.102113E+00	.730
28	.100001E+01	.381026E+01	.300000E+03	.796427E-02	.329002E-02	.977915E-01	.939
29	.100002E+01	.391293E+01	.300000E+03	.796427E-02	.337867E-02	.934703E-01	.104
30	.100003E+01	.398245E+01	.300000E+03	.796427E-02	.343870E-02	.884378E-01	.123
31	.100003E+01	.404792E+01	.300000E+03	.796427E-02	.349523E-02	.833184E-01	.124
32	.100004E+01	.410676E+01	.300000E+03	.796427E-02	.354604E-02	.786156E-01	.129
33	.100005E+01	.415924E+01	.300000E+03	.796427E-02	.359135E-02	.743132E-01	.128
34	.100005E+01	.421140E+01	.300000E+03	.796427E-02	.363639E-02	.700073E-01	.128
35	.100006E+01	.425861E+01	.300000E+03	.796427E-02	.367580E-02	.656273E-01	.127
36	.100006E+01	.430223E+01	.300000E+03	.796427E-02	.371402E-02	.612473E-01	.12
37	.100007E+01	.434460E+01	.300000E+03	.796427E-02	.375158E-02	.557697E-01	.11
38	.100008E+01	.438458E+01	.300000E+03	.796427E-02	.378593E-02	.492765E-01	.10
39	.100008E+01	.442437E+01	.300000E+03	.796427E-02	.382026E-02	.427633E-01	.97
40	.100009E+01	.445888E+01	.300000E+03	.796427E-02	.385008E-02	.371020E-01	.91
41	.100009E+01	.449260E+01	.300000E+03	.796427E-02	.387937E-02	.315340E-01	.79
42	.100010E+01	.452520E+01	.300000E+03	.796427E-02	.390735E-02	.260590E-01	.72
43	.100010E+01	.455275E+01	.300000E+03	.796427E-02	.393114E-02	.208796E-01	.62
44	.100011E+01	.458032E+01	.300000E+03	.796427E-02	.395494E-02	.157002E-01	.49
45	.100011E+01	.460436E+01	.300000E+03	.796427E-02	.397570E-02	.110234E-01	.42
46	.100012E+01	.462527E+01	.300000E+03	.796427E-02	.399375E-02	.652893E-02	.33
47	.100013E+01	.464510E+01	.300000E+03	.796427E-02	.401180E-02	.543444E-02	.24
48	.100013E+01	.466179E+01	.300000E+03	.796427E-02	.402526E-02	.387276E-02	.21
49	.100014E+01	.467509E+01	.300000E+03	.796427E-02	.403746E-02	.274630E-02	.15
50	.100014E+01	.469000E+01	.300000E+03	.796427E-02	.404904E-02	.162000E-02	0.

USL	Y9U	U10	Y10	SPRD	DEL
.299[illegible]E+02	.999929E+00	.750200E+01	.999993E+00	-.633502E-04	-.15666

DELWPRAVG
.815076E+00

PRECEDING PAGE BLANK-NOT FILMED

DATA-BL PROFILE + TKE PROFILES$$$$$

WJWDK6Y
6 FEB 79

	GFNCT	FFNCT
…E+01	.100000E+01	0.

…U.	ENTH-TKE (Z/(F/S))**2	VISCOSITY LB/FT/SEC	PSI	PR-XE	UNORM
…597E-02	.791000E-01	0.	.269169E+01	0.	1.000
…506E-02	.135215E+00	.158402E-05	.269170E+01	.716588E+02	.997
…615E-02	.187330E+00	.214968E-05	.269172E+01	.104416E+03	.993
…496E-02	.257048E+00	.240865E-05	.269173E+01	.175460E+03	.989
…232E-02	.405544E+00	.330363E-05	.269175E+01	.318407E+03	.984
…967E-02	.554041E+00	.427647E-05	.269176E+01	.459115E+03	.979
…169E-02	.758475E+00	.494665E-05	.269177E+01	.704868E+03	.974
…500E-02	.976640E+00	.611921E-05	.269179E+01	.101794E+04	.967
…610E-02	.123521E+01	.723257E-05	.269180E+01	.134930E+04	.960
…137E-02	.144479E+01	.798616E-05	.269182E+01	.178911E+04	.952
…436E-02	.176204E+01	.913969E-05	.269183E+01	.217281E+04	.944
…7496E-02	.202926E+01	.984187E-05	.269185E+01	.267626E+04	.936
…9480E-02	.233625E+01	.105653E-04	.269186E+01	.330430E+04	.926
…1316E-02	.264867E+01	.117919E-04	.269188E+01	.380536E+04	.917
…2697E-02	.294592E+01	.123827E-04	.269189E+01	.448281E+04	.907
…3588E-02	.319033E+01	.129023E-04	.269190E+01	.504574E+04	.896
…4260E-02	.343473E+01	.133609E-04	.269192E+01	.564772E+04	.885
…4029E-02	.363277E+01	.132862E-04	.269193E+01	.635326E+04	.872
…3233E-02	.380394E+01	.135467E-04	.269195E+01	.683216E+04	.860
…2144E-02	.398365E+01	.129047E-04	.269196E+01	.786649E+04	.846
…0859E-02	.422934E+01	.127888E-04	.269198E+01	.896174E+04	.831
…3574E-02	.447483E+01	.114437E-04	.269199E+01	.111920E+05	.815
…0992E-02	.469398E+01	.989126E-05	.269201E+01	.142480E+05	.793
…0010E-02	.490118E+01	.143064E-05	.269202E+01	.107397E+06	.768
…2048E-02	.565708E+01	.979603E-06	.269204E+01	.418880E+06	.444
…9580E-03	.532162E+01	.297123E-04	.269205E+01	.286113E+05	-.131
…0137E-02	.102113E+00	.736953E-06	.269206E+01	.633017E+03	-.035
…9002E-02	.577915E-01	.939898E-05	.269208E+01	.455215E+02	-.031
…7867E-02	.934703E-01	.104319E-04	.269209E+01	.374695E+02	-.028
…3870E-02	.884378E-01	.123701E-04	.269211E+01	.282878E+02	-.025
…9523E-02	.833184E-01	.124503E-04	.269212E+01	.249458E+02	-.023
…4804E-02	.786158E-01	.129315E-04	.269214E+01	.213828E+02	-.021
…9135E-02	.743132E-01	.128401E-04	.269215E+01	.192424E+02	-.019
…3039E-02	.700073E-01	.128104E-04	.269217E+01	.171166E+02	-.017
…7580E-02	.656273E-01	.127635E-04	.269218E+01	.150972E+02	-.015
…1402E-02	.612473E-01	.121668E-04	.269219E+01	.137941E+02	-.014
…5158E-02	.557897E-01	.117241E-04	.269221E+01	.118775E+02	-.012
…0593E-02	.492765E-01	.106206E-04	.269222E+01	.102289E+02	-.011
…2028E-02	.427633E-01	.978313E-05	.269224E+01	.836297E+01	-.009
…5008E-02	.371020E-01	.914340E-05	.269225E+01	.673568E+01	-.008
…7937E-02	.315340E-01	.795728E-05	.269227E+01	.559098E+01	-.007
…0735E-02	.260590E-01	.722219E-05	.269228E+01	.420672E+01	-.006
…3114E-02	.208798E-01	.625714E-05	.269230E+01	.311720E+01	-.005
…5494E-02	.157002E-01	.499537E-05	.269231E+01	.220768E+01	-.004
…7570E-02	.116234E-01	.422310E-05	.269232E+01	.143130E+01	-.003
…9375E-02	.652693E-02	.331584E-05	.269234E+01	.981500E+00	-.002
…1180E-02	.543444E-02	.240837E-05	.269235E+01	.548633E+00	-.002
…2526E-02	.387276E-02	.210205E-05	.269237E+01	.319222E+00	-.001
…3746E-02	.274630E-02	.156543E-05	.269238E+01	.215567E+00	-.001
…4984E-02	.162000E-02	0.	.269240E+01	0.	0.000

…U	SPRD	DELW	DELWPRIME	DUDYM	JM
…93E+00	-.633502E-04	-.156685E-03	.376045E-01	-.179468E+06	26

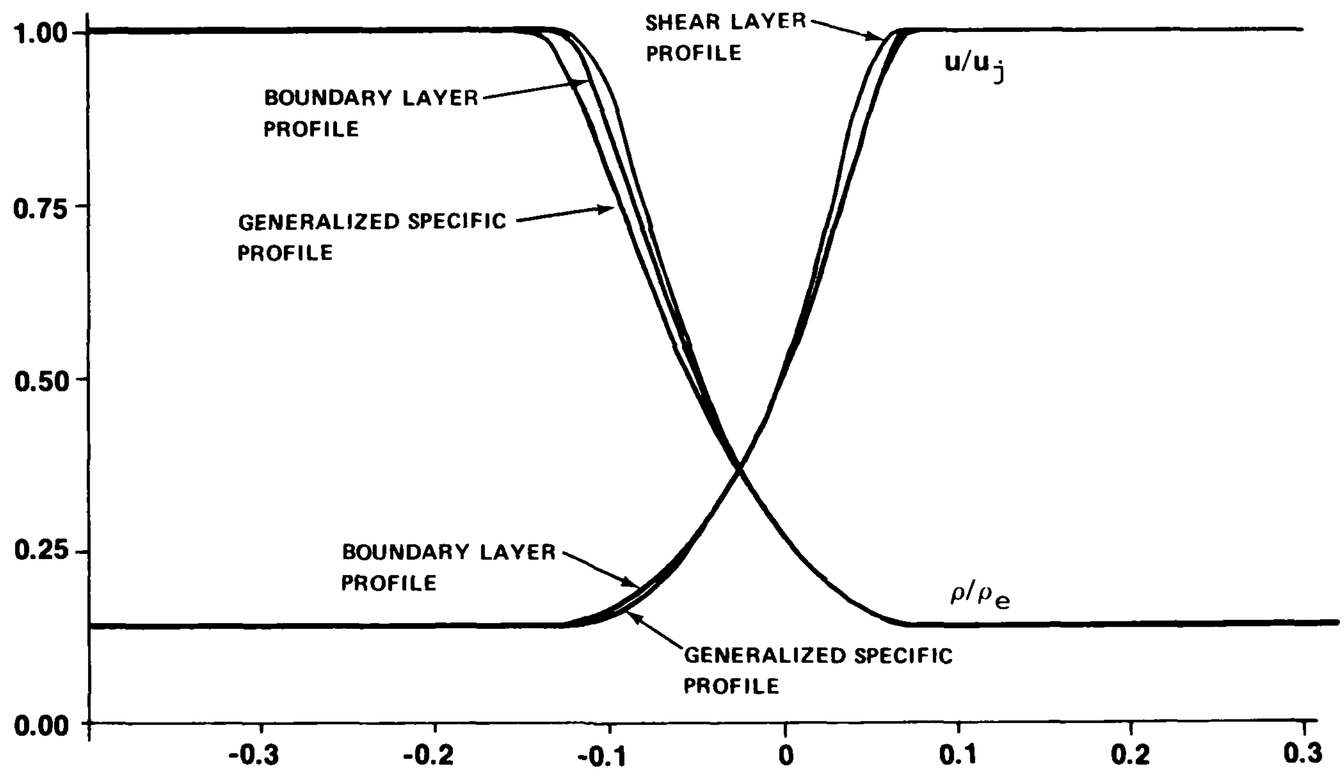

Figure 8. Comparison of results utilizing the three (3) input methods for determining the initial profile.

- Launder-Spalding kϵ2 turbulence kinetic energy model

- Saffman kω^2 turbulence kinetic energy model.

The Saffman model was chosen because this model has been formulated to account for a specific physical phenomena which is not explicitly modeled in the other three. This model was formulated, primarily on empirical arguments, to account for shear flows which do not have a constant density. These density differences arise either due to differences in molecular weights of the shear layer fluids (heterogeneous fluids) or due to compressibility effects (Mach Number) in homogeneous fluids. Both of these effects are modeled in the turbulence equations formulation.

Compressibility effects are accounted for in the kϵ2 turbulence model, but in an ad hoc manner. The turbulent viscosity contains an empirical correction term $k(M_{\tau_{max}})$ which was formulated using only a very limited set of experimental data. There are no additional terms in the model that account for this effect.

In order to use the Saffman model to make comparisons with data it was necessary to extend this model to a cylindrical geometry and to formulate it using a finite differencing scheme common to the other three models investigated. Only in this way can differences in results be solely due to the turbulence modeling and not due to the numerics. In addition, the equations are formulated in a stream function coordinate system.

Consider the Saffman formulation

$$\bar{\rho}U \frac{\partial e}{\partial x} + \bar{\rho}V \frac{\partial e}{\partial y} = \alpha'' \bar{\rho} e \left|\frac{\partial U}{\partial y}\right| - \bar{\rho} e \omega + \frac{1}{2} A \frac{\partial}{\partial y} \left(\frac{\bar{\rho} e}{\omega} \frac{\partial e}{\partial y}\right)$$

k-EQUATION

$$\bar{\rho}U \frac{\partial (\omega^2)}{\partial x} + \bar{\rho}V \frac{\partial \omega^2}{\partial y} = \alpha' \bar{\rho} \omega^2 \left|\frac{\partial U}{\partial y}\right| - \beta' \bar{\rho} \omega^3 + \frac{1}{2} A \frac{\partial}{\partial y} \left(\frac{\bar{\rho} e}{\omega} \frac{\partial (\omega^2)}{\partial y}\right) - A\gamma \frac{\omega}{\bar{\rho}} \frac{\partial \bar{\rho}}{\partial y} \frac{\partial}{\partial y} \left(\bar{\rho} e\right)$$

VORTICITY EQUATION

where

$$A = 0.09 \quad \alpha'' = A^{\frac{1}{2}} \quad \beta' = 5/3 \quad \alpha' = \beta'\alpha'' - 2k^2$$

These equations can be generalized for either 2-D or axisymmetric flow to be

$$\rho\frac{De}{Dt} = \frac{A}{2}\frac{1}{y^j}\frac{\partial}{\partial y}\left(y^j \frac{\rho e}{\omega}\frac{\partial e}{\partial y}\right) + \alpha''\bar{\rho}e\left|\left(\frac{\partial u}{\partial y}\right)\right| - \rho e\omega$$

$$\rho\frac{D\omega^2}{Dt} = \frac{A}{2}\frac{1}{y^j}\frac{\partial}{\partial y}\left(y^j \frac{\rho e}{\omega}\frac{\partial \omega^2}{\partial y}\right) + \alpha'\rho\omega^2\left|\frac{\partial u}{\partial y}\right| - \beta'\rho\omega^3$$

$$- A\gamma\frac{\omega}{\rho}\frac{\partial\rho}{\partial y}\frac{\partial}{\partial y}\left(\rho e\right)$$

In order to apply these equations to an axisymmetric rocket exhaust plume, choose $j = 1$; $y = r$. Utilizing different notations for the turbulence kinetic energy $\left(k^2 = \frac{u'^2 + v'^2}{2}\right)$, these equations become

$$\rho\frac{Dk}{Dt} = \frac{1}{2}\frac{1}{r}\frac{\partial}{\partial r}\left(r\mu_t\frac{\partial k}{\partial r}\right) + \frac{\alpha''}{A}\omega\mu_t\left|\frac{\partial u}{\partial r}\right| - \rho k\omega$$

$$\rho\frac{D\omega^2}{Dt} = \frac{1}{2}\frac{1}{r}\frac{\partial}{\partial r}\left(r\mu_t\frac{\partial \omega^2}{\partial r}\right) + \alpha'\rho\omega^2\left|\frac{\partial u}{\partial r}\right| - \frac{A\gamma\omega}{\rho}\frac{\partial\rho}{\partial r}\frac{\partial}{\partial r}\rho k$$

$$- \beta'\rho\omega^3$$

where $e = k$ & $\mu_t = \frac{A\rho e}{\omega}$

so rewriting these equations,

$$\rho\frac{Dk}{Dt} = \frac{1}{2r}\frac{\partial}{\partial r}\left(r\mu_t\frac{\partial k}{\partial r}\right) + C_1\omega\mu_t\left|\frac{\partial u}{\partial r}\right| - \rho k\omega$$

$$\rho\frac{D\omega^2}{Dt} = \frac{1}{2r}\frac{\partial}{\partial r}\left(r\mu_t\frac{\partial \omega^2}{\partial r}\right) + C_2\rho\omega^2\left|\frac{\partial u}{\partial r}\right| + \frac{C_3\omega}{\rho}\left(\frac{\partial\rho}{\partial r}\right)\frac{\partial}{\partial r}\left(\rho k\right)$$

$$+ C_4\rho\omega^3$$

where:

$$C_1 = \frac{\alpha''}{A} \quad C_2 = \alpha' \quad C_3 = -A\gamma \quad C_4 = -\beta' \quad \gamma = 1$$

$$C_1 = \frac{A^{1/2}}{A} \quad C_2 = \beta'\alpha'' - 2k^2 \quad C_3 = -(0.09)^{1/2}(1) \quad C_4 = -5/3$$

$$C_1 = A^{-1/2} \quad C_2 = \frac{5}{3}(0.9)^{1/2} - 2(.41)^2$$

$$C_1 = (.09)^{-1/2} \quad C_2 = 0.1638 \quad C_3 = -0.3 \quad C_4 = -1.6667$$

$$C_1 = 3.33333 \quad C_2 = 0.1638 \quad C_3 = -0.3 \quad C_4 = 1.66667$$

Now define

$$z \equiv \omega^2$$

$$\boxed{\begin{aligned} \rho \frac{Dk}{Dt} &= \frac{1}{2r}\frac{\partial}{\partial r}\left(r\mu_t \frac{\partial k}{\partial r}\right) + C_1 z^{1/2}\mu_t \left|\frac{\partial u}{\partial r}\right| - \rho k z^{1/2} && (37) \\ \rho \frac{Dz}{Dt} &= \frac{1}{2r}\frac{\partial}{\partial r}\left(r\mu_t \frac{\partial z}{\partial r}\right) + C_2 \rho z \left|\frac{\partial u}{\partial r}\right| + \frac{C_3 z^{1/2}}{\rho}\left(\frac{\partial \rho}{\partial r}\right)\frac{\partial}{\partial r}(\rho k) \\ &\quad + C_4 \rho z^{3/2} && (38) \end{aligned}}$$

where
$$\mu_t = \frac{C_5 \rho k}{z^{1/2}}$$
and

$$C_5 = 0.09$$

Expanding (1) for a steady flow gives —

$$\rho u \frac{\partial k}{\partial x} + \rho v \frac{\partial k}{\partial r} = \frac{1}{2r}\frac{\partial}{\partial r}\left(r\mu_t \frac{\partial k}{\partial r}\right) + C_1 z^{1/2}\mu_t \left|\frac{\partial u}{\partial r}\right| - \rho k z^{1/2} \quad (39)$$

This equation can be transformed from $(x,r) \rightarrow (x,\psi)$ utilizing a transformation of dependent variables.

$$\psi \frac{\partial \psi}{\partial r} = \rho u r \tag{40}$$

$$\psi \frac{\partial \psi}{\partial x} = \rho v r \tag{41}$$

$$\left(\frac{\partial}{\partial r}\right)_x = \frac{\rho u r}{\psi} \left(\frac{\partial}{\partial \psi}\right)_x \tag{42}$$

$$\left(\frac{\partial}{\partial x}\right)_r = \left(\frac{\partial}{\partial x}\right)_\psi - \frac{\rho v r}{\psi} \left(\frac{\partial}{\partial \psi}\right)_x \tag{43}$$

utilizing (42) and (43) in (39)

$$\rho u \left\{ \frac{\partial k}{\partial x} - \cancel{\frac{\rho v r}{\psi} \frac{\partial k}{\partial \psi}} \right\} + \rho v \left\{ \cancel{\frac{\rho u r}{\psi} \frac{\partial k}{\partial \psi}} \right\} = \frac{1}{2r} \frac{\rho u r}{\psi} \frac{\partial}{\partial \psi} \left\{ r \mu_t \left[\frac{\rho u r}{\psi} \frac{\partial k}{\partial \psi} \right] \right\}$$

$$+ C_1 z^{1/2} \mu_t \left| \frac{\rho u r}{\psi} \frac{\partial u}{\partial \psi} \right| - \rho k z^{1/2}$$

$$\rho u \frac{\partial k}{\partial x} = \frac{\rho u}{2\psi} \frac{\partial}{\partial \psi} \left\{ \frac{\rho u r^2}{\psi} \mu_t \frac{\partial k}{\partial \psi} \right\} + C_1 \mu_t z^{1/2} \left| \frac{\rho u r}{\psi} \frac{\partial u}{\partial \psi} \right| - \rho k z^{1/2}$$

$$\frac{\partial k}{\partial x} = \frac{1}{2\psi} \frac{\partial}{\partial \psi} \left\{ \frac{\rho u r^2}{\psi} \mu_t \frac{\partial k}{\partial \psi} \right\} + C_1 \mu_t z^{1/2} \left| \frac{r}{\psi} \frac{\partial u}{\partial \psi} \right| - \frac{k z^{1/2}}{u} \tag{44}$$

Expanding (38) for steady flow gives —

$$\rho u \frac{\partial z}{\partial x} + \rho v \frac{\partial z}{\partial r} = \frac{1}{2r} \frac{\partial}{\partial r} \left(r \mu_t \frac{\partial z}{\partial r} \right)$$

$$+ C_2 \rho z \left| \frac{\partial u}{\partial r} \right| + \frac{C_3 z^{1/2}}{\rho} \left(\frac{\partial \rho}{\partial r} \right) \frac{\partial}{\partial r} \left(\rho k \right) + C_4 \rho z^{3/2} \tag{45}$$

utilizing (42) and (43) in (45) gives --

$$\rho u \left\{ \frac{\partial z}{\partial x} - \frac{\rho v r}{\psi} \frac{\partial z}{\partial \psi} \right\} + \rho v \left\{ \frac{\rho u r}{\psi} \frac{\partial z}{\partial \psi} \right\} = \frac{1}{2r} \frac{\rho u r}{\psi} \frac{\partial}{\partial \psi} \left\{ r \mu_t \left[\frac{\rho u r}{\psi} \frac{\partial z}{\partial \psi} \right] \right\}$$

$$+ C_2 \rho z \left| \frac{\rho u r}{\psi} \frac{\partial u}{\partial \psi} \right| + \frac{C_3 z^{\frac{1}{2}}}{\rho} \frac{\rho u r}{\psi} \frac{\partial \rho}{\partial \psi} \frac{\rho u r}{\psi} \frac{\partial}{\partial \psi} \left(\rho k \right) + C_4 \rho z^{3/2}$$

$$\rho u \frac{\partial z}{\partial x} = \frac{\rho u}{2\psi} \frac{\partial}{\partial \psi} \left\{ \frac{\rho u r^2}{\psi} \mu_t \frac{\partial z}{\partial \psi} \right\} + C_2 z \left| \frac{\rho^2 u r}{\psi} \frac{\partial u}{\partial \psi} \right|$$

$$+ C_3 z^{\frac{1}{2}} \frac{\rho u^2 r^2}{\psi^2} \left(\frac{\partial \rho}{\partial \psi} \right) \frac{\partial}{\partial \psi} \left(\rho k \right) + C_4 \rho z^{3/2}$$

since ρ is always positive. Dividing by ρu gives

$$\frac{\partial z}{\partial x} = \frac{1}{2\psi} \frac{\partial}{\partial \psi} \left\{ \frac{\rho u r^2 \mu_t}{\psi} \frac{\partial z}{\partial \psi} \right\} + \frac{C_2 z}{u} \left| \frac{\rho u r}{\psi} \frac{\partial u}{\partial \psi} \right|$$

$$+ C_3 z^{\frac{1}{2}} \frac{u r^2}{\psi^2} \left(\frac{\partial \rho}{\partial \psi} \right) \frac{\partial}{\partial \psi} \left(\rho k \right) + \frac{C_4 z^{3/2}}{u} \tag{46}$$

Hence, the turbulence model equations in the transformed plane are (44) and (46)

$$\boxed{\begin{aligned} \frac{\partial k}{\partial x} &= \frac{1}{2\psi} \frac{\partial}{\partial \psi} \left\{ \frac{\rho u r^2 \mu_t}{\psi} \frac{\partial k}{\partial \psi} \right\} + C_1 \mu_t z^{\frac{1}{2}} \left| \frac{r}{\psi} \frac{\partial u}{\partial \psi} \right| - \frac{k z^{\frac{1}{2}}}{u} && (44) \\ \frac{\partial z}{\partial x} &= \frac{1}{2\psi} \frac{\partial}{\partial \psi} \left\{ \frac{\rho u r^2 \mu_t}{\psi} \frac{\partial z}{\partial \psi} \right\} + \frac{C_2 z}{u} \left| \frac{\rho u r}{\psi} \frac{\partial u}{\partial \psi} \right| \\ &\quad + C_3 z^{\frac{1}{2}} \frac{u r^2}{\psi^2} \left(\frac{\partial \rho}{\partial \psi} \right) \frac{\partial}{\partial \psi} \left(\rho k \right) + \frac{C_4 z^{3/2}}{u} && (46) \end{aligned}}$$

where:

$$\mu_t = \frac{C_5 \rho k}{z^{\frac{1}{2}}}$$

$$z = \omega^2$$

$$C_5 = 0.09$$

and the other constants are as they appear on page 34. To account for the effects of compressibility, Saffman introduces an additional term into the k-equation. This is the last term in his equation given below

$$\bar{\rho} U \frac{\partial e}{\partial x} + \bar{\rho} V \frac{\partial e}{\partial y} = \alpha'' \bar{\rho} e \left| \frac{\partial U}{\partial y} \right| + \frac{1}{2} A \frac{\partial}{\partial y} \left(\frac{\bar{\rho} e}{\omega} \frac{\partial e}{\partial y} \right) - \bar{\rho} e \omega$$

$$- A\xi \frac{\gamma - 1}{\rho_1 a_1^2} \frac{\bar{\rho}^2 e^2}{\omega} \left(\frac{\partial U}{\partial y} \right)^2$$

where the subscript "1" in the last term refers to properties of the external stream. Rewriting this equation

$$\bar{\rho} U \frac{\partial e}{\partial x} + \bar{\rho} V \frac{\partial e}{\partial y} = \alpha'' \bar{\rho} e \left| \frac{\partial U}{\partial y} \right| + \frac{1}{2} \frac{\partial}{\partial y} \left(\frac{A \bar{\rho} e}{\omega} \frac{\partial e}{\partial y} \right)$$

$$- \xi \frac{(\gamma - 1)}{\rho_1 a_1^2} \bar{\rho} e \left\{ \frac{A \bar{\rho} e}{\omega} \right\} \left(\frac{\partial U}{\partial y} \right)^2 - \bar{\rho} e \omega \tag{47}$$

The turbulent eddy viscosity has been given previously by

$$\mu_t = A \frac{\bar{\rho} e}{\omega}$$

Substituting this into the previous equation gives

$$\bar{\rho} U \frac{\partial e}{\partial k} + \bar{\rho} V \frac{\partial e}{\partial y} = \alpha'' \bar{\rho} e \left| \frac{\partial U}{\partial y} \right| + \frac{1}{2} \frac{\partial}{\partial y} \left(\mu_t \frac{\partial e}{\partial y} \right)$$

$$- \xi \left(\frac{\gamma - 1}{\rho_1 a_1^2} \right) \left(\bar{\rho} e \right) \mu_t \left(\frac{\partial U}{\partial y} \right)^2 - \bar{\rho} e \omega \tag{48}$$

Now if we utilize the notation that the turbulent kinetic energy is given by k, Equation (48) becomes

$$\bar{\rho}U \frac{\partial k}{\partial x} + \bar{\rho}V \frac{\partial k}{\partial y} = \frac{1}{2} \frac{\partial}{\partial y} \left(\mu_t \frac{\partial k}{\partial y}\right) + \alpha'' \bar{\rho} k \left|\frac{\partial U}{\partial y}\right|$$
$$- \bar{\rho} k \omega - \xi \left(\frac{\gamma - 1}{\rho_1 a_1^2}\right) \left(\bar{\rho} k\right) \mu_t \left(\frac{\partial U}{\partial y}\right)^2 \tag{49}$$

where as before $k \equiv e$

writing this equation in terms of the substantial derivative

$$\bar{\rho} \frac{Dk}{Dt} = \frac{1}{2} \frac{\partial}{\partial y} \left(\mu_t \frac{\partial k}{\partial y}\right) + \alpha'' \bar{\rho} k \left|\frac{\partial U}{\partial y}\right|$$
$$- \bar{\rho} k \omega - \xi \left(\frac{\gamma - 1}{\rho_1 a_1^2}\right) \left(\bar{\rho} k \mu_t\right) \left(\frac{\partial U}{\partial y}\right)^2 \tag{50}$$

Now for a perfect gas, the sonic velocity of the external stream, a_1 is given by

$$a_1^2 = \gamma R T_1 = \frac{\gamma p_1}{\rho_1}$$

Also for a perfect gas

$$C_p - C_v = R$$

and

$$1 - \frac{1}{\gamma} = \frac{R}{C_p}$$

$$\frac{\gamma - 1}{\gamma} = \frac{R}{C_p}$$

Utilizing these two relations

$$\frac{\gamma - 1}{\rho_1 a_1^{\,2}} = \left(\frac{\gamma - 1}{\gamma}\right)\left(\frac{1}{a_1^{\,2}}\right)\left(\frac{\gamma}{\rho_1}\right)$$

$$= \frac{R_1}{C_{p_1}} \; \frac{\rho_1}{\gamma p_1} \; \frac{\gamma}{\rho_1}$$

$$= \frac{R_1}{C_{p_1} p_1}$$

$$\frac{\gamma - 1}{\rho_1 a_1^{\,2}} = \frac{\bar{R}}{MW_1 C_{p_1} p_1} \tag{51}$$

Where the subscript 1 refers to the external stream. Utilizing this relation *(51)* in *(50)* above leads to

$$\bar{\rho} \frac{Dk}{Dt} = \frac{1}{2} \frac{\partial}{\partial y}\left(\mu_t \frac{\partial k}{\partial y}\right) + \alpha'' \bar{\rho} k \left|\frac{\partial U}{\partial y}\right| - \bar{\rho} k \omega$$

$$- \xi \left\{\frac{\bar{R}}{MW_{ex} C_{p_{ex}} p_{ex}}\right\} \bar{\rho} k \mu_t \left(\frac{\partial U}{\partial y}\right)^2 \tag{52}$$

Transforming this equation to cylindrical coordinates

$$\bar{\rho} \frac{Dk}{Dt} = \frac{1}{2r} \frac{\partial}{\partial r}\left(r \mu_t \frac{\partial k}{\partial r}\right) + \alpha'' \bar{\rho} k \left|\frac{\partial U}{\partial r}\right| - \bar{\rho} k \omega$$

$$- \xi \left\{\frac{\bar{R}}{MW_{ex} C_{p_{ex}} p_{ex}}\right\} \bar{\rho} k \mu_t \left(\frac{\partial U}{\partial r}\right)^2 \tag{53}$$

Now if we define

$$z \equiv \omega^2 \tag{54}$$

and drop the mean value notation (53) becomes --

$$\rho \frac{Dk}{Dt} = \frac{1}{2r} \frac{\partial}{\partial r}\left(r\mu_t \frac{\partial k}{\partial r}\right) + \alpha'' \rho k \left|\frac{\partial u}{\partial r}\right| - \rho k z^{\frac{1}{2}}$$

$$- \xi \left\{\frac{\bar{R}}{MW_{ex} C_{pex} P_{ex}}\right\} \rho k \mu_t \left(\frac{\partial u}{\partial r}\right)^2 \tag{55}$$

where

$$\mu_t = \frac{A\rho k}{\omega} = \frac{A\rho k}{z^{\frac{1}{2}}} \tag{56}$$

Utilizing (56) the second term on the right hand side (RHS) of (55) becomes

$$\alpha'' \rho k \left|\frac{\partial u}{\partial r}\right| = \alpha'' \left|\frac{\partial u}{\partial r}\right| \frac{\mu_t z^{\frac{1}{2}}}{A} \tag{57}$$

$$\alpha'' \rho k \left|\frac{\partial u}{\partial r}\right| = \frac{\alpha''}{A} z^{\frac{1}{2}} \mu_t \left|\frac{\partial u}{\partial r}\right|$$

Substituting (57) back into (56)

$$\rho \frac{Dk}{Dt} = \frac{1}{2r} \frac{\partial}{\partial r}\left(r\mu_t \frac{\partial k}{\partial r}\right) + \frac{\alpha''}{A} z^{\frac{1}{2}} \mu_t \left|\frac{\partial u}{\partial r}\right| \tag{58}$$

$$- \rho k z^{\frac{1}{2}} - \xi \left\{\frac{\bar{R}}{MW_{ex} C_{pex} P_{ex}}\right\} \rho k \mu_t \left(\frac{\partial u}{\partial r}\right)^2$$

Hence, if we let

$$C_1 \equiv \frac{\alpha''}{A} = \frac{A^{\frac{1}{2}}}{A} = A^{-\frac{1}{2}} = 0.09^{-\frac{1}{2}} = 3.33333$$

$$C_6 \equiv \xi = 2.5$$

Equation (58) becomes

$$\boxed{\rho \frac{Dk}{Dt} = \frac{1}{2r}\frac{\partial}{\partial r}\left(r\mu_t \frac{\partial k}{\partial r}\right) + C_1 z^{\frac{1}{2}}\mu_t \left|\frac{\partial u}{\partial r}\right| - \rho k z^{\frac{1}{2}} - \frac{C_6 \bar{R}\rho k \mu_t}{MW_{ex} C_{pex} P_{ex}}\left(\frac{\partial u}{\partial r}\right)^2} \tag{59}$$

Where (59) differs from (47) in the previous formulation only by the last term.

Expanding (59) for a steady flow gives

$$\rho u \frac{\partial k}{\partial x} + \rho v \frac{\partial k}{\partial r} = \frac{1}{2r}\frac{\partial}{\partial r}\left(r\mu_t \frac{\partial k}{\partial r}\right) + C_1 z^{\frac{1}{2}}\mu_t \left|\frac{\partial u}{\partial r}\right| - \rho k z^{\frac{1}{2}} - \frac{C_6 \bar{R}\rho k \mu_t}{MW_e C_{pe} P_e}\left(\frac{\partial u}{\partial r}\right)^2 \tag{60}$$

Now (60) can be transformed from $(x,r) \rightarrow (x,\psi)$ using the transformation of dependent variable

$$\left(\frac{\partial}{\partial r}\right)_x = \frac{\rho u r}{\psi}\left(\frac{\partial}{\partial \psi}\right)_x \tag{61}$$

$$\left(\frac{\partial}{\partial x}\right)_r = \left(\frac{\partial}{\partial x}\right)_\psi - \frac{\rho v r}{\psi}\left(\frac{\partial}{\partial \psi}\right)_x \tag{62}$$

Utilizing (61) and (62) in (60)

$$\begin{aligned} \rho u \left\{\frac{\partial k}{\partial x} - \cancel{\frac{\rho v r}{\psi}\frac{\partial k}{\partial \psi}}\right\} + \rho v \left\{\cancel{\frac{\rho u r}{\psi}\frac{\partial k}{\partial \psi}}\right\} \\ = \frac{1}{2r}\frac{\rho u r}{\psi}\frac{\partial}{\partial \psi}\left(r\mu_t \frac{\rho u r}{\psi}\frac{\partial k}{\partial \psi}\right) + C_1 z^{\frac{1}{2}}\mu_t \left|\frac{\rho u r}{\psi}\frac{\partial u}{\partial \psi}\right| \\ - \rho k z^{\frac{1}{2}} - \frac{C_6 \bar{R}\rho k \mu_t}{MW_e C_{pe} P_e}\frac{\rho^2 u^2 r^2}{\psi^2}\left(\frac{\partial u}{\partial \psi}\right)^2 \end{aligned} \tag{63}$$

$$\rho u \frac{\partial k}{\partial x} = \frac{\rho u}{2\psi}\frac{\partial}{\partial \psi}\left(\frac{\rho u r}{\psi}^{2} \mu_t \frac{\partial k}{\partial \psi}\right) + C_1 z^{\frac{1}{2}} \mu_t \left|\frac{\rho u r}{\psi}\left(\frac{\partial u}{\partial \psi}\right)\right|$$

$$- \rho k z^{\frac{1}{2}} - \frac{C_6 \bar{R} \rho^3 k \mu_t u^2 r^2}{MW_e C_{pe} P_e \psi^2} \left(\frac{\partial u}{\partial \psi}\right)^2 \tag{64}$$

Since ρu always > 0 for the shear flows considered here

$$\boxed{\begin{aligned} \frac{\partial k}{\partial x} &= \frac{1}{2\psi}\frac{\partial}{\partial \psi}\left(\frac{\rho u r^2}{\psi} \mu_t \frac{\partial k}{\partial \psi}\right) + C_1 z^{\frac{1}{2}} \mu_t \left|\frac{r}{\psi}\left(\frac{\partial u}{\partial \psi}\right)\right| \\ &- \frac{k z^{\frac{1}{2}}}{u} - \frac{C_6 \bar{R} \rho^2 k \mu_t u r^2}{MW_e C_{pe} P_e \psi^2} \left(\frac{\partial u}{\partial \psi}\right)^2 \end{aligned}} \tag{65}$$

Where it will be noted that (65) differs from (54) only in the addition of the last term

From Equations (65) and (56) —

$$\frac{\partial k}{\partial x} = \frac{1}{2\psi}\frac{\partial}{\partial \psi}\left\{\frac{\rho u r^2 \mu_t}{\psi} \frac{\partial k}{\partial \psi}\right\} + C_1 \mu_t z^{\frac{1}{2}} \left|\frac{r}{\psi}\frac{\partial u}{\partial \psi}\right| - k\frac{z^{\frac{1}{2}}}{u}$$

$$- \frac{C_6 \bar{R} \rho^2 k u r^2 \mu_t}{C_{p_2} MW_2 P_2 \psi^2} \left(\frac{\partial u}{\partial \psi}\right)^2 \tag{66}$$

$$\frac{\partial z}{\partial x} = \frac{1}{2\psi}\frac{\partial}{\partial \psi}\left\{\frac{\rho u r^2 \mu_t}{\psi} \frac{\partial z}{\partial \psi}\right\} + \frac{C_2 z^2}{u}\left|\frac{\rho u r}{\psi} \frac{\partial u}{\partial \psi}\right| + C_3 z^{\frac{1}{2}} \frac{u r^2}{\psi^2}\left(\frac{\partial \rho}{\partial \psi}\right)$$

$$\frac{\partial}{\partial \psi}(\rho k) + \frac{C_4 z^{3/2}}{u} \tag{67}$$

where the subscripts "2" and "ex" are synonomous. Now let $A \equiv (\mu_t + \rho u r^2)/\psi$ and utilize the following finite difference formulation

$$\frac{\partial}{\partial\psi}\left(a\frac{\partial f}{\partial\psi}\right) = a_{n,m+\frac{1}{2}}\frac{\left(f_{n,m+1}-f_{n,m}\right)}{\left(\Delta\psi\right)^2}$$

$$- a_{n,m-\frac{1}{2}}\frac{\left(f_{n,m}-f_{n,m-1}\right)}{\left(\Delta\psi\right)^2}$$

Where:

$$a_{n,m+\frac{1}{2}} = \frac{a_{n,m}+a_{n,m+1}}{2}$$

$$a_{n,m-\frac{1}{2}} = \frac{a_{n,m}+a_{n,m-1}}{2}$$

$$\left(\frac{\partial f}{\partial\psi}\right)_{n,m} = \frac{f_{n,m+1}-f_{n,m-1}}{2\Delta\psi} \quad (68)$$

Utilizing these formulas in (66)

$$\Delta k_{n,m} =$$

$$\frac{\Delta x}{2\psi_{n,m}}\left[\frac{A_{n,m+\frac{1}{2}}\left\{k_{n,m+1}-k_{n,m}\right\}-A_{n,m-\frac{1}{2}}\left\{k_{n,m}-k_{n,m-1}\right\}}{\left(\Delta\psi\right)^2}\right.$$

$$+ C_1\mu_t z^{\frac{1}{2}}_{n,m}\,\Delta x\left|\frac{r}{\psi_{n,m}}\quad\frac{u_{n,m+1}-u_{n,m-1}}{2\Delta\psi}\right|$$

$$-\frac{k_{n,m}\,z^{\frac{1}{2}}_{n,m}}{u_{n,m}}\Delta x - \frac{C_6\,\bar{R}\rho^2 k_{n,m}u_{n,m}r^2\mu_t}{C_{p2}\,MW_2\,P_2\psi^2_{n,m}}\Delta x$$

$$\left\{\frac{u_{n,m+1}-u_{n,m-1}}{2\Delta\psi}\right\}^2$$

and

$$k_{n+1,\,m} = k_{n,m} + \frac{\Delta x}{2\psi_{n,m}(\Delta\psi)^2}$$

$$\left\{A_{n,m+\frac{1}{2}}\left[k_{n,m+1} - k_{n,m}\right] - A_{n,m-\frac{1}{2}}\left[k_{n,m} - k_{n,m-1}\right]\right\}$$

$$+ C_1\mu_t\Delta x\, z^{\frac{1}{2}}_{n,m}\left|\frac{r}{2\psi_{n,m}\Delta\psi}\left\{u_{n,m+1} - u_{n,m-1}\right\}\right| - \frac{k_{n,m}\, z^{\frac{1}{2}}_{n,m}\Delta x}{u_{n,m}}$$

$$- \frac{C_6\bar{R}\rho^2 k_{n,m}u_{n,m}r^2\mu_t\ \Delta x}{4C_{p2}MW_2P_2\psi^2_{n,m}(\Delta\psi)^2}\left\{u_{n,m+1} - u_{n,m-1}\right\}^2 \qquad (69)$$

Utilizing the same difference formulas for equation (67)

$$\Delta z_{n,m} = \frac{\Delta x}{2\psi_{n,m}\Delta\psi^2}\Bigg\langle A_{n,m+\frac{1}{2}}\left\{z_{n,m+1} - z_{n,m}\right\}$$

$$- A_{n,m-\frac{1}{2}}\left\{z_{n,m} - z_{n-1,\,m}\right\}$$

$$+ \frac{C_2 z_{n,m}\Delta x}{u_{n,m}}\left|\frac{\rho u_{n,m}r}{\psi_{n,m}}\left(\frac{u_{n,m+1} - u_{n,\,m-1}}{2\Delta\psi}\right)\right|$$

$$+ \frac{C_3 z^{\frac{1}{2}}_{n,m}u_{n,m}r^2\Delta x}{\psi^2_{n,m}}\left\{\frac{\rho_{n,m+1} - \rho_{n,m-1}}{2\Delta\psi}\right\}$$

$$\Bigg[\mu_{n,m}\left\{\frac{k_{n,m+1} - k_{n,m-1}}{2\Delta\psi}\right\}$$

$$+ k_{n,m}\left\{\frac{\rho_{n,m+1} - \rho_{n,m-1}}{2\Delta\psi}\right\}\Bigg]\Bigg\rangle + \frac{C_4\ z^{3/2}_{n,m}\ \Delta x}{u_{n,m}} \qquad (70)$$

and

$$
\begin{aligned}
z_{n+1,m} = z_{n,m} &+ \frac{\Delta x}{2\psi_{n,m}(\Delta\psi)^2}\Big\{A_{n,m+\frac{1}{2}}\left[z_{n,m+1} - z_{n,m}\right] \\
&- A_{n,m-\frac{1}{2}}\left[z_{n,m} - z_{n,m-1}\right]\Big\} + \frac{C_2 z_{n,m}\Delta x}{u_{n,m}}\Bigg|\frac{\rho u_{n,m} r}{\psi_{n,m}} \\
&\left[\frac{u_{n,m+1} - u_{n,m-1}}{2(\Delta\psi)}\right]\Bigg| + \frac{C_3 z_{n,m}^{\frac{1}{2}} u_{n,m} r^2 \Delta x}{4\psi_{n,m}^2(\Delta\psi)^2}\Big\{\rho_{n,m+1} \\
&- \rho_{n,m-1}\Big\}\Big[\rho_{n,m}\left\{k_{n,m+1} - k_{n,m-1}\right\} \\
&+ k_{n,m}\left\{\rho_{n,m+1} - \rho_{n,m-1}\right\}\Big] + \frac{C_4 z_{n,m}^{\frac{3}{2}}\Delta x}{u_{n,m}}
\end{aligned}
\tag{71}
$$

and finally

$$
\boxed{
\begin{aligned}
z_{n+1,m} = z_{n,m} &+ \frac{\Delta x}{2\psi_{n,m}(\Delta\psi)^2}\Big\{A_{n,m+\frac{1}{2}}\Big[z_{n,m+1} \\
&- z_{n,m}\Big] - A_{n,m-\frac{1}{2}}\left[z_{n,m} - z_{n,m-1}\right]\Big\} \\
&+ \frac{C_2 z_{n,m}\Delta x}{u_{n,m}}\left|\rho\frac{u_{n,m} r}{2\psi_{n,m}(\Delta\psi)}\left\{u_{n,m+1} - u_{n,m-1}\right\}\right| \\
&+ \frac{C_3 z_{n,m}^{\frac{1}{2}} u_{n,m} r^2 \Delta x}{4\psi_{n,m}^2(\Delta\psi)^2}\left\{\rho_{n,m+1} - \rho_{n,m-1}\right\} \\
&\Big[\rho_{n,m}\left\{k_{n,m+1} - k_{n,m-1}\right\} + k_{n,m}\Big\{\rho_{n,m+1} \\
&- \rho_{n,m-1}\Big\}\Big] + \frac{C_4 z_{n,m}^{\frac{3}{2}}\Delta x}{u_{n,m}}
\end{aligned}
}
\tag{72}
$$

Hence equations (69) and (72) are utilized to calculate the changes in k and z along the marching direction at mesh points inside the calculational field. However, special treatment of these equations is necessary along the axis of the flow as shown below.

The turbulent kinetic energy equation is given by (73)

$$\frac{\partial k}{\partial x} = \frac{1}{2\psi} \frac{\partial}{\partial \psi} \left\{ \frac{\rho u r^2 \mu_t}{\psi} \frac{\partial k}{\partial \psi} \right\} + C_1 \mu_t z^{\frac{1}{2}} \left| \frac{r}{\psi} \frac{\partial u}{\partial \psi} \right| - \frac{k z^{\frac{1}{2}}}{u} \tag{73}$$

Now along the axis $r = \psi = 0$

$$\frac{\partial k}{\partial \psi} = \frac{\partial u}{\partial \psi} = 0$$

Hence, the first and second terms on the RHS of (73) must be evaluated along the axis since these terms are indefinite.

The first term is

$$\frac{1}{2\psi} \frac{\partial}{\partial \psi} \left\{ \frac{\rho u r^2 \mu_t}{\psi} \frac{\partial k}{\partial \psi} \right\} \tag{76}$$

Define

$$\xi \equiv \frac{\psi^2}{2} \qquad R \equiv \frac{r^2}{2}$$

Then $d\xi = \psi d\psi \qquad dR = rdr$

From (69)

$$\psi \frac{\partial \psi}{\partial r} = \rho u r$$

and

$$\psi \partial \psi = \rho u r \partial r$$

$$d\xi = \rho u dR$$

and

$$\frac{dR}{d\xi} = \frac{1}{\rho u}$$

Hence, [illegible] becomes

$$\frac{1}{\partial\xi} \left\{ \frac{\rho u r^2 \mu_t}{2} \frac{\partial k}{\partial r} \frac{\partial r}{\partial\psi} \right\} \frac{\partial\xi}{\partial\psi}$$

$$= \frac{1}{\partial\xi} \left\{ \frac{\rho u r^2 \mu_t}{2} \frac{\partial k}{\partial\psi} \right\}$$

$$= \frac{\partial}{\partial\xi} \left\{ \frac{\rho u r^2 \mu_t}{2} \frac{\partial k}{\partial\xi} \right\}$$

$$= \frac{\partial}{\partial\xi} \left\{ \rho u R \mu_t \frac{\partial k}{\partial\xi} \right\}$$

Differentiating

$$R \frac{\partial}{\partial\xi} \left\{ \rho u \mu_t \frac{\partial k}{\partial\xi} \right\} + \left\{ \rho u \mu_t \frac{\partial k}{\partial\xi} \right\} \frac{\partial R}{\partial\xi}$$

Taking the limit as $r \to o$

$$= R \frac{\partial}{\partial\xi} \left\{ \rho u \mu_t \frac{\partial k}{\partial\xi} \right\} + \left\{ \rho u \mu_t \frac{\partial k}{\partial\xi} \right\} \frac{1}{\rho u}$$

$$= \mu_t \frac{\partial k}{\partial\xi} = \mu_t \frac{\partial k}{\partial\psi} \frac{\partial\psi}{\partial\xi} = \frac{\mu_t}{\psi} \frac{\partial k}{\partial\psi}$$

now using L'Hospital's rule

$$h(\psi) = \frac{f(\psi)}{g(\psi)} = \frac{\mu_t \frac{\partial k}{\partial\psi}}{\psi}$$

$$\frac{f'(\psi)}{g'(\psi)} = \frac{\frac{\partial}{\partial\psi}\left(\mu_t \frac{\partial k}{\partial\psi}\right)}{1} = \mu_t \frac{\partial^2 k}{\partial\psi^2} + \frac{\partial k}{\partial\psi} \frac{\partial\mu_t}{\partial\psi}$$

$$\lim_{\psi \to 0}$$

but

$$\lim_{\psi \to 0} \frac{\partial k}{\partial \psi} = 0$$

Therefore the first term becomes

$$\mu_t \frac{\partial^2 k}{\partial \psi^2}$$

The second term is given by

$$C_1 \mu_t z^{\frac{1}{2}} \left| \frac{r}{\psi} \frac{\partial u}{\partial \psi} \right|$$

Applying L'Hospital's rule to a portion of this term gives

$$h(\psi) = \frac{f(\psi)}{g(\psi)} = \frac{r \frac{\partial u}{\partial \psi}}{\psi}$$

$$\lim_{\psi \to 0} \frac{f'(\psi)}{g'(\psi)} = \frac{r \frac{\partial^2 u}{\partial \psi^2} + \frac{\partial u}{\partial \psi} \frac{\partial r}{\partial \psi}}{1}$$

Now taking the limit as r → o; $\frac{\delta u}{\delta \psi}$ → o and hence the second term → o. The third term is unaffected by the limit process and we have

$$\boxed{\frac{\partial k}{\partial x} = \mu_t \frac{\partial^2 k}{\partial \psi^2} - \frac{k z^{\frac{1}{2}}}{u}} \qquad \text{Along the axis} \qquad (77)$$

The z equation is given by (75)

$$\frac{\partial z}{\partial x} = \frac{1}{2\psi}\frac{\partial}{\partial\psi}\left\{\frac{\rho u r^2 \mu_t}{\psi}\frac{\partial z}{\partial\psi}\right\} + \frac{C_2 z}{u}\left|\frac{\rho u r}{\psi}\frac{\partial u}{\partial\psi}\right|$$

$$+ C_3 z^{1/2}\frac{ur^2}{\psi^2}\left(\frac{\partial\rho}{\partial\psi}\right)\frac{\partial}{\partial\psi}(\rho k) + \frac{C_4 z^{3/2}}{u} \tag{75}$$

The first two terms on the RHS of (75) are analogous to the first two terms on the RHS of (74), and are evaluated analogously. Hence looking at the third term

$$C_3 z^{1/2}\frac{ur^2}{\psi^2}\left(\frac{\partial\rho}{\partial\psi}\right)\frac{\partial}{\partial\psi}(\rho k) \tag{78}$$

$$\lim r = \psi \rightarrow o$$

Making the same substitution as before, define

$$\xi = \frac{\psi^2}{2}$$

then $\frac{d\xi}{d\psi} = \psi$

and the third term (78) becomes

$$C_3 z^{1/2}\frac{ur^2}{\psi^2}\left(\frac{\partial\rho}{\partial\xi}\right)\frac{\partial\xi}{\partial\psi}\left[\frac{\partial}{\partial\xi}(\rho k)\frac{\partial\xi}{\partial\psi}\right]$$

$$C_3 z^{1/2}\frac{ur^2}{\psi^2}\left(\frac{\partial\rho}{\partial\xi}\right)\psi\left[\frac{\partial}{\partial\xi}(\rho k)\ \psi\right]$$

and taking the limit as $r \to o$

$$\lim_{r \to 0} \; C_3 z^{\frac{1}{2}} u r^2 \left(\frac{\partial \rho}{\partial \xi}\right) \frac{\partial}{\partial \xi} (\rho k) = 0$$

The fourth term remains as is and the z-equation along the axis becomes --

$$\boxed{\frac{\partial z}{\partial x} = \mu_t \frac{\partial^2 z}{\partial \psi^2} + C_4 \frac{z^{3/2}}{u}} \qquad \text{Along the axis} \tag{79}$$

Hence, evaluation of the turbulence model equations for the case when $r = o$ along the axis becomes according to (77) and (78)

$$\boxed{\begin{aligned} \frac{\partial k}{\partial x} &= \mu_t \frac{\partial^2 k}{\partial \psi^2} - \frac{k z^{\frac{1}{2}}}{u} \\ \frac{\partial z}{\partial x} &= \mu_t \frac{\partial^2 z}{\partial \psi^2} + C_4 \frac{z^{3/2}}{u} \end{aligned}}$$

Now when compressibility effects are important the last term in the k-equation must also be evaluated along the axis

$$\frac{C_6 \bar{R} \rho^2 k u r^2 \mu_t}{MW_2 C_{p_2} P_2 \psi^2} \left(\frac{\partial u}{\partial \psi}\right)^2 \tag{80}$$

Investigate this term in the limit as

$$r \to 0 \qquad \psi \to 0$$

$$\frac{\partial k}{\partial \psi} \to 0 \qquad \frac{\partial u}{\partial \psi} \to 0$$

Rewrite (80) as

$$\frac{B}{\psi}\left(\frac{\partial u}{\partial \psi}\right)^2 \tag{81}$$

where

$$B = \frac{C_6 \bar{R}\rho^2 k u r^2 \mu_t}{MW_2 C_{p_2} p_2 \psi}$$

Then using L'Hospital's rule to (81)

$$h(\psi) = \frac{f(\psi)}{g(\psi)} = \frac{B\left(\frac{\partial u}{\partial \psi}\right)^2}{\psi}$$

$$\frac{f'(\psi)}{g'(\psi)} = \frac{2B\left(\frac{\partial u}{\partial \psi}\right)\left(\frac{\partial^2 u}{\partial \psi^2}\right) + \left(\frac{\partial u}{\partial \psi}\right)^2\left(\frac{\partial B}{\partial \psi}\right)}{1}$$

$$= 0$$

Hence in the limit as $r \to o$ this term adds nothing.

Therefore equations (69) and (72) for field mesh points and (84) and (85) for points along the axis determine the turbulence kinetic energy and the pseudo vorticity in the shear layer.

This formulation was coded and added to the BOAT portion of the SPF code now under development. These coding changes were input via an update to the main code and are detailed in Appendix B.

The TKE equations along the axis are

$$\frac{\partial k}{\partial x} = \mu_t \frac{\partial^2 k}{\partial \psi^2} - \frac{k z^{\frac{1}{2}}}{u} \tag{82}$$

$$\frac{\partial z}{\partial x} = \mu_t \frac{\partial^2 z}{\partial \psi^2} + C_4 \frac{z^{3/2}}{u} \tag{83}$$

$$\frac{\partial^2 f}{\partial \psi^2} = \frac{f_{n,m+1} - 2f_{n,m} + f_{n,m-1}}{\Delta\psi^2}$$

Since $f_{n-1,m}$ does not exist, assume

$$f_{n,m-1} = f_{n,m}$$

then

$$\frac{\partial^2 f}{\partial \psi^2} = \frac{f_{n,m+1} - f_{n,m}}{(\Delta\psi)^2}$$

and for the special case along the axis

$$\left.\frac{\partial^2 f}{\partial \psi^2}\right|_{r=0} = \frac{f_{n,2} - f_{n,1}}{(\Delta\psi)^2}$$

Therefore, equation (82) becomes

$$\Delta k_{n,m} = \frac{\mu_t \Delta x}{(\Delta\psi)^2}\left(k_{n,2} - k_{n,1}\right) - \frac{k_{n,1}\, z^{1/2}_{n,1}\, \Delta x}{u_{n,1}}$$

So that

$$\boxed{k_{n+1,1} = k_{n,1} + \frac{\mu_t \Delta x}{(\Delta\psi)^2}\left(k_{n,2} - k_{n,1}\right) - \frac{\Delta x\, k_{n,1} z^{1/2}_{n,1}}{u_{n,1}}} \tag{84}$$

Along the axis

and likewise

$$\boxed{z_{n+1,1} = z_{n,1} + \frac{\mu_t \Delta x}{(\Delta\psi)^2}\left(z_{n,2} - z_{n,1}\right) - C_4 \frac{\Delta x \; z_{n,1}^{3/2}}{u_{n,1}}} \tag{85}$$

Along the axis

V. NON-REACTING SHEAR LAYER COMPARISON

In order to evaluate the various turbulence mixing models, predictions were made corresponding to the careful experimental measurements made by Brown and Roshko [1] over an extended period of time. The experiments were made in a laboratory utilizing a splitter plate separating two 4 x 1-inch 2-D nozzles. The principal aim of this experimental work was to investigate the effect of density differences between the two mixing layers. This was accomplished experimentally by using various mixtures of He and N_2. Ar was also used in some rare instances. These two streams were turbulent with the Re number $\frac{U_\infty x}{\nu}$ in the range of $\approx 10^6$. The experimental device was run at low speeds in the range of $\approx$ 50 fps. Freestream velocity and density ratios on the order of $\approx$ 7 were run experimentally. This work showed that the large structure existed over all the density ranges tested.

Predictions were made for all the experimental runs made by Brown and Roshko and are presented subsequently. Velocity and density profiles were calculated as a function of y (x-x_0) where x_0 is the virtual origin of the shear layer and y is the distance above or below the dividing streamline. The dividing streamline was located utilizing a numerical integration scheme. The details and limitations of this calculation is given in Appendix A.

In addition to the velocity and density profiles that were compared for the data of Brown and Roshko, the growth of the shear layer as a function of velocity ratio was compared. As a basis for this comparison, they used the velocity profile maximum slope thickness and its derivative

$$\delta_\omega = \frac{U_j - U_e}{\left(\frac{\partial U}{\partial y}\right)_{max}} \tag{86}$$

$$\delta'_\omega = \frac{d\delta\omega}{dx} = \frac{\delta\omega}{x - x_o}$$

or

$$\delta'_\omega = \frac{U_j - U_e}{\left(\frac{\partial U}{\partial y}\right)_{max} (x - x_o)} \qquad (87)$$

Equation (87) was used for the comparison.

Results comparing the shear layer flow utilizing the two turbulence kinetic energy models with experimental data are shown in *Figure 9*. This is a comparison of the constant density air/air case with a jet velocity of 32.8 feet/second and an external stream velocity of 4.7 feet/second. The flow was at a constant pressure of 102.9 psia.

Note that the agreement between theory and experiment is very good for both the kϵ2 and the kω' turbulence models. The shear width agreement is excellent and velocity profile slope is very good. The kϵ2 model shows a little better agreement with the slope while the kω' model shows a slightly better shear width agreement. Overall it can be said that the agreement with both is very good.

The next comparison made was another constant density air/air case for which the pressure was maintained constant at 102.9 psia. For this case, the jet velocity was held at 32.8 feet/second while the external stream velocity was increased to 12.5 feet/second. This comparison is shown in *Figure 10*.

Note that the agreement between theory and experiment is again pretty good for both turbulence models. The slope is reasonable for both and the width of the shear layer is approximately the same for both. The kω' model falls closer to the actual data than does the kϵ2 model.

Hence, for the constant density turbulent 2-D shear layer, the turbulence prediction models are doing reasonably well at predicting the growth and velocity profiles.

In order to evaluate shear layer flows, where multiple species are involved such as for the He/N_2 experiments, it is necessary to know the value of the turbulent Prandtl number. This

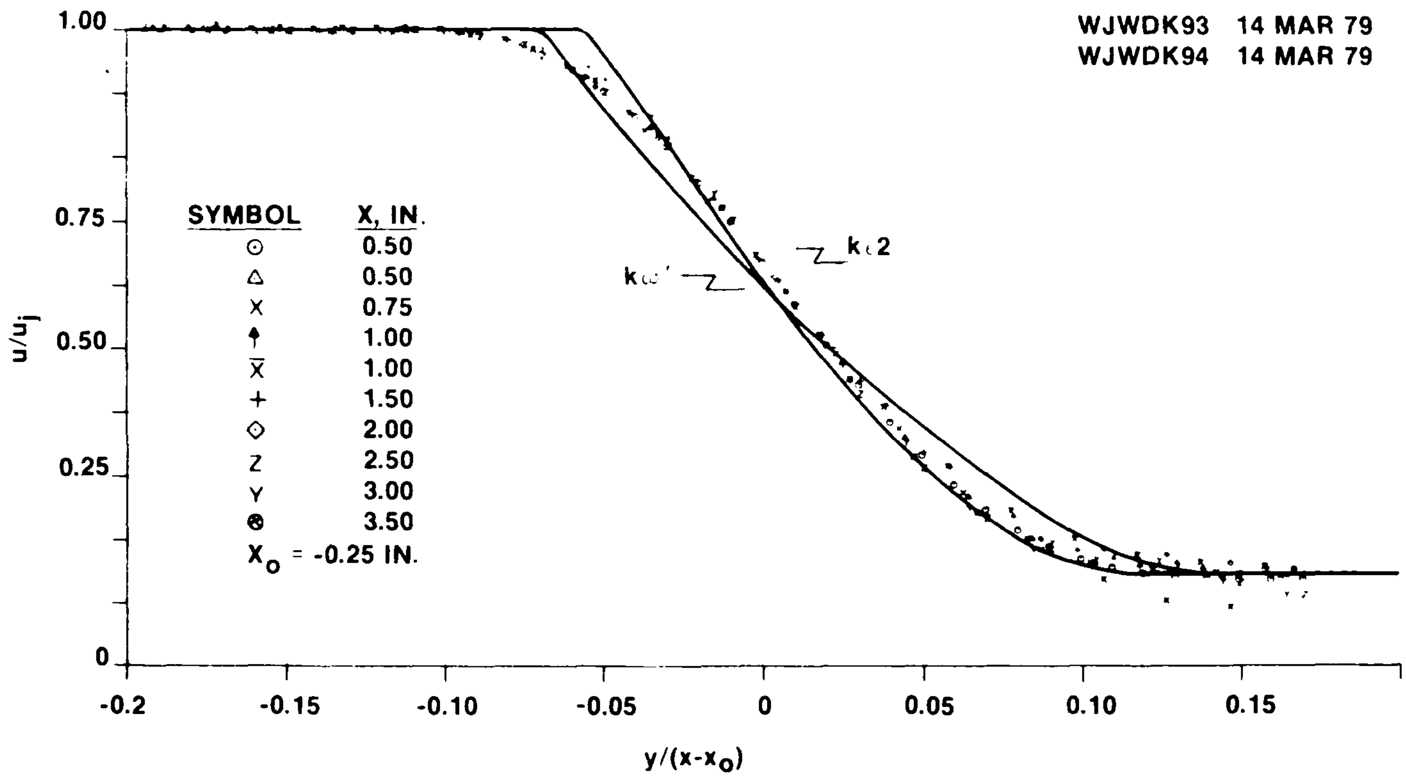

Figure 9. Velocity profile comparison for air/air shear layer - Table 6, case number I.

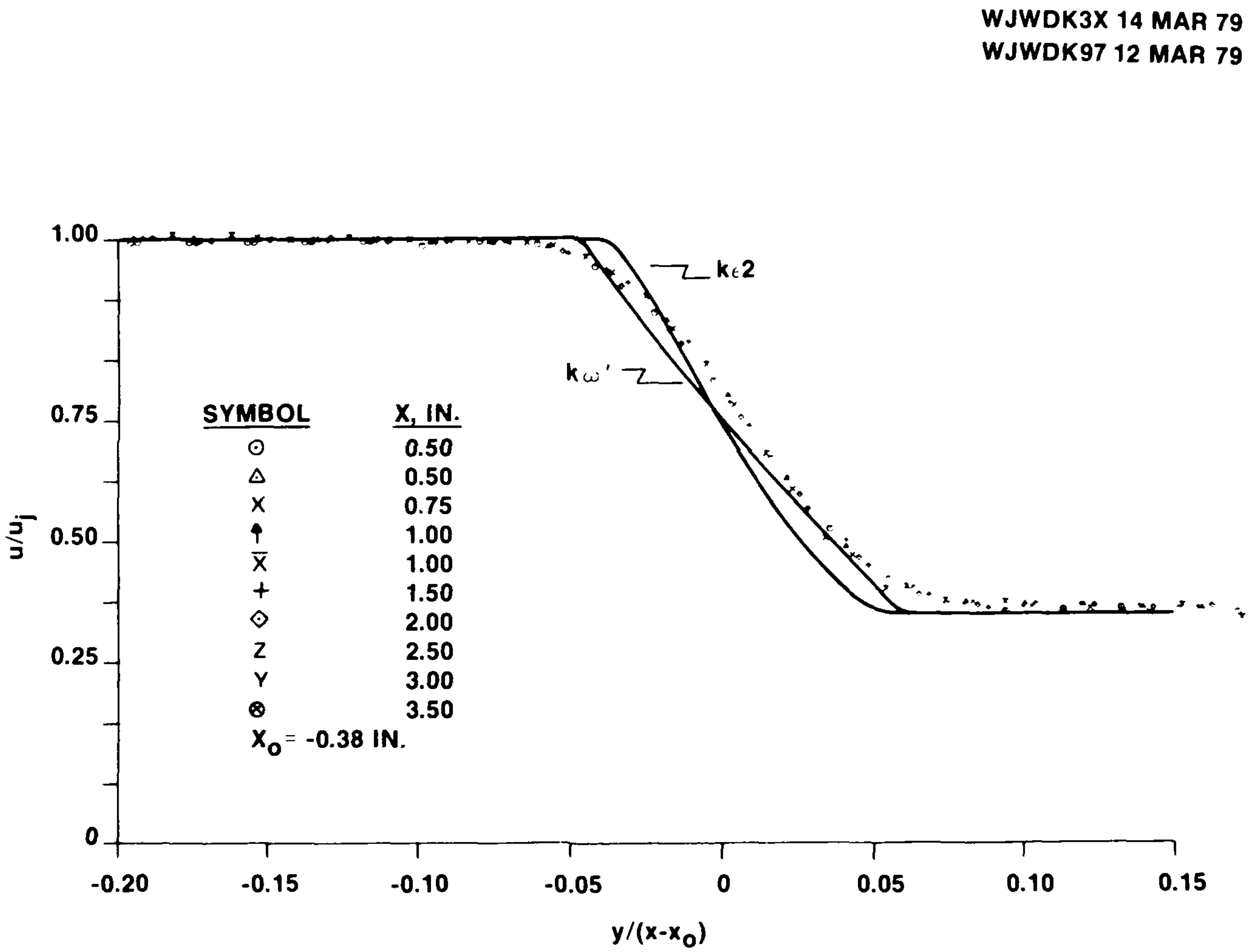

Figure 10. Velocity profile comparison for air/air shear layer - Table 6 case number II.

parameter arises in the governing differential equations to account for differences between the velocity profile and the specie profiles. This parameter is not known *a priori*. It can be determined however from the experimental data.

Brown and Roshio [1] found that for all cases of He/N_2 shear layers, the spreading angle of the density profile was greater than that for the velocity profile. In order to evaluate this, they constructed an eddy-viscosity model and deduced that the turbulent Prandtl number should be between 0.2 and 0.3.

Figure 11 compares the predicted ρu profile for the conditions of Case V shown in *Table 6* utilizing the present $k\epsilon 2$ turbulence kinetic energy model. Note that there is qualitative agreement between the predictions and the experiment for a turbulent Prandtl number of 0.3. Had this been for the constant density case, the functional relationship would have been much different, approaching a constant value of 1.0. The trend toward matching the experimental data is to run at lower Pr_t numbers. However, this study did not investigate the quantitative differences as a lower Pr_t is utilized. One reason for this was the marked increase in computer runtime that would have been necessary. This is, however, a parameter that needs to be investigated in future investigations of turbulence modeling. Therefore, $Pr_t = 0.3$ was chosen for the corresponding calculation.

TABLE 6. INITIAL CONDITIONS FOR SHEAR LAYER COMPARISON CASES

CASE NO.	u_j/u_e	ρ_j/ρ_e	JET STREAM CONSTITUENT	EXTERNAL STREAM CONSTITUENT
I	7.00	1.00	AIR	AIR
II	2.62	1.00	AIR	AIR
III	2.65	7.00	N_2	He
IV	2.65	0.143	He	N_2
V	7.00	0.143	He	N_2

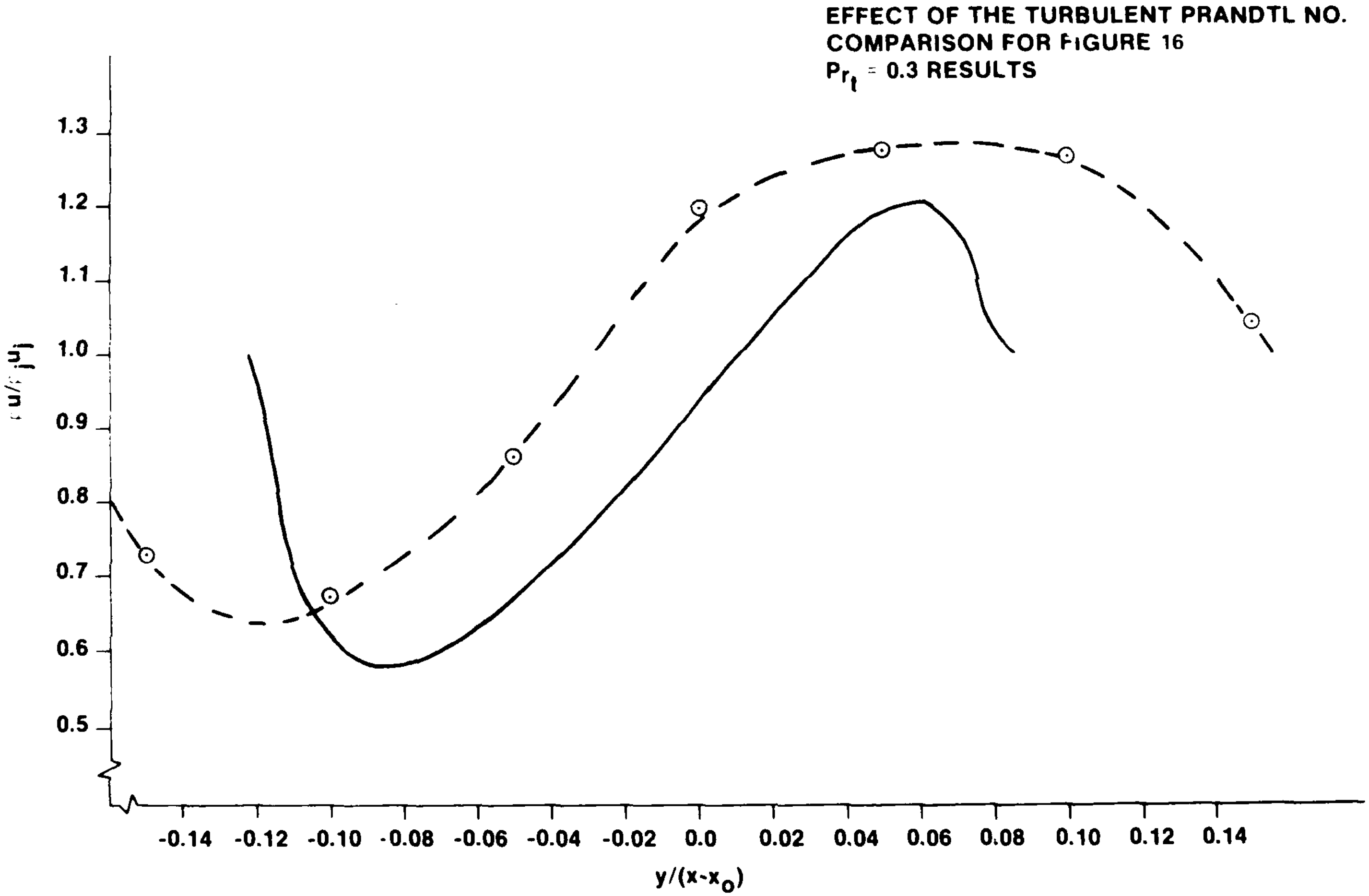

Figure 11. ρu Profile comparison for He/N_2 shear layer Table 6-case number V.

A comparison of the two turbulent kinetic energy models with experiment is shown in terms of the velocity profile in *Figure 12* for case III (*Table 6*). For this case, the jet velocity was 32.8 feet/second while the external stream velocity was 12.4 feet/second. The jet-fluid was N_2 while the external fluid was He giving a density ratio of 7. As before, the pressure was held constant at 102.9 psia.

Both models show reasonable agreement with the data. The velocity profile slope is more nearly constant for the $k\epsilon 2$ as opposed to the $k\omega'$ model. There is some disagreement with the width of the mixing layer between the models where the width is too great on the high velocity side on one and too narrow on the low velocity side on the other and vice versa.

The first density profile comparison is shown in *Figure 13*. (Case III) The most notable aspect of this comparison is the lack of agreement between theory and experiment. In particular the slope of density profile on the N_2 side is far too large: the $k\epsilon 2$ model demonstrating the worst agreement between the two. The width of the density layer is very close for the $k\omega'$ model and somewhat worse for the $k\epsilon 2$ model. The absolute agreement between experiment and theory is poor everywhere across the mixing layer and density errors of $\approx$ 100 percent can be seen. Had the disagreement occurred only in the edge regions of the shear layer, concern for this would have been lessened. Unfortunately, the agreement is uniformly poor.

The next comparison of the turbulent kinetic energy models with experiment is shown in terms of the velocity profile in *Figure 14* for case IV (*Table 6*). For this case, the jet velocity was 32.8 feet/second while the external stream velocity was 12.4 feet/second. The jet fluid was He while the external fluid was N_2 giving a density ratio of 0.143, the external stream being the more dense. Again the pressure was held constant at 102.9 psia. A turbulent Prandtl number of 0.7 was used in the predictions.

For this case, the velocity profile comparison begins to look poor, especially on the He side of the shear layer. Some of this poor agreement can be attributed to being in the edge region of the shear layer. However, it is clear that this is not the only reason for the disagreement. Notice that the shear layer width is predicted much more narrow than that observed experimentally. Further, the velocity profile slope on the He side is considerably in error. This velocity profile comparison is the worst that has occurred so far.

The density profile comparison for Case IV is shown in *Figure 15*. The same problems that were evident in the velocity profile comparison are magnified for the density profile. The predicted density width is too narrow and discrepancies are most notable in the slope of the

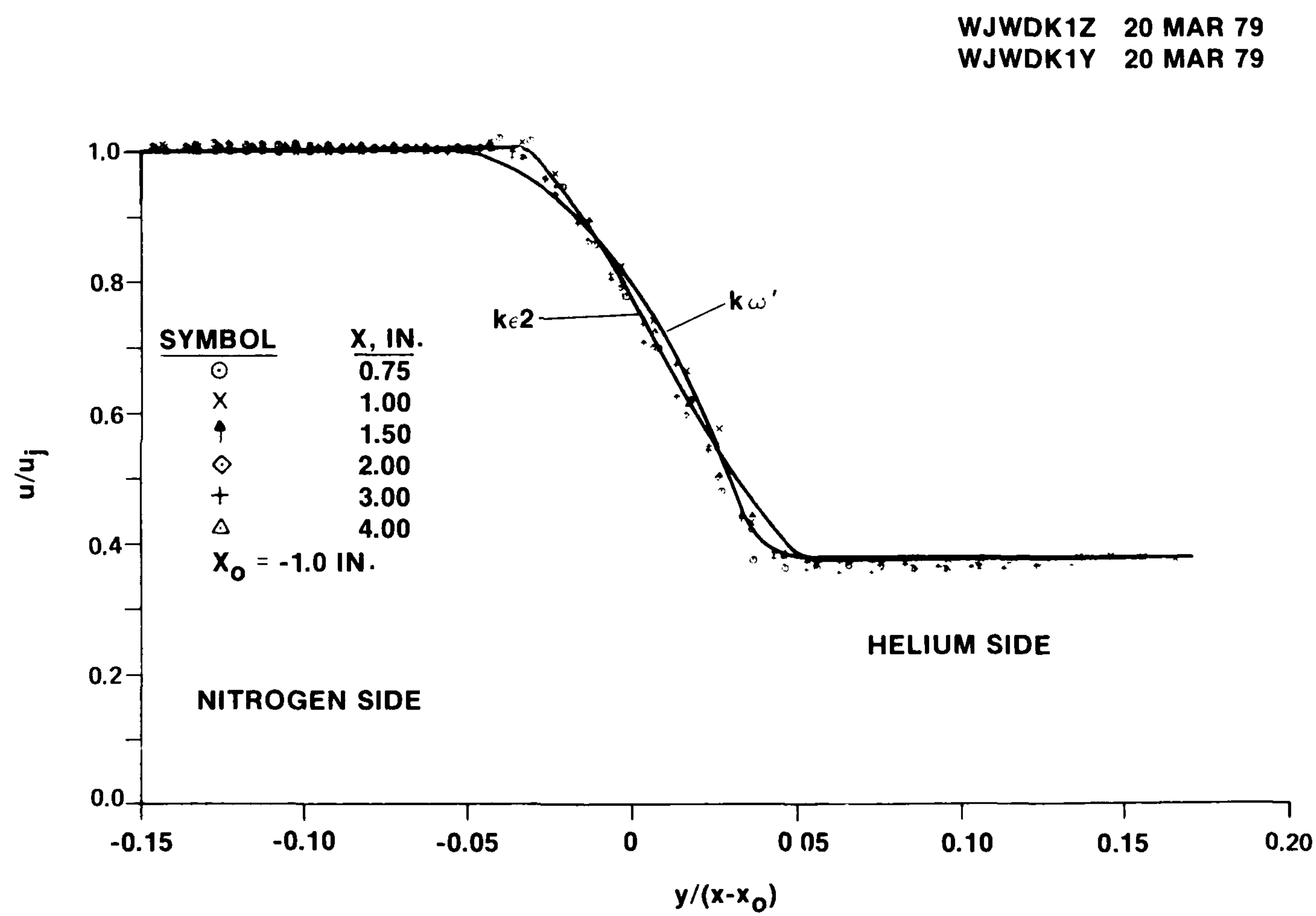

Figure 12. Velocity profile comparison for He/N_2 shear layer Table 6 - case number III.

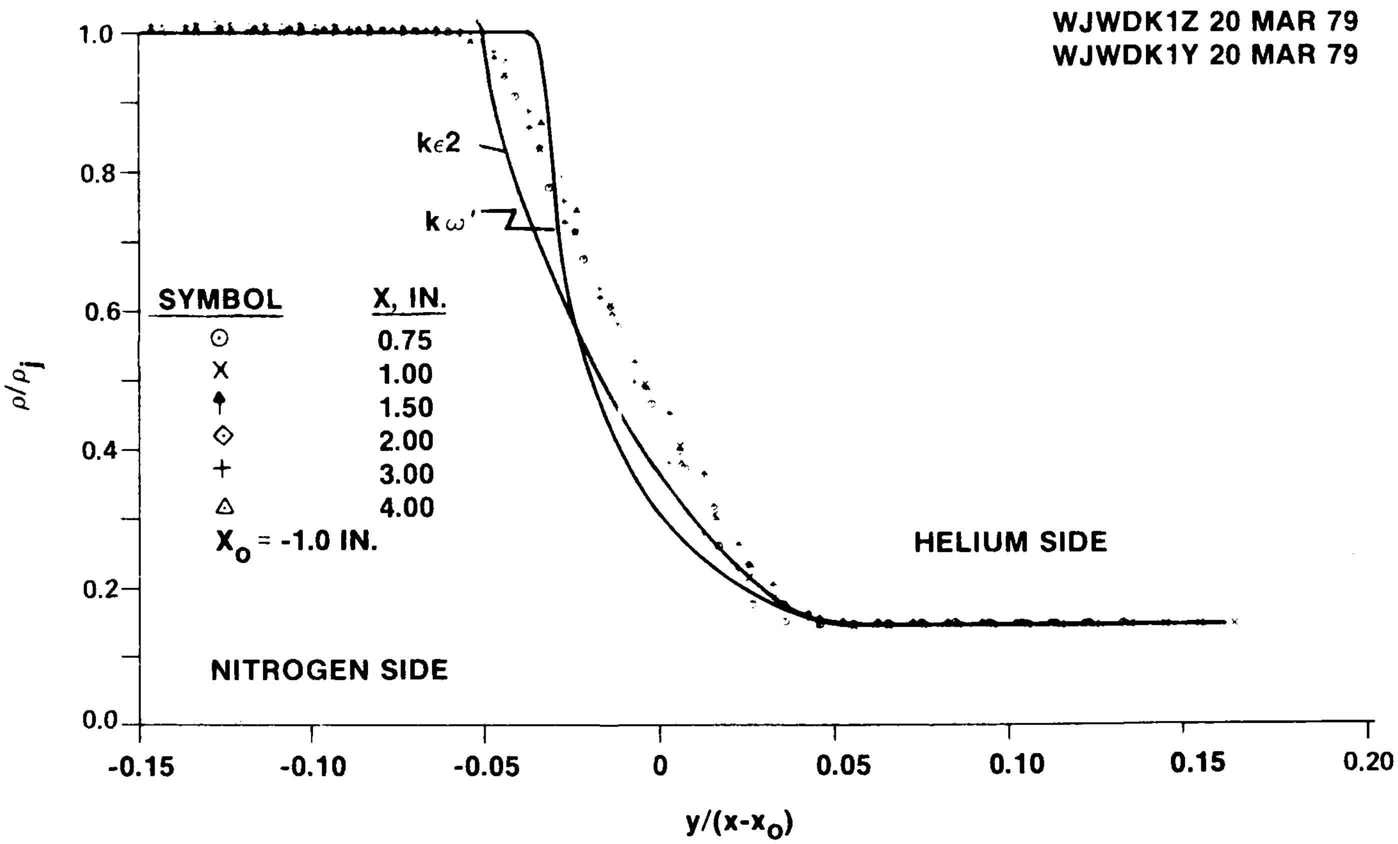

Figure 13. Density profile comparison for He/N_2 shear layer - Table 6, case number III.

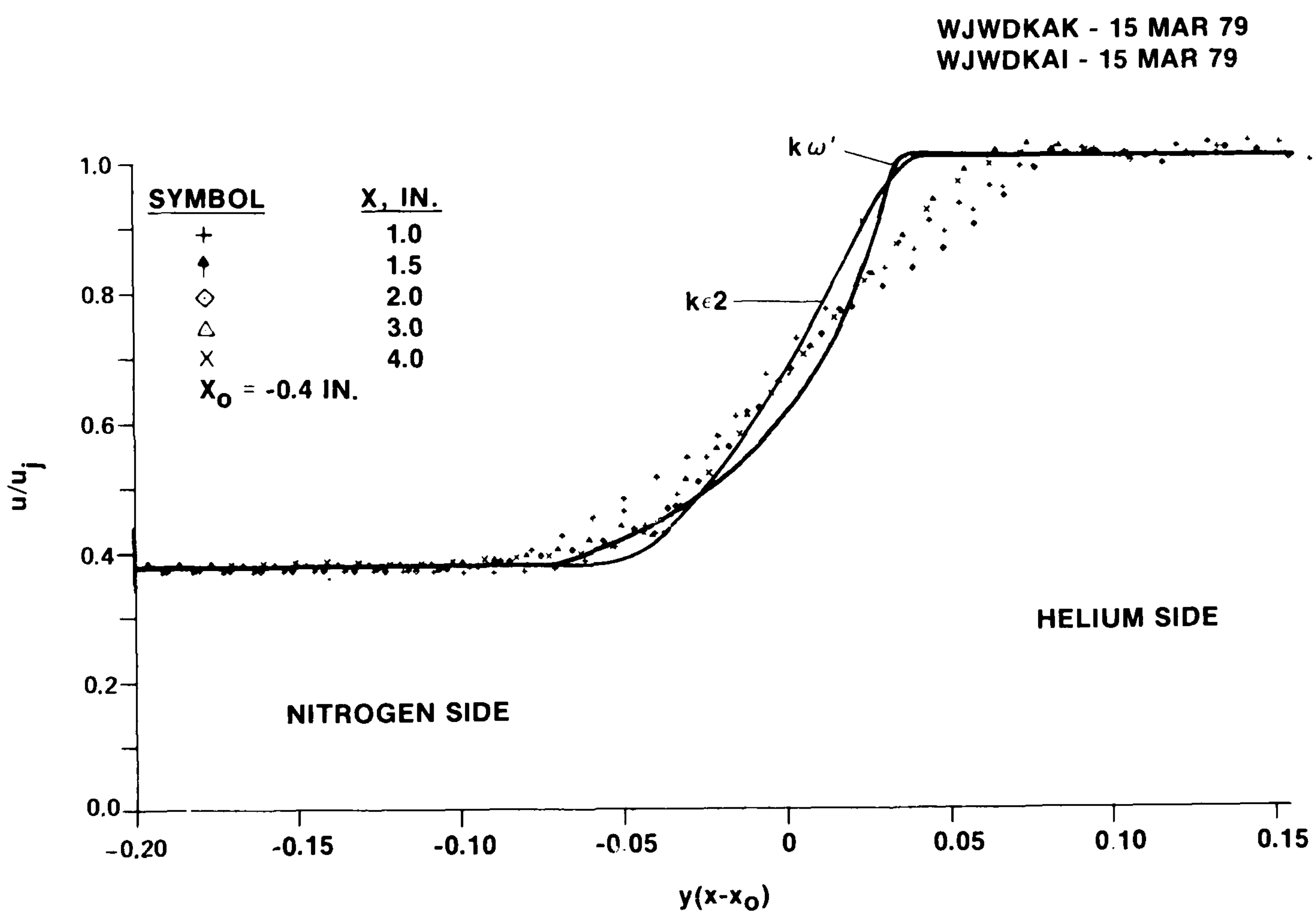

Figure 14. Velocity profile comparison for He/N_2 shear layer, Table 6 - case number IV.

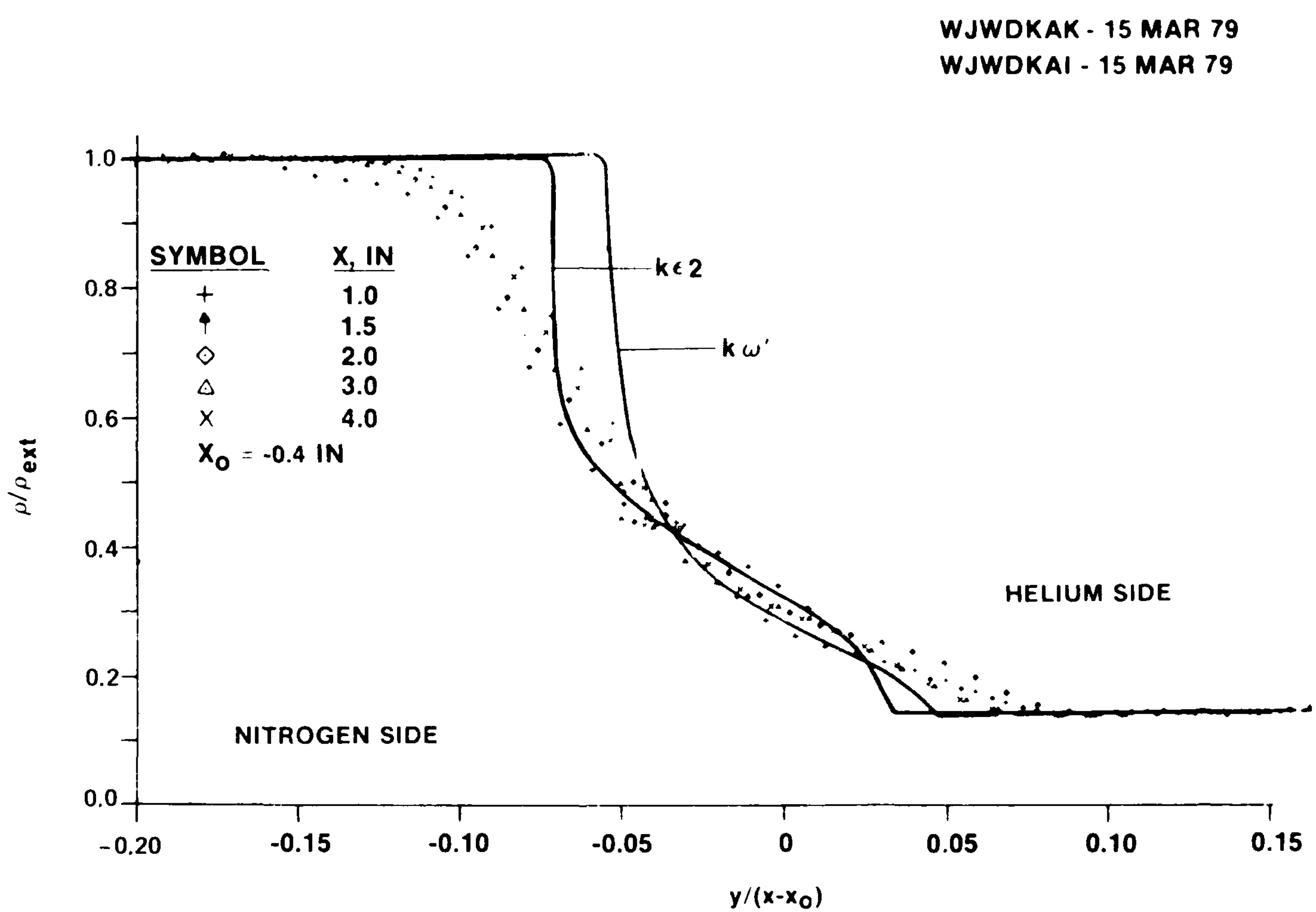

Figure 15. Density profile comparison for He/N_2 shear layer - Table 6, case number IV.

density profile on the N_2 side. The differences in width between the velocity and density profiles was accounted for in the model by running the model at a turbulent Prandtl number, $Pr_t=0.3$ as described earlier. It is obvious that the resulting theoretical difference in width of the two layers is far less than the experimental width difference. Thus, it is obvious that there are some serious problems in the turbulence modeling for flows have a large density difference.

The next comparison of the turbulent kinetic energy models with experiment are the most interesting of the shear flows compared since the density ratio of 7 that was run is very nearly that seen in rocket exhaust plume firings. The velocity profile is shown in *Figure 16* for Case V (*Table 6*). For this case, the jet velocity was 32.8 feet second while the external stream velocity was 4.7 feet second. The jet fluid was He while the external fluid was N_2 giving a density ratio of 7, the jet stream being the less dense stream. The pressure was held constant at 102.9 psia.

The velocity profile comparison for this case is shown in *Figure 16*. As was the situation in Case IV, the velocity profile comparison looks poor, especially on the He side of the mixing layer. Note the substantial difference between the velocity profile slopes predicted by both models and measured. Again the shear layer width predicted is more narrow than that measured. The comparison is very similar to that of Case IV.

The density profile comparison for Case V is shown in *Figure 17*. Again as in Case IV, the predicted density width is too narrow and discrepancies are most notable in the slope of the density profile on the N_2 side. The differences in width between the velocity and density profiles were accounted for in the model by running at a $Pr_t=0.3$. Again the predicted width difference between the predicted density and velocity profiles are far less than between the measured profiles. The comparison between experiment and theory is the worst thus far seen and as mentioned earlier, this is the case of most interest since it more closely matches a real rocket plume in terms of density ratio.

The spreading rate for all the previous cases was calculated and compared with the experimental data. *Figure 18* shows the comparison for the $k\epsilon 2$ model and the comparison for the $k\omega'$ model is shown in *Figure 19*. There is one difference between the velocity profile slope of the experimental data and the theoretical calculations Brown and Roshko used $\left(\frac{\delta u}{\delta y}\right)MAX$ while $\left(\frac{\delta u}{\delta y}\right)AVG$ was utilized for the theoretical calculations. In calculating the $\left(\frac{\delta u}{\delta y}\right)AVG$, only the center 50 percent of the profile was utilized in determining the average slope to minimize edge gradient effects.

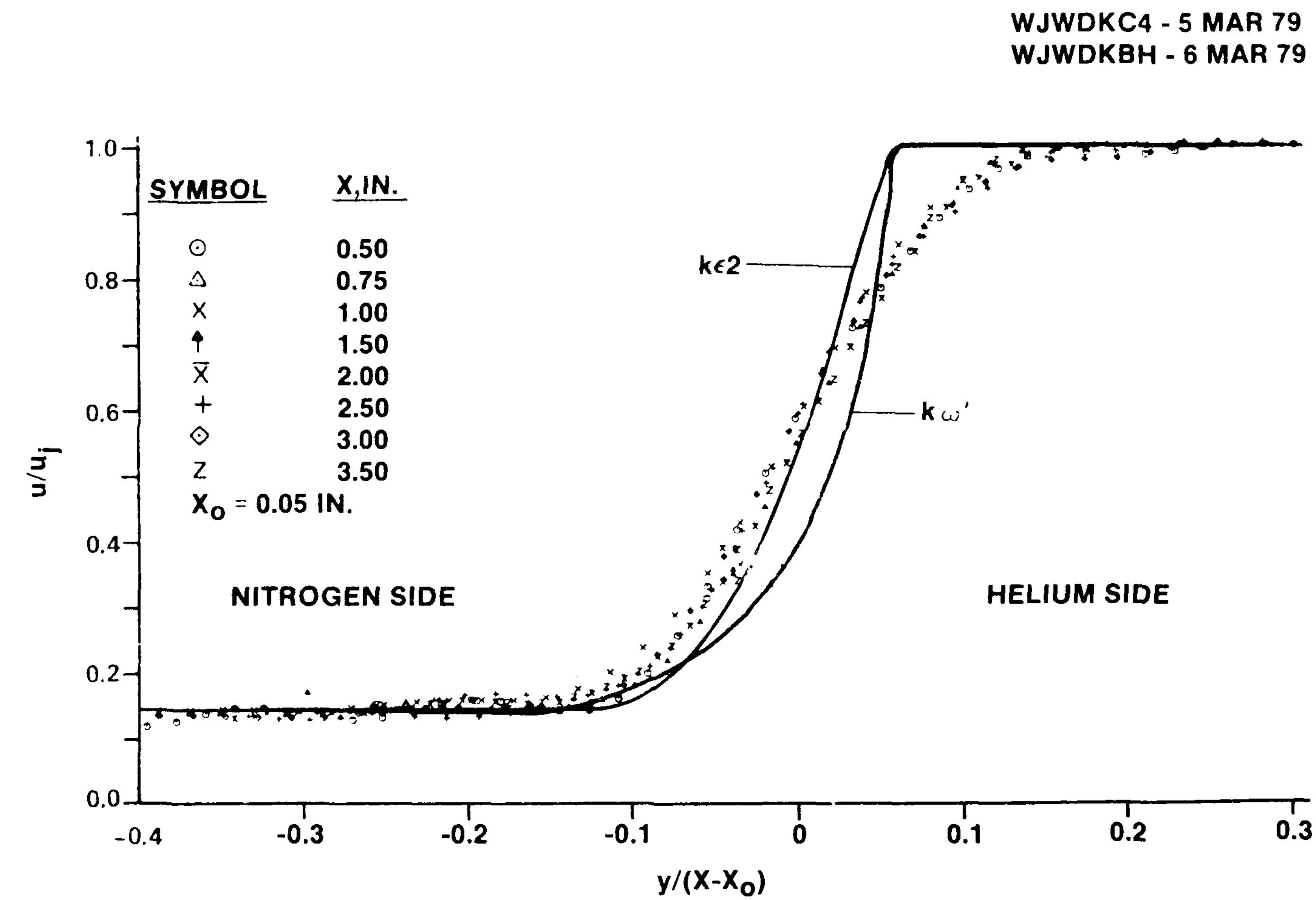

Figure 16. Velocity profile comparison for He/N_2 shear layer - Table 6 - case number V.

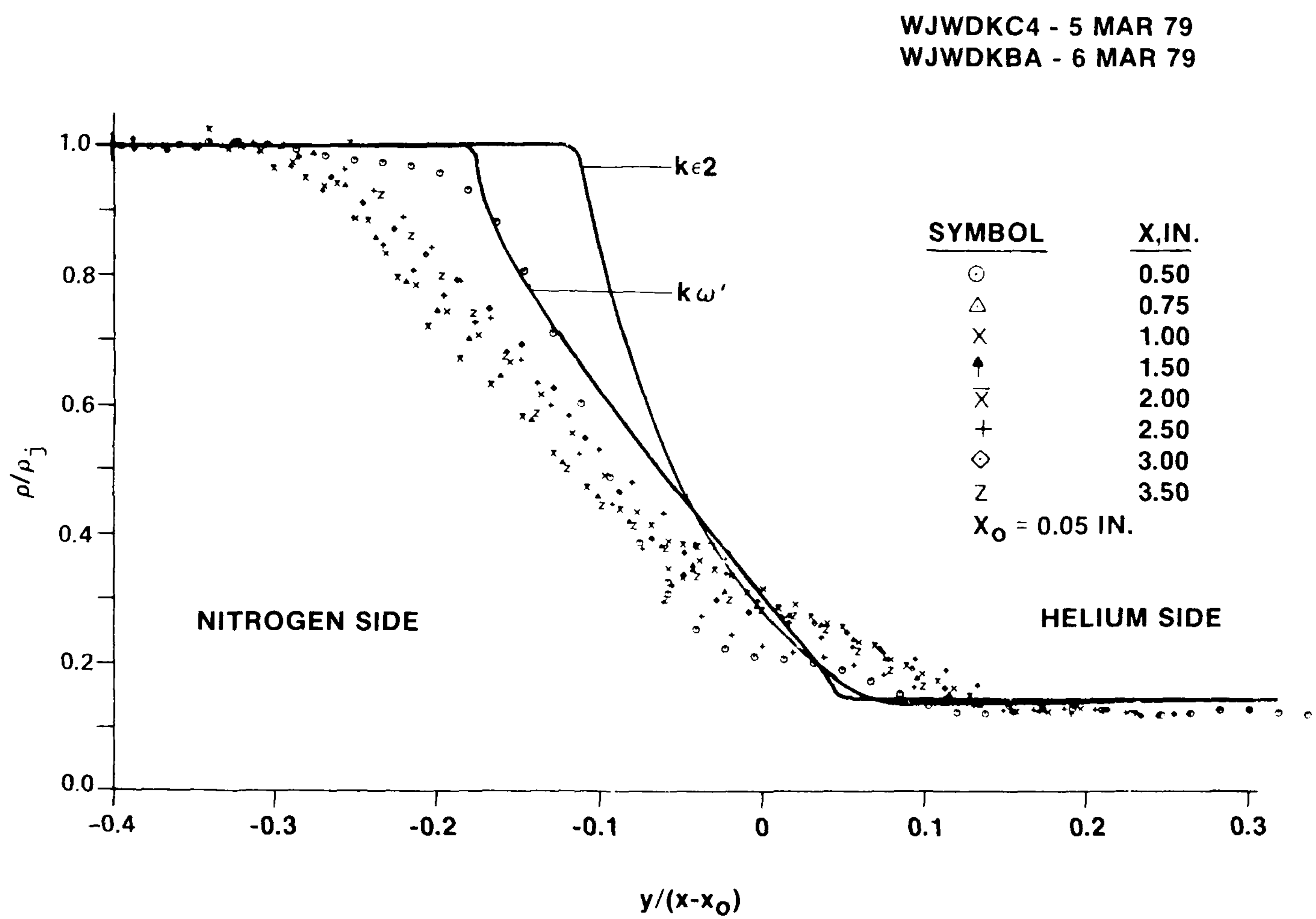

Figure 17. Density profile comparison for He/N_2 shear layer - Table 6, case number V.

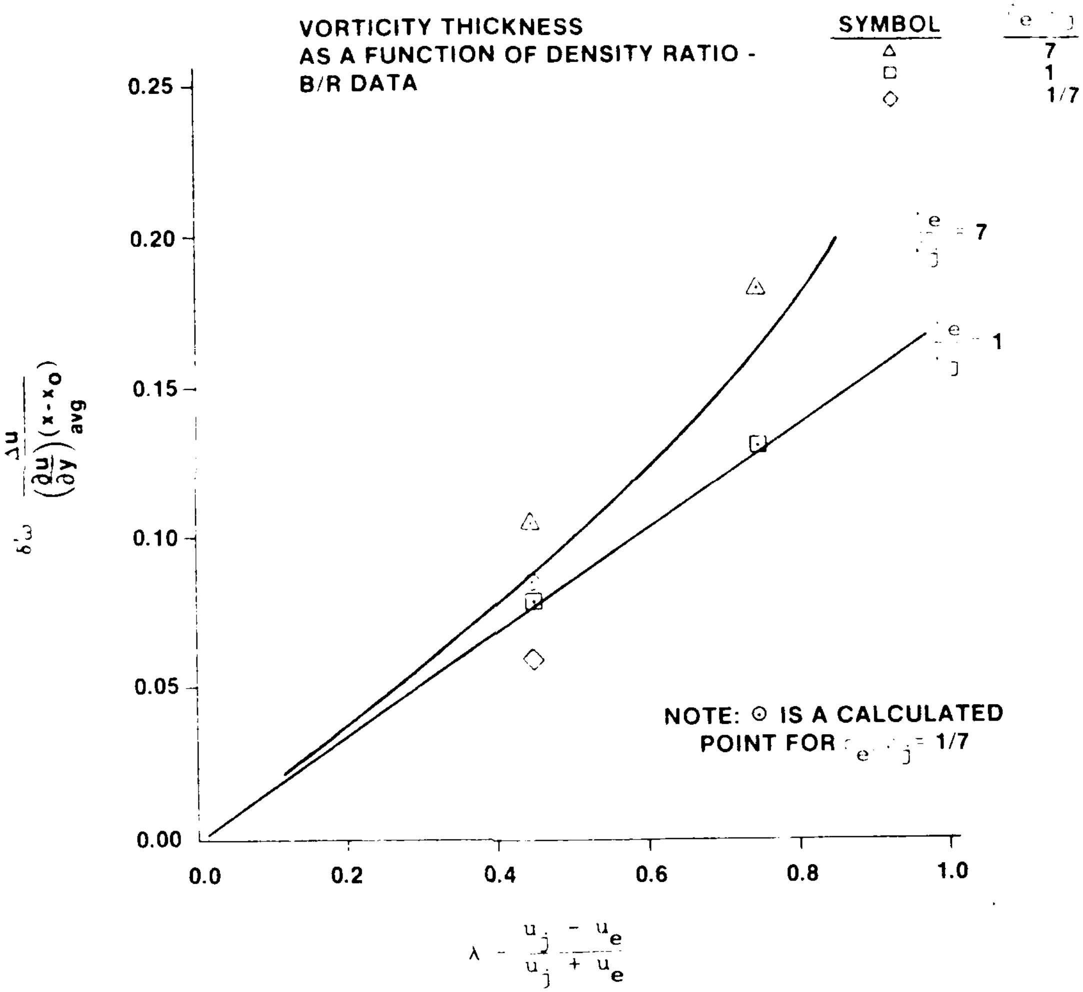

Figure 18. Comparison of calculated and measured effect of density ratio on spreading rate (k ε 2 turbulence model).

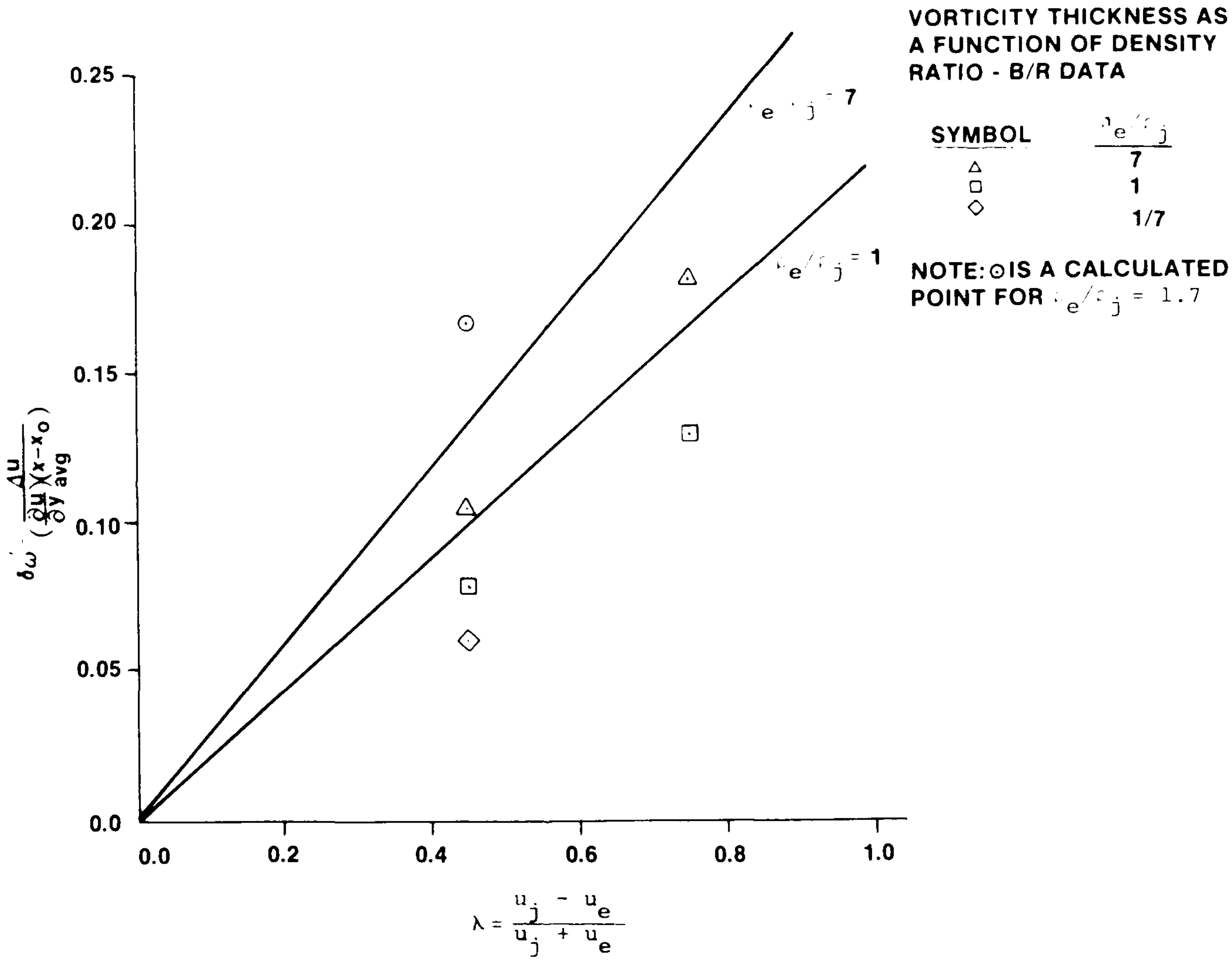

Figure 19. Comparison of calculated and measured effect of density ratio on spreading rate (Saffman $k\omega'$ turbulence model).

It should be noted that the kε2 model gave the best agreement between theory and experiment. For the case with equal densities for both the jet and external streams, the data points fall exactly on the theoretical curve.

The agreement between theory and experiment is the worst for the case where $\rho_e / \rho = 1$ for both models.

The agreement or lack thereof between experiment and theory is almost totally governed by $\frac{\delta u}{\delta y}$. Since the spreading rate is so sensitive to this parameter, these comparisons are much less meaningful than the density profile for example.

VI. NON-REACTING JET COMPARISON

The previous comparisons of the turbulence mixing models were made utilizing the experimental data of Brown and Roshko which were for two dimensional shear layers at low velocities (30 feet second or less). Since the applications of interest for this work are all at much higher velocities and since the geometry is axisymmetric, it was felt that comparison with some of the NASA Shear Flow Conference Data [7] was in order. Hence comparisons were made for axisymmetric jet data in order to compare the turbulence models. Two sets of experimental data were chosen from the NASA Shear Flow Conference for comparison with the two turbulence kinetic energy models, the kε2 and kω'. *Table 7* details the flow conditions that were run during the experiments.

These two cases cover the spectrum of expected velocity and density ratios that one might expect to see in a realistic rocket plume case. They are, however, not in the same experiment. For both of these cases only experimental velocity profiles were measured. This is

TABLE 7. INITIAL CONDITIONS FOR JET MIXING COMPARISON CASES

CASE NO.	u_j/u_e	ρ_j/ρ_e	JET STREAM CONSTITUENT	JET STREAM CONSTITUENT	M_j	M_e
I	∞	1.97	AIR	AIR	2.2	0
II	2.72	0.06	H_2	AIR	0.89	1.32

unfortunate since, as was seen in the preceding comparisons for the shear layer, the density profiles are a much more stringent test for the accuracy of the theoretical models. Furthermore, since species concentration is the one of the quantities used directly in rocket plume applications, it is a more important measure of the accuracy of the turbulence models.

Another important consideration for rocket exhaust plumes is the compressibility effects. The importance of this effect is addressed for Case 1 *(Table 7)* where there is an infinite velocity ratio between the jet and the external stream. Certainly Brown and Roshko have pointed out the importance of this effect and the accuracy with which this effect is accounted for is shown below.

The first comparison made was for an M_j=2.2 air jet exhausting into still air. The jet velocity was 1765 feet second and the pressure was ambient. The density ratio was as shown in *Table 7* for Case 1.

This is the homogeneous case in which the density ratio is determined by the Mach number as opposed to molecular weight differences in the jet and the external stream. Hence, compressibility effects are important for this case. Since the kϵ2 turbulence model does not account for compressibility effects, a compressibility correction factor originating from some empirical work at General Applied Science Laboratory (GASL) was utilized to account for this effect. The details of this correction were presented in an earlier section.

Figure 20 compares model predictions for the kϵ2 and kω' turbulence models without compressibility with the experimental data. It should be noted from the centerline velocity profile that the predicted core length of the jet is too short compared with experiment. The kω' core length being much shorter than the kϵ2 core length. This indicates that the entrainment of the ambient stream is much too large and the mixing distance much too short for the case of a high relative velocity between the two streams.

However, when the compressibility effects are accounted for by utilizing the GASL compressibility factor for the kϵ2 turbulence model and via the addition of a term in the modeling equation for the kω' model, the results show a marked improvement. In fact the agreement between prediction and experiment is excellent for the kω' turbulence model with compressibility. This agreement is shown in *Figure 21*. Note that the core length prediction is correct and the centerline velocity agreement is excellent out to 60 jet nozzle radii. The agreement deteriorates from that point on downstream but is still quite reasonable. The kϵ2 model with compressibility correction predicts a core length that is too long and centerline velocities that are too high until the centerline velocity has dropped to 30 percent of its original

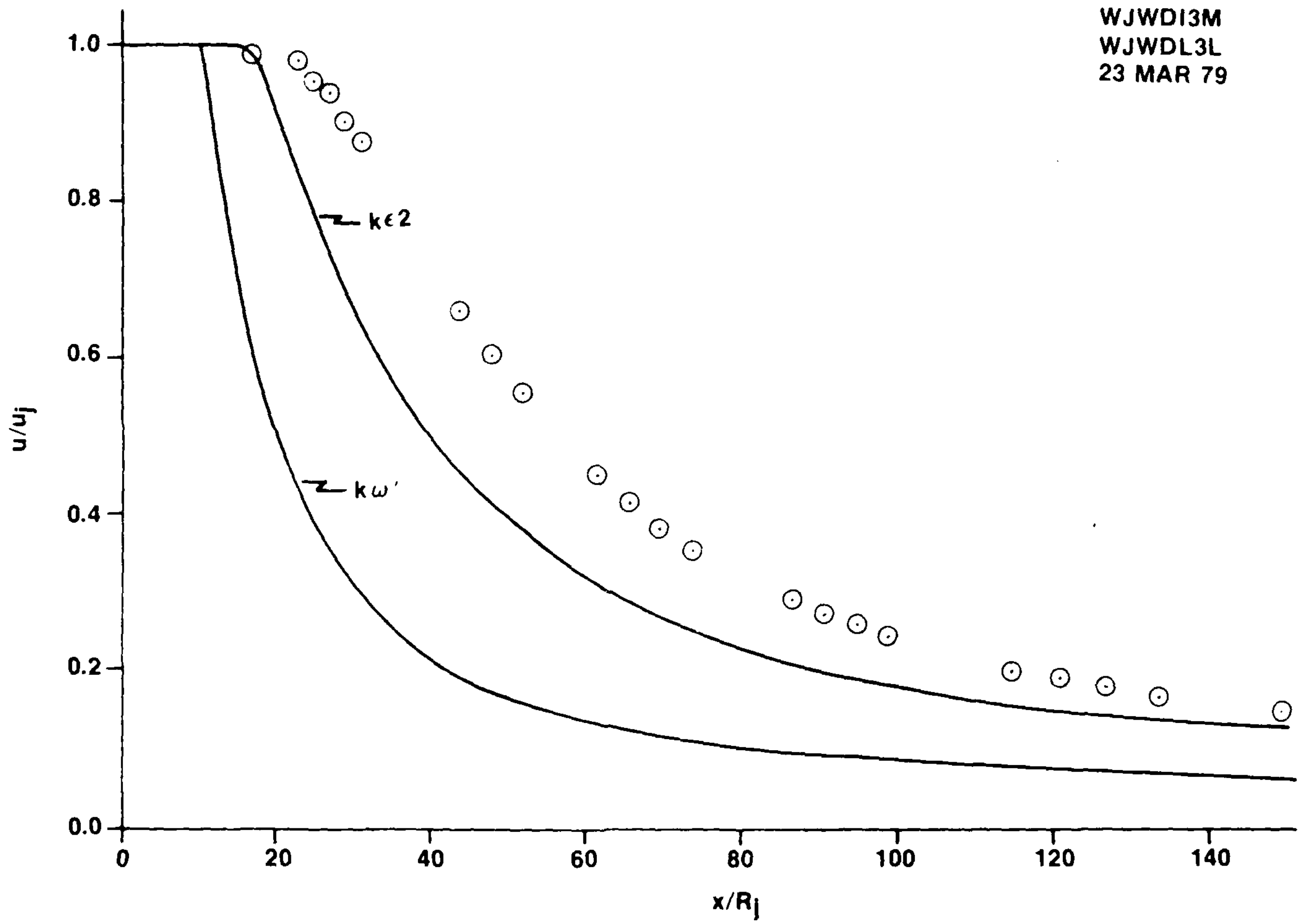

Figure 20. $M_j = 2.2$ air jet into still air. Comparison of $k\epsilon 2$ and $k\omega'$ turbulence models without compressibility centerline velocity profile.

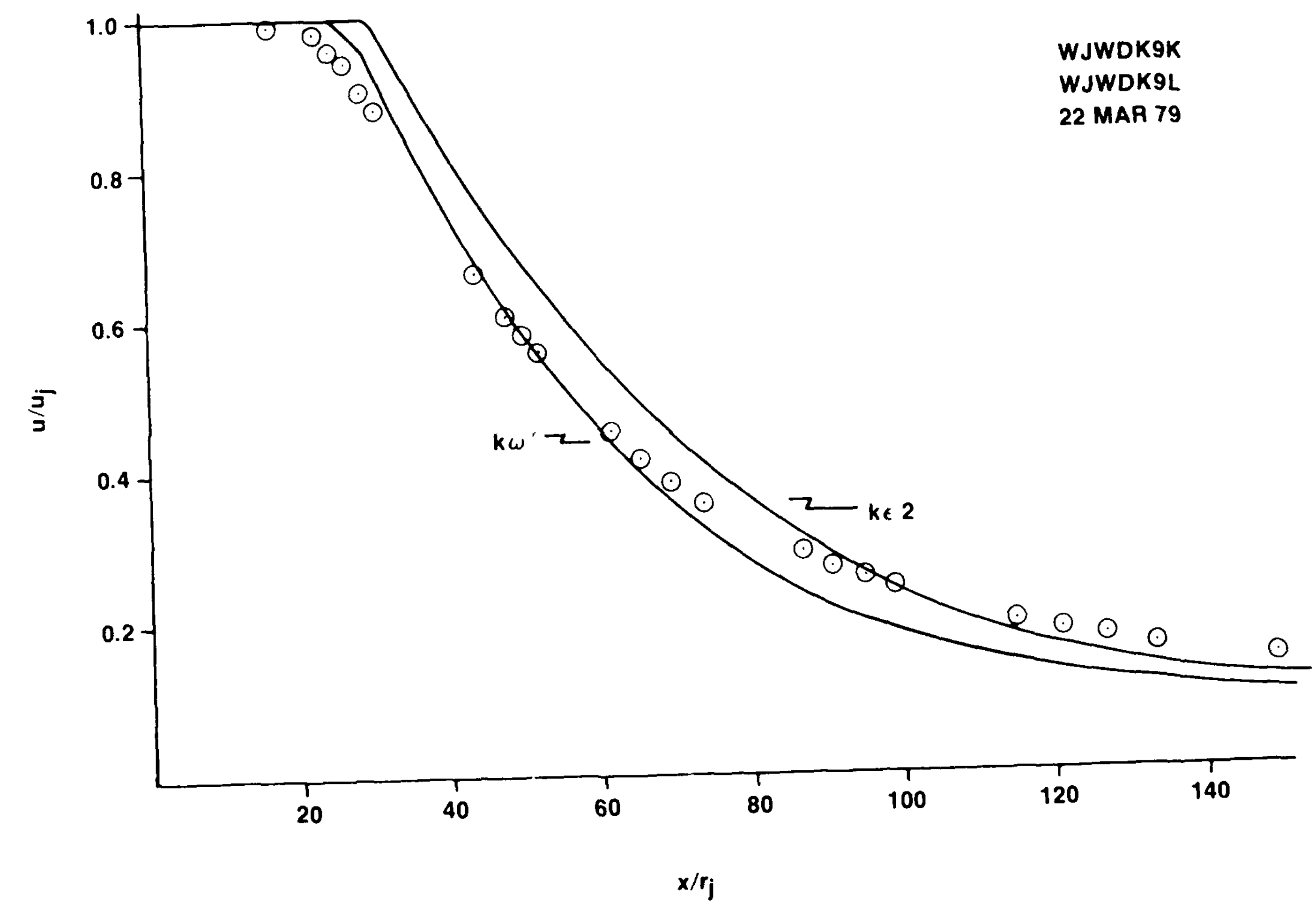

Figure 21. M_j = 2.2 air jet into still air. Comparison of $k\epsilon$ 2 and $k\omega'$ turbulence models with compressibility centerline velocity profile.

value. Hence, both models agree reasonably well with the experimental data with the kω' model showing the better agreement of the two. Further, it has been established that the compressibility effects are important and will be retained for the remainder of the jet comparisons in this section.

The next test of the model predictive capability comes about by comparing the radial velocity profiles at downstream axial stations. The first station chosen was near the end of the jet potential core as shown in *Figure 20* at 22.9 jet radii downstream of the nozzle exit. Note that the velocity profile in *Figure 22* shows a small diameter potential core at this distance downstream and a gradual velocity reduction as the radial distance increases. Note that both turbulence models show excellent agreement with the experimental data with the kω' model showing slightly better agreement.

The next point chosen for comparison was at 43.9 nozzle radii downstream. The radial profile at this axial station is shown in *Figure 23*. The agreement between the kω' model and experiment is near perfect at this axial location. The kϵ2 model prediction shows a reduced velocity compared with experiment indicating that mixing is occurring slightly too rapidly.

The last point chosen for comparison was at 61.7 nozzle radii downstream. The radial profile at this axial station is shown in *Figure 24*. The agreement between the kω' model and experiment is very good at this axial location. The kϵ2 model prediction again shows a reduced velocity compared with experiment.

It is thus concluded that compressibility effects are important for Case I (*Table 7*) and must be accounted for to achieve a reasonable agreement between theory and experiment. It is also concluded that the kω' turbulence model shows improved agreement with the experimental data compared with the kϵ2 model.

The second comparison made was for a $M_j = 0.89$ H_2 jet into a supersonic $M_e = 1.32$ air jet. The jet velocity was 3520 ft/sec and the external velocity was 1295 ft/sec. The pressure was ambient and the initial density ratio is shown in *Table VII*.

Figure 22 compares model predictions for the kϵ2 and kω' turbulence models with compressibility. It should be noted that the agreement between theory and experiment for the core length is reasonable. The kω' model shows a slightly better agreement with the experimentally determined length.

The radial velocity profiles were first compared at an axial distance downstream of 11.02 nozzle radii. This can be seen from *Figure 25* to still be in the potential core region. Note in *Figure 26* that the predicted radial profile utilizing the kω' model is reasonable but certainly does not agree as closely as it did in Case I above. Discrepancies between experiment and theory became apparent when the velocity difference ratio has dropped to approximately 60

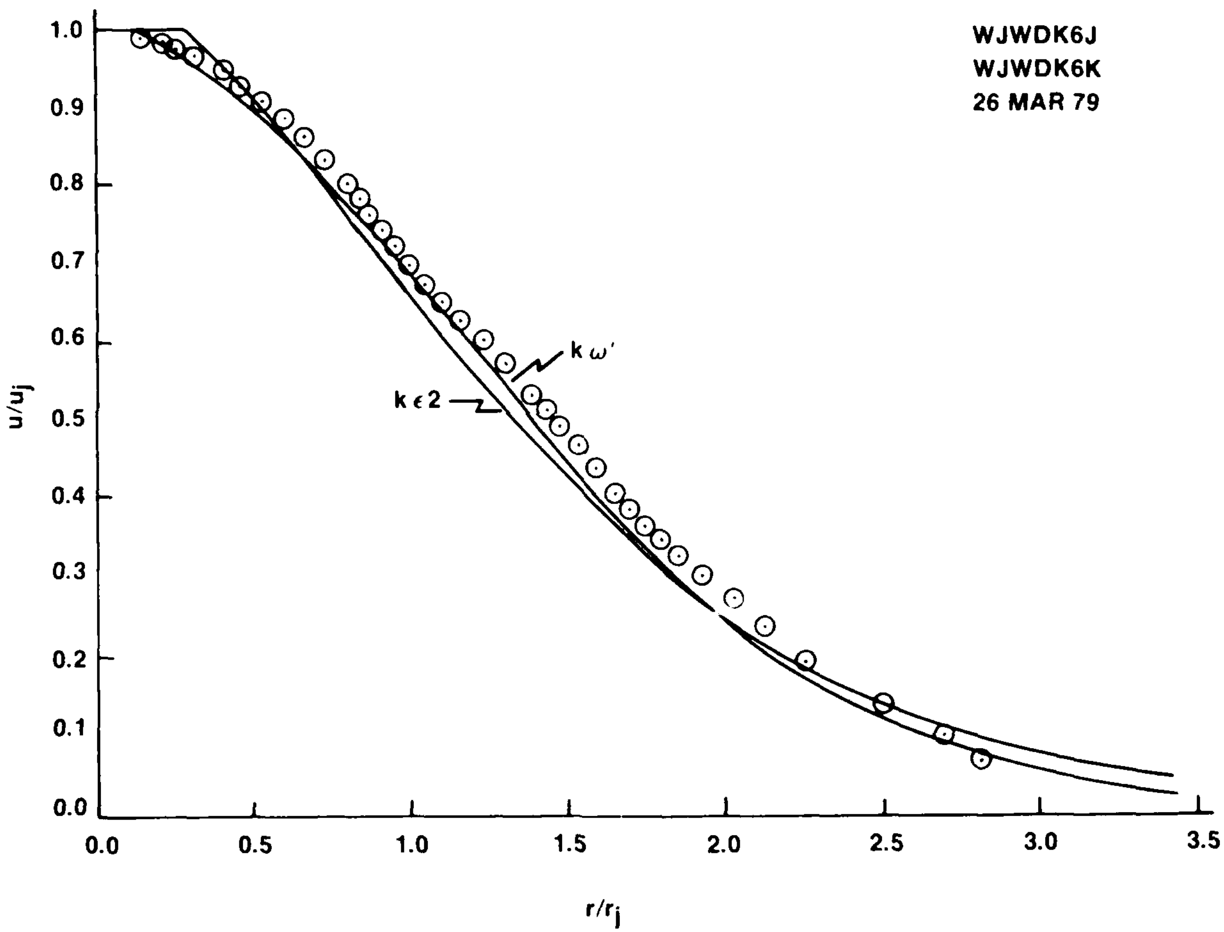

Figure 22. M_j = 2.2 air jet into still air. Comparison of k ε 2 and k ω' turbulence models with compressibility radial profile at x/r_j = 22.9.

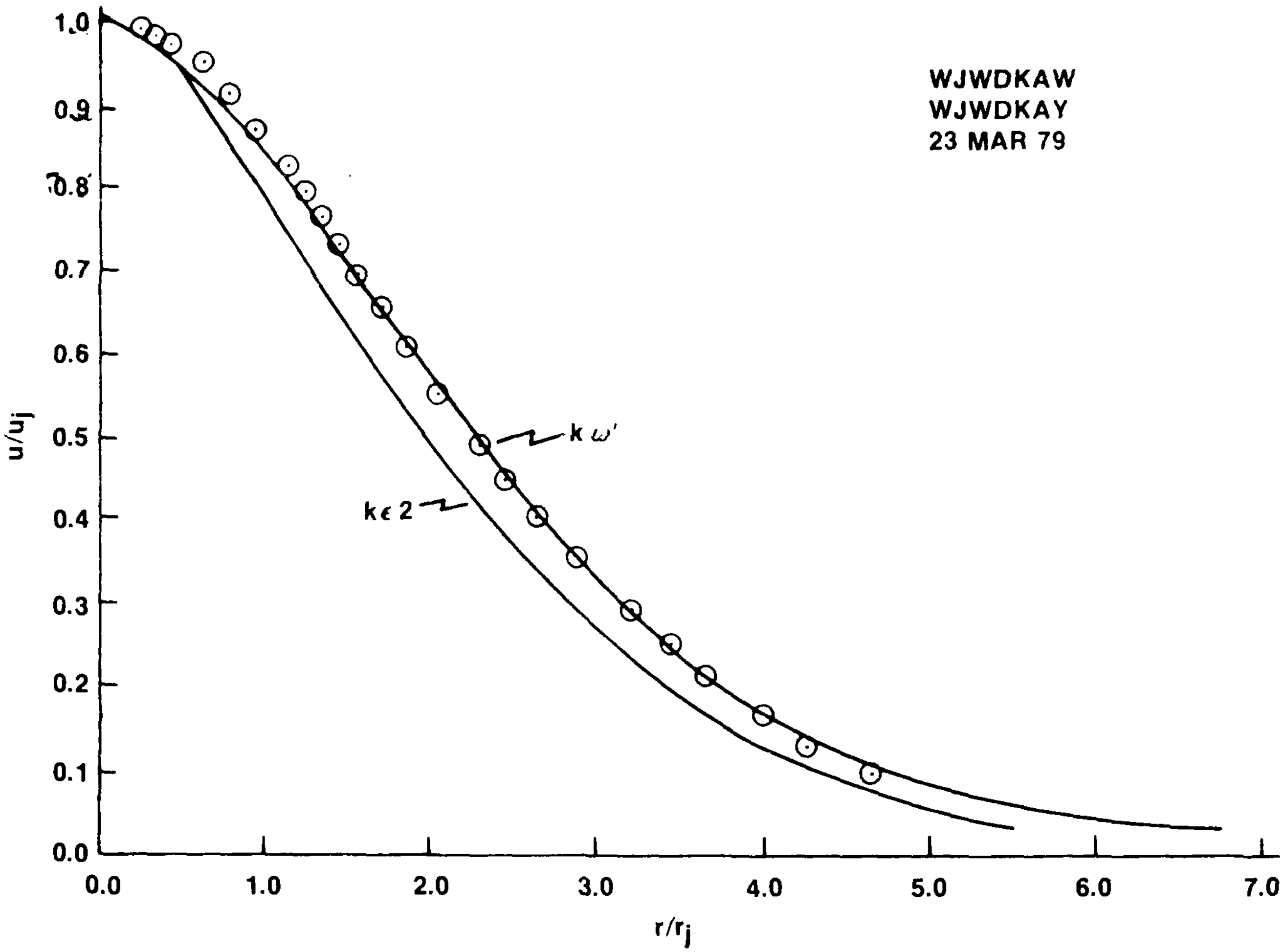

Figure 23. $M_j = 2.2$ air jet into still air. Comparison of $k\epsilon 2$ and $k\omega'$ turbulence models with compressibility radial profile at $x/r_j = 43.9$.

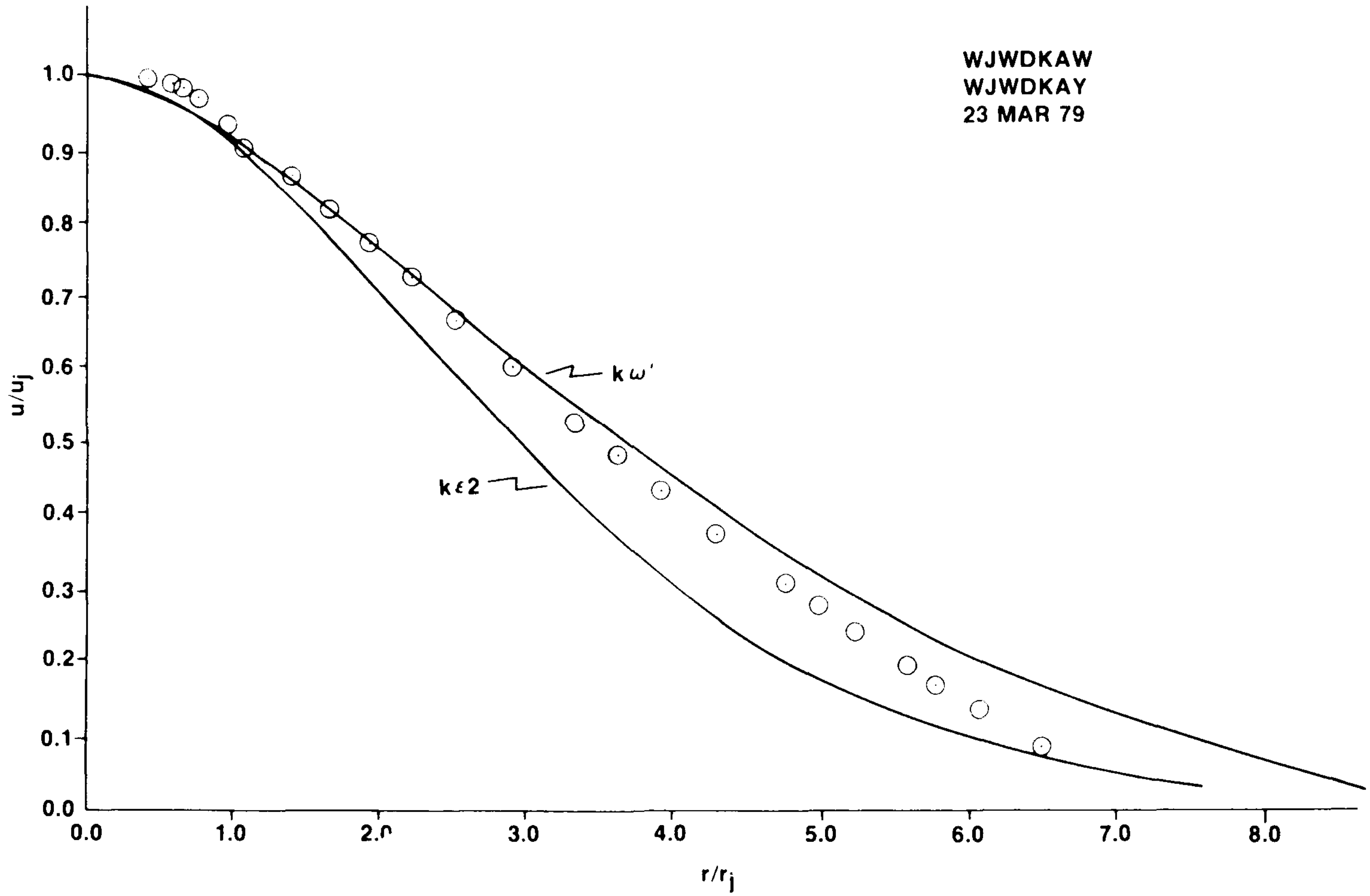

Figure 24. $M_j = 2.2$ air jet into still air. Comparison of $k\epsilon 2$ and $k\omega'$ turbulence models with compressibility radial profile at $x/r_j = 61.7$.

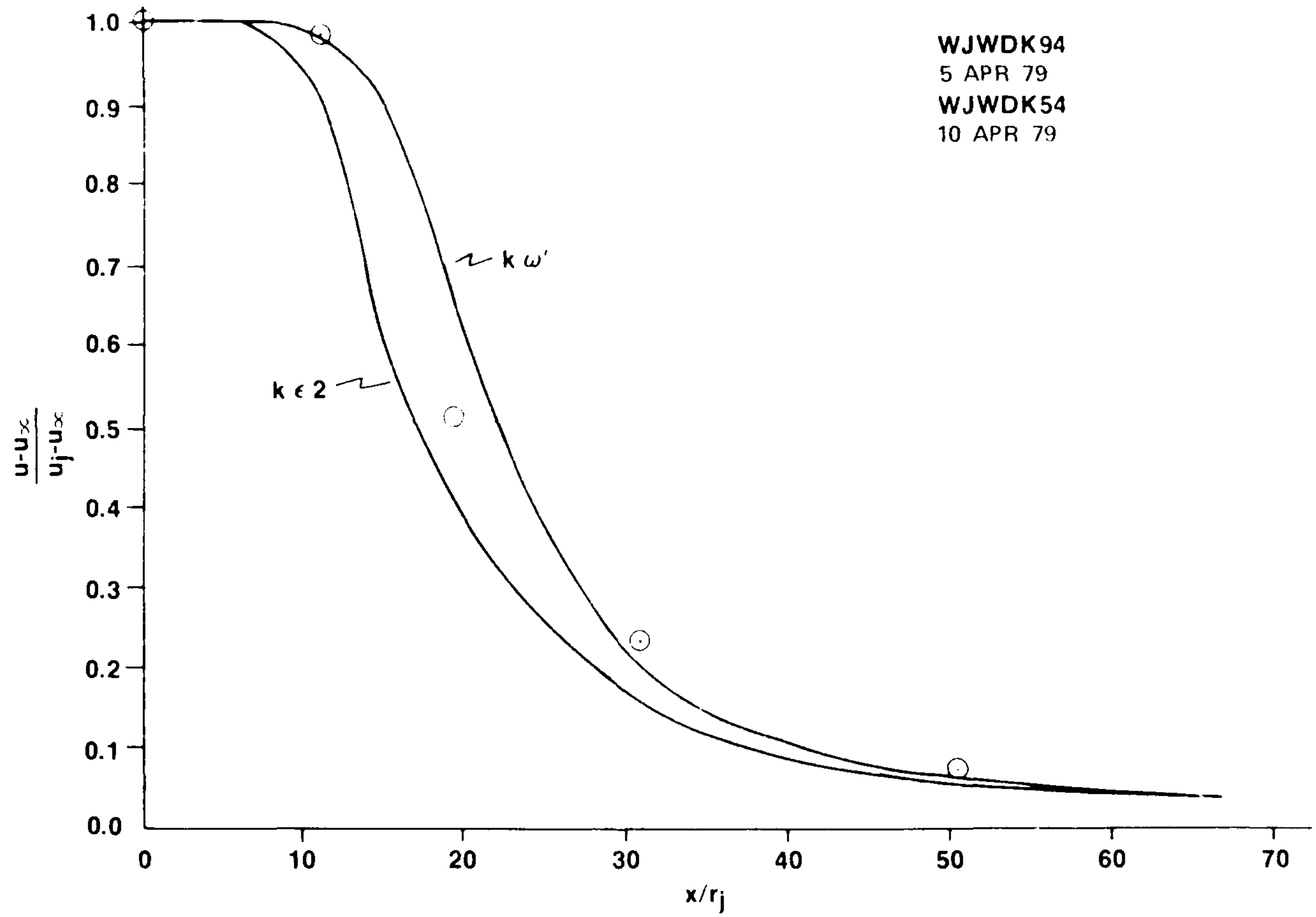

Figure 25. $M_j = 0.89$ H_2 jet into $M_\infty = 1.32$ air. Comparison of $k\epsilon 2$ and $k\omega'$ turbulence models with compressibility centerline velocity profile.

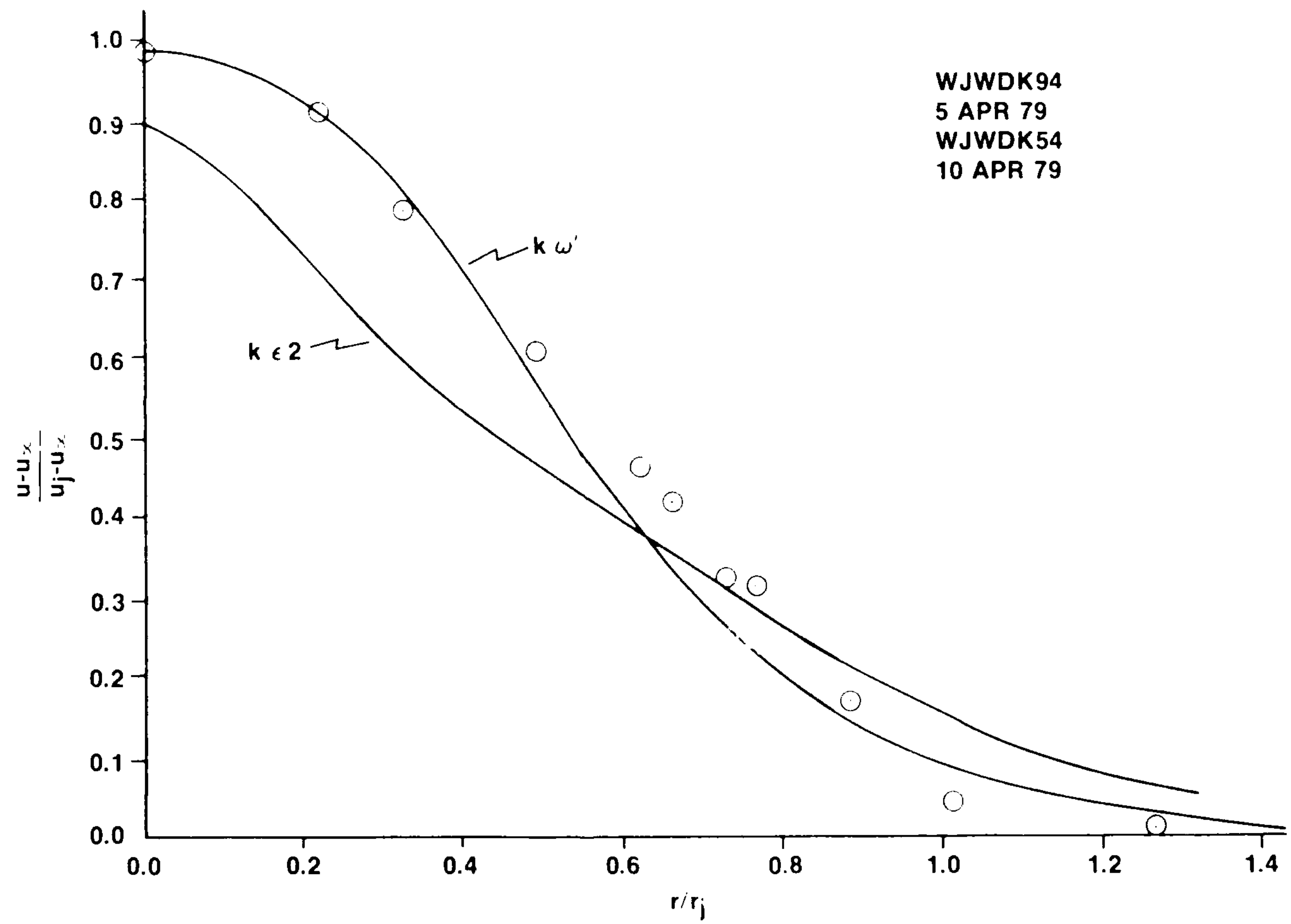

Figure 26. $M_j = 0.89$ H_2 jet into $M_\infty = 1.32$ air. Comparison of kε2 and kω' turbulence models with compressibility radial profile at $x/r_j = 11.02$.

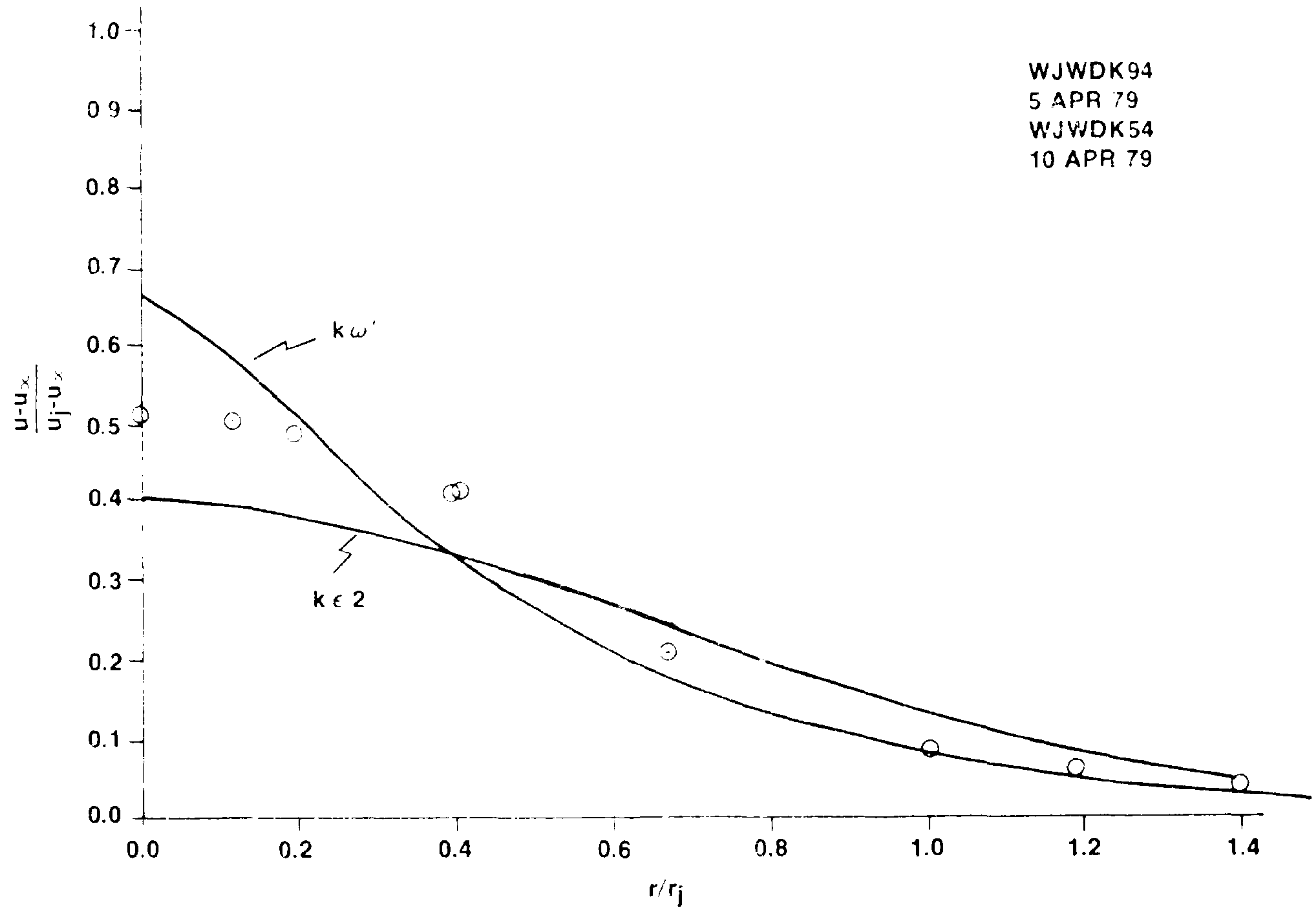

Figure 27. $M_j = 0.89$ H_2 jet into $M_\infty = 1.32$ air. Comparison of $k\epsilon 2$ and $k\omega'$ turbulence models with compressibility radial profile at $x/r_j = 19.16$.

percent of its initial value. Use of the kε2 model gives a noticeably poorer agreement with experiment over the entire range of comparison.

The next radial profile to be compared is shown in *Figure 27* at a downstream distance of 19.16 nozzle radii. Note that the comparisons do not agree at the r = 0 point because the core length is incorrectly predicted by both turbulence models. Both models do equally well over the entire range of parameters at this downstream distance with the most serious discrepancies occurring at r = 0.

The last radial profile comparison was made at a distance of 30.88 nozzle radii downstream of the exit plane as shown in *Figure 28*. Both models do reasonably well over the radius range covered with the largest discrepancy occurring at the lower values of the radius ratio.

The preceding comparisons demonstrate that the turbulence kinetic energy methods predict the velocity profiles, both radially and axially, reasonably well over a fairly wide range of velocities and densities. "Reasonably well" means an accuracy within ≈30 percent for a maximum error. They also demonstrate that compressibility effects are important and must be accounted for in the modeling in order to achieve this accuracy. Otherwise, even larger errors will occur.

These comparisons also demonstrate that the kω′ turbulence model show closer agreement to experiment than the kε2 model over the range of comparisons made. Hence this model can be considered as a viable alternative to the kε2 model.

VII. REACTING SHEAR LAYER COMPARISON

Thus far the turbulent mixing models have been compared against flows which have different velocities for each of the two streams or different velocities and different densities. The latter type flow is certainly more applicable to the rocket exhaust plume flows since large density ratios occur for these cases and since it is important to know the species distribution across the mixing layer. The next level of complexity in the modeling procedure is to examine the turbulent mixing of a reacting shear layer, preferably one in which the initial densities of the two streams are the same. This eliminates another variable in the problem if the initial density ratio can be held at unity. In addition, a kinetically simple reacting flow system is mandatory for an accurate test of the turbulence models since chemical reaction rates constantly change.

Reacting shear layer experiments of this kind have recently been completed at the University of Adelaide in Australia and have been reported at the Second Symposium on *Turbulent Shear Flows* by Wallace and Brown [5].

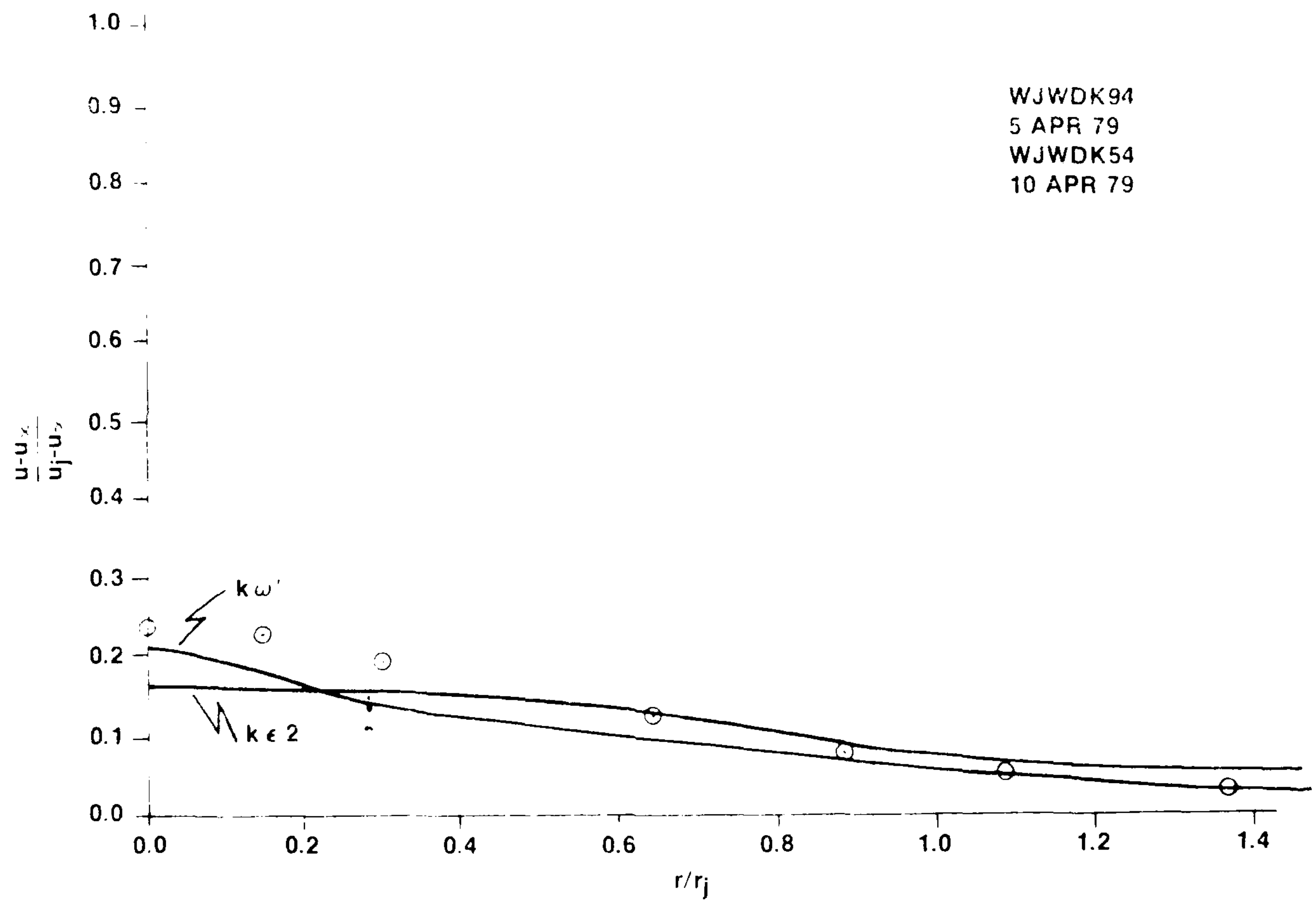

Figure 28. $M_j = 0.89$ H_2 jet into $M_\infty = 1.32$ air. Comparison of kε2 and kω' turbulence models with compressibility radial profile at $x/r_j = 30.88$.

In these experiments, the jet stream consisted of NO mixed with N_2 in various low level concentrations and the external stream consisted of O_3 mixed with N_2 in various other low level concentrations. The jet stream velocity was 82 feet/second and the external stream velocity was 16 feet/second. The flow channel was 3.94 inches wide and the height of the jet stream nozzle was 0.98 inches while the height of the external stream nozzle was 1.97 inches. The Re number based on the boundary layer height was ≈ 100.

The chemical reaction involved in this experiment is very simple

$$NO + O_3 \longrightarrow NO_2 + O_2$$

This is a well known chemical reaction and its rate is known with a high degree of accuracy as long as the temperature remains below 500 degrees K. Therefore, this experiment allows the comparison of the turbulent mixing model directly since the chemical kinetics of this reaction are so well known.

Comparisons were made for three two-dimensional reacting shear layer cases shown in *Figure 29* and further details in *Table 8*.

Note in *Figure 29* that the jet stream contains the fuel NO and the external stream contains the oxidizer O_3. The low concentrations of fuel and oxidizer mixed with the carrier

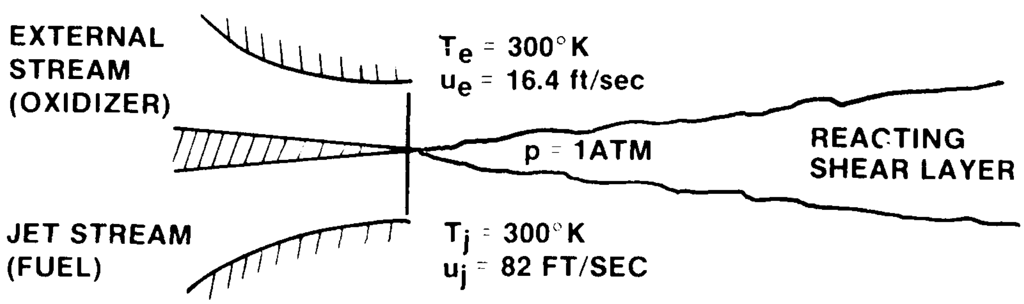

Figure 29. Two-dimensional reacting shear flow schematic.

TABLE 8. INITIAL CONDITIONS FOR REACTIVE SHEAR LAYER COMPARISONS

CASE NO.	u_j/u_e	p_j/p_e	T_j/T_e	JET STREAM CONSTITUENT*		EXTERNAL STREAM CONSTITUENT*	
				NO	N_2	O_3	N_2
I	5.0	0.996	1.0	0.05	0.95	0.010	0.990
II	5.0	0.977	1.0	0.05	0.95	0.0379	0.9621
III	5.0	0.95	1.0	0.05	0.95	0.078	0.922

* Constituents given as mole fractions.

stream. N_2 is detailed in *Table 8* for the cases that were compared. The reason for such low concentrations of reactants is the degree of reactivity of the NO/O_3 reaction. A large amount of heat is produced from minute quantities of reactants.

Comparisons were made for the cases shown in *Table 8* where the amount of oxidizer in the external stream was constantly increased from 1 to 7.8 percent. This increased the O/F ratio and resulted in increasingly higher shear layer temperatures. Comparisons were made of both the velocity and temperature profiles for these cases. Density profiles were not measured.

The virtual origin x_o was not determined in these tests as it was for the non-reacting shear layer experiments presented earlier. Hence, for the theoretical predictions, x_o was taken as zero indicating that the shear layer starts growing exactly at the exit plane of the nozzle. This will produce some error by scaling the width of the predicted shear layer incorrectly. Hence, even if the theoretical and experimental results agreed perfectly, the width of the shear layer would show a discrepancy between the predicted and measured results. However, this is not considered to be a serious discrepancy in light of the magnitude of the disagreement of the temperature profiles as will be subsequently shown.

Both the kε2 turbulence model and the kω' turbulence models were utilized in the predictions of the reacting shear layers. These models produced virtually identical results and therefore the predictions shown were those obtained utilizing the kω' turbulence model.

Results comparing the reacting shear layer for Case I given in *Table 8* predicted and measured are shown in *Figure 30*. This is a comparison of the velocity profile across the shear layer. The agreement between theory and experiment is excellent. This agreement compares favorably with the non-reacting shear layer results presented earlier for the case where the initial density ratio is 1. That is the situation here. The density ratio is 0.996 initially as shown in *Table 8*. Therefore it appears that the velocity profile is little affected by the reacting flow at least at this level and similarly good agreement between experiment and theory is shown.

Figure 31 compares the temperature profile predicted across the reacting shear layer with that actually measured. In contrast to the excellent agreement between the velocity profile determined from experiment and theory, these results are quite the opposite. The predicted temperature rise profile across the shear layer looks nothing like the measured profile. The predicted maximum temperature rise is more than twice what was actually measured. Likewise the predicted temperature gradient is much larger than that found experimentally. The shear layer width also does not agree but as was mentioned previously, this is scaled by the virtual origin x_0 and therefore cannot agree unless the origin of the shear layer lies at the exit plane of the two flows. In addition, it is worth noting that the location of the predicted maximum temperature rise from the dividing streamline is displaced toward the jet (fuel stream) side relative to the experimental results.

The results shown for both *Figures 30* and *31* were for an axial distance of 100 mm downstream of the shear layer exit plane.

For the 3.79 percent (mole) O_3 case given as Case II in *Table 8*, no experimental results were available with which to make a comparison of the velocity profile across the shear layer. Hence the temperature profile is compared again at 100 mm downstream of the shear layer exit plane. This comparison is shown in *Figure 32*. Note that the essential features that were discussed for the 1 percent O_3 case shown in *Figure 31* are applicable here as well. The predicted maximum temperature rise is more than twice the measured value. The location of the maximum is again shifted toward the jet stream side and the width of the shear layer is in disagreement.

A Lewis number variation was made to determine its effect on the width of the temperature shear layer compared with the velocity shear layer but only minor variations resulted. This did not affect the overall poor comparison between theory and experiment.

The next case compared is shown as Case Number III in *Table 8*. The O_3 mole fraction was increased to 7.8 percent for this comparison. The velocity profile is compared in *Figure 33*. Note that the agreement, while not as good as for the 1 percent O_3 case, is again excellent. This

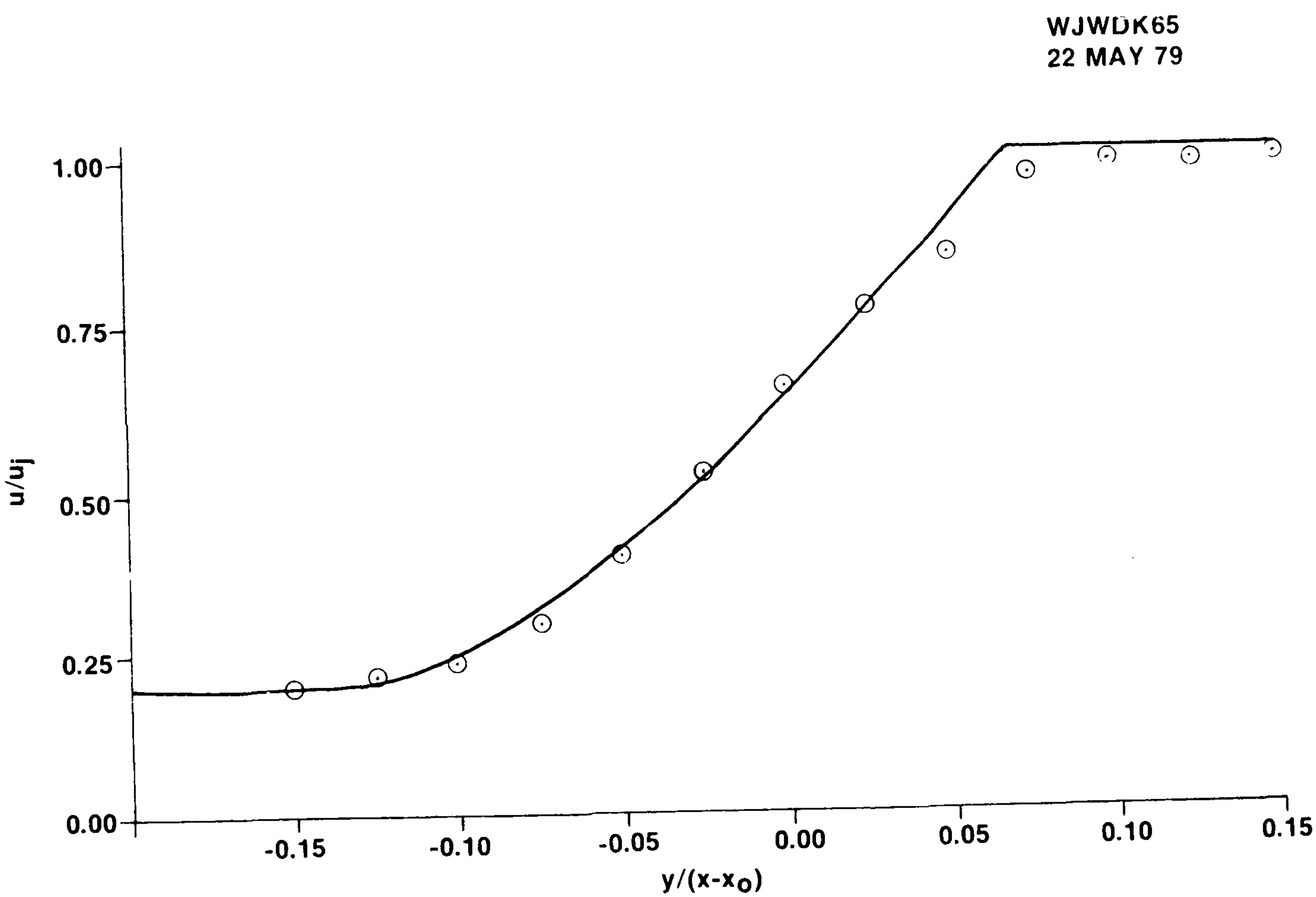

Figure 30. Velocity profile comparison for reacting shear layer - Table 8, case number I.

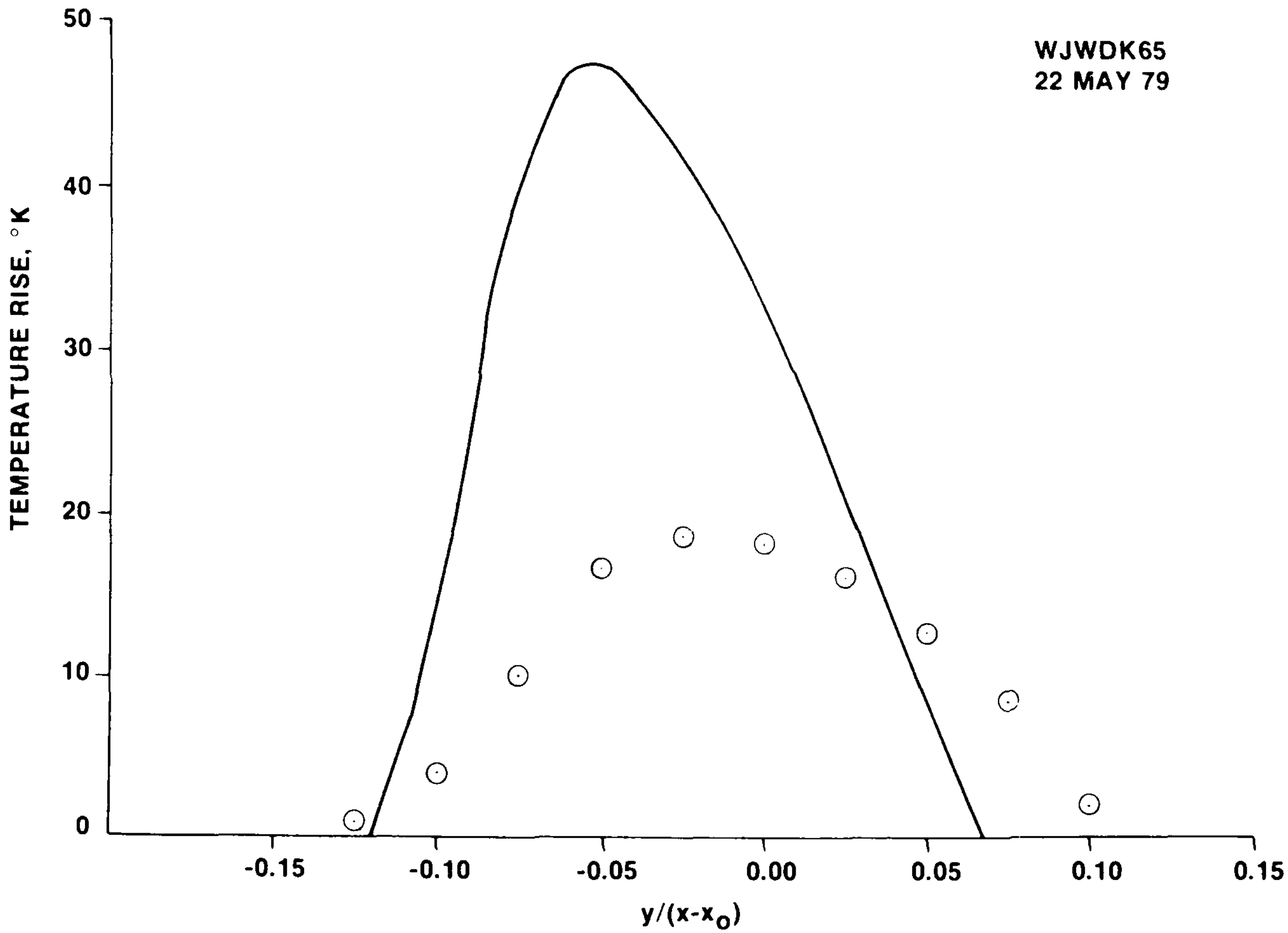

Figure 31. Temperature profile comparison for reacting shear layer - Table 8, case number I.

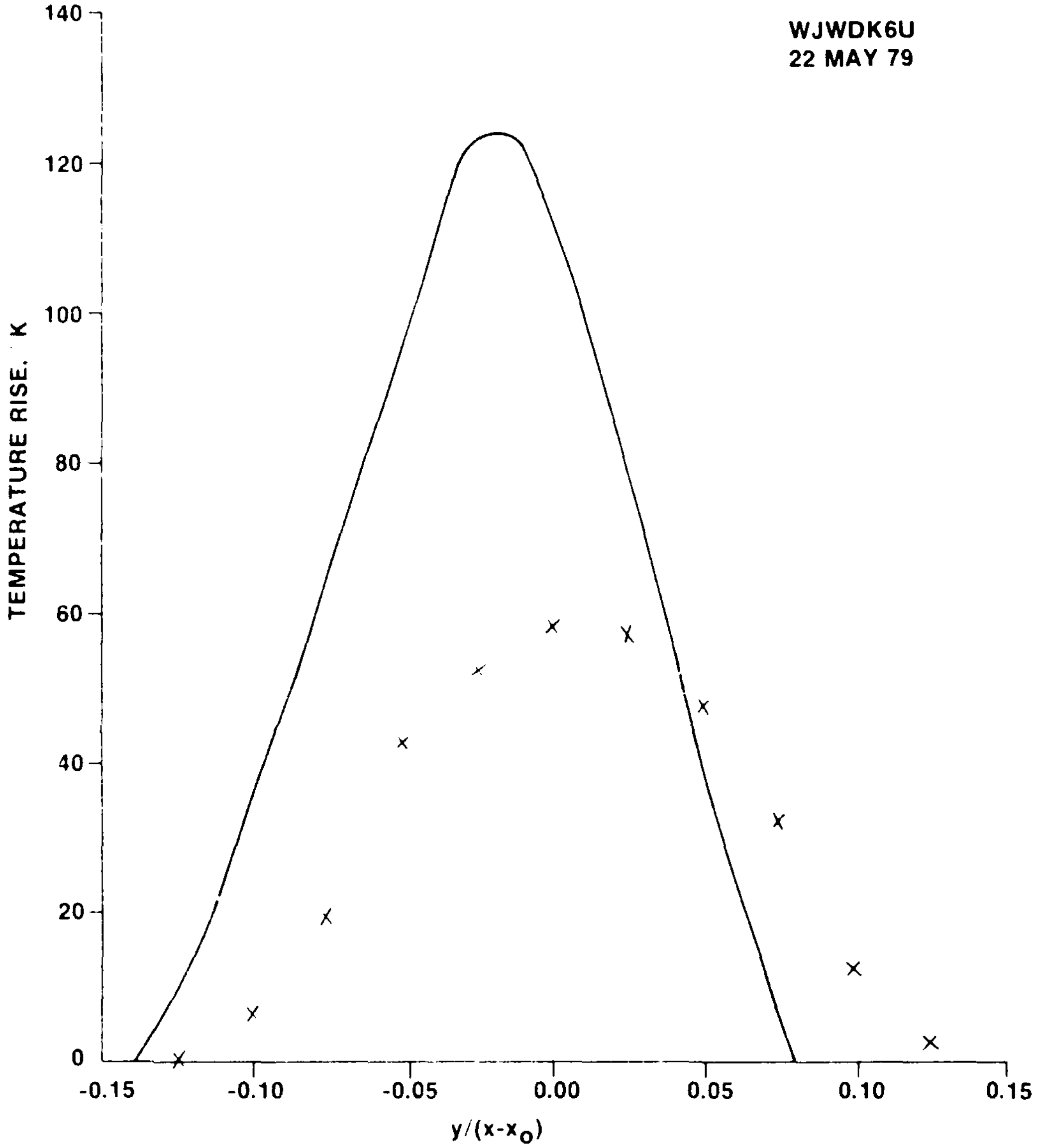

Figure 32. Temperature profile comparison for reacting shear layer - Table 8, case number II.

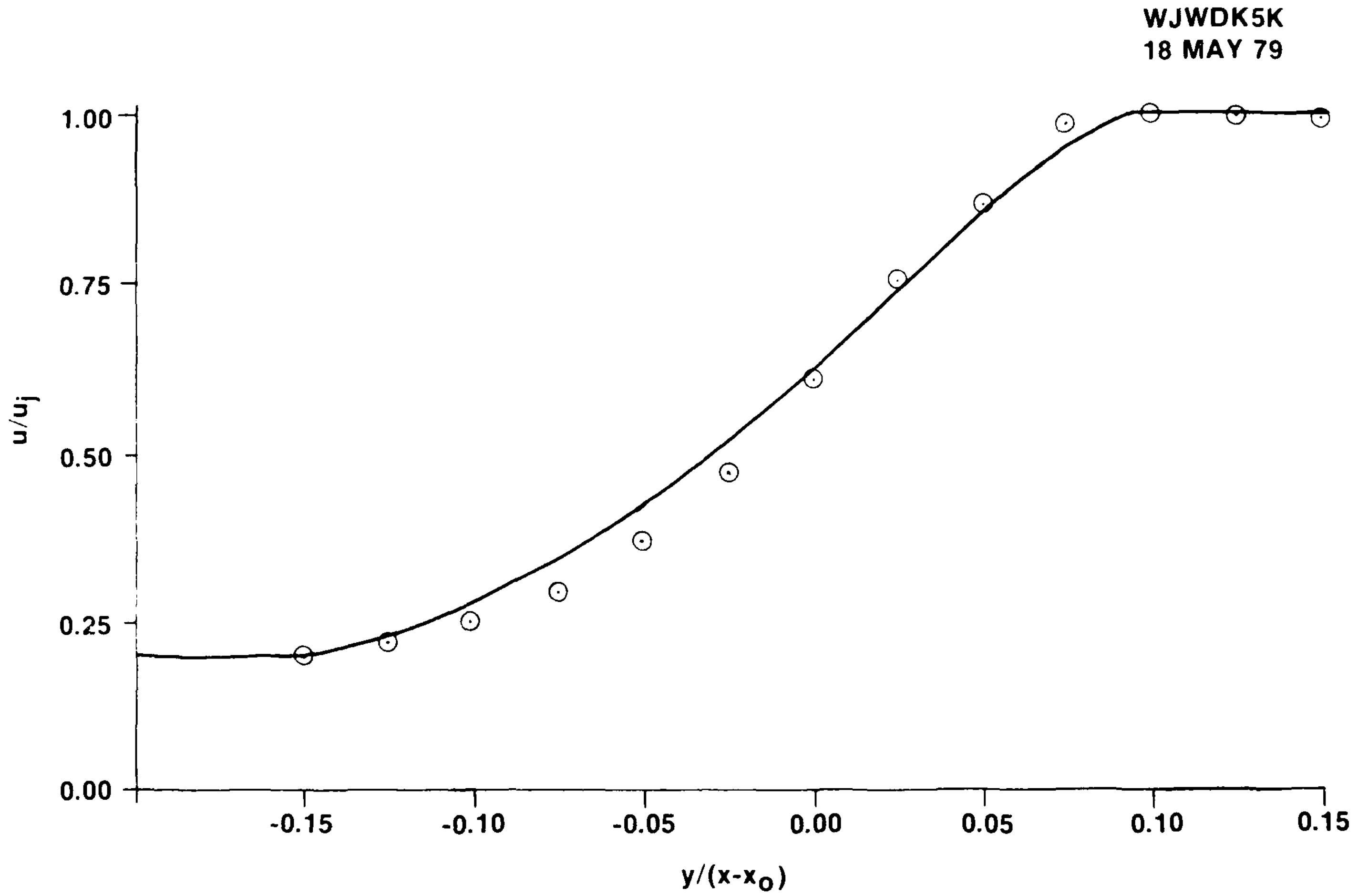

Figure 33. Velocity profile comparison for reacting shear layer - Table 8, case number III.

should be expected however in light of the results presented in *Figure 29*. Again this is a nearly constant initial density case, the density ratio being 0.95 as given in *Table 8*.

Figure 34 illustrates the comparison of the predicted and measured temperature profile across the reacting shear layer. Similarly for this case the predicted maximum temperature rise is nearly twice the measured value. The predicted maximum is similarly skewed to the jet stream side. Hence the common features that were noted in Cases I & II (*Table 8*), are similarly evident in Case III.

It is instructive to examine the results for an increasing amount of oxidizer and noting the shift toward the fuel side. This is shown in *Figure 35* where the maximum temperature rise location moves toward the oxidizer stream monatonically with increasing oxidizer. This leads one to suspect that the turbulence model utilized in the predictions is behaving in a "laminar manner". Note that the experimental results show very little shift in the maximum temperature rise.

This hypothesis was confirmed after programming a laminar mixing model and introducing it as an option into the BOAT analysis. This was accomplished [8] and the results are shown in *Figure 36*. Note that the laminar mixing case results in virtually the same maximum temperature rise as for the $k\omega'$ turbulence model. The only difference is the spreading rate of the laminar shear layer compared to the turbulent shear layer.

Finally predictions were made with two other turbulence models; (i) Prandtl mixing length model and (ii) Donaldson-Gray eddy viscosity model. The results are shown in *Figures 37* and *38*, respectively. It is evident from these figures that neither of the simple models offers any hope of better agreement between experiment and theory.

VIII. CONCLUSIONS

Results of this study clearly show that matching of a theoretical velocity profile for mean velocities with experimental results is not a good indicator of the correctness of a turbulence model. This was shown most vividly for the reacting shear layer experiments where the velocity profile match was excellent and the temperature profile through the shear layer was in error by more than a factor of two. The velocity profile was the easiest parameter to match when utilizing the turbulence kinetic energy models given in this investigation. The constant initial density cases showed excellent agreement between experiment and theory for

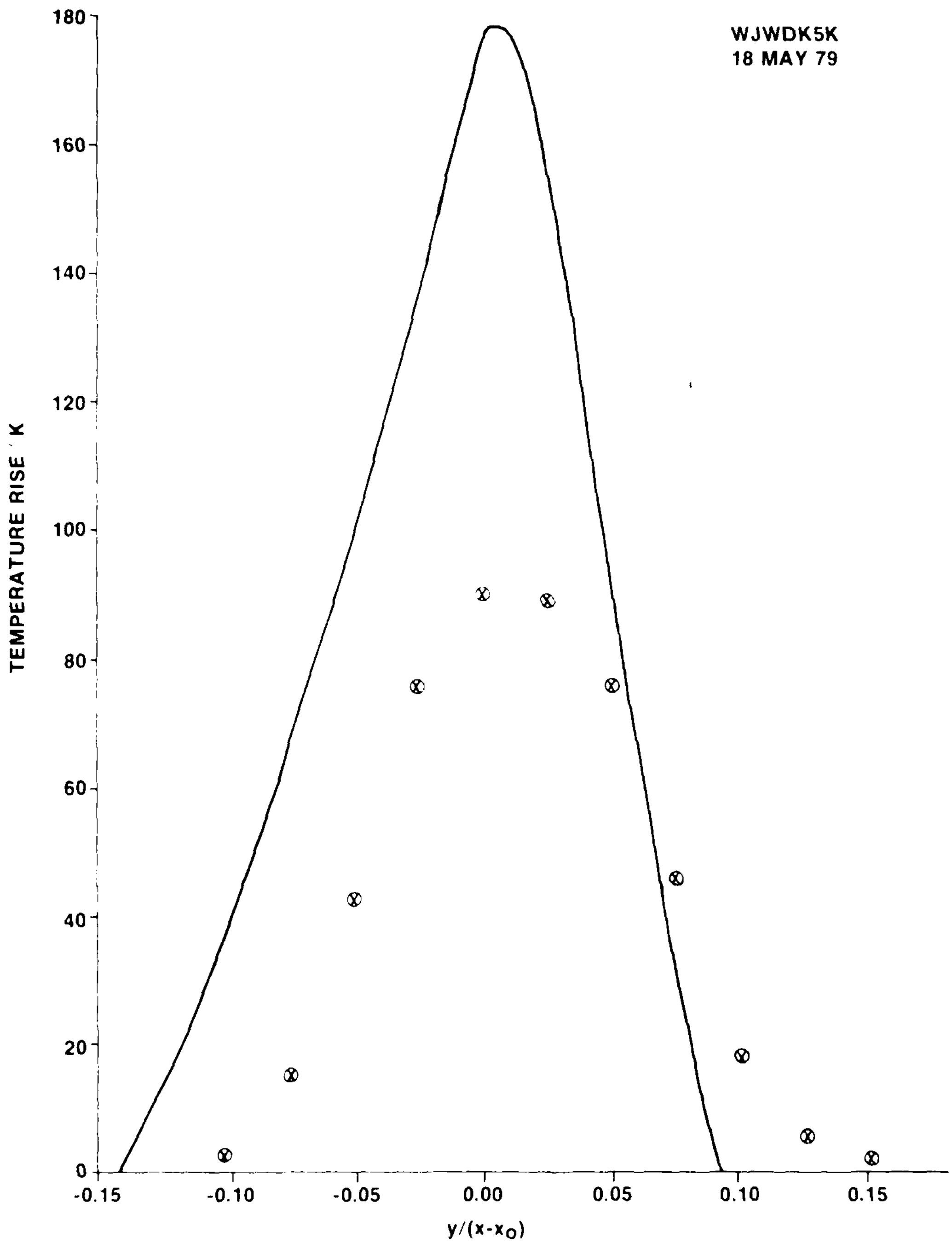

Figure 34. Temperature profile comparison for reacting shear layer - Table 8, case number III.

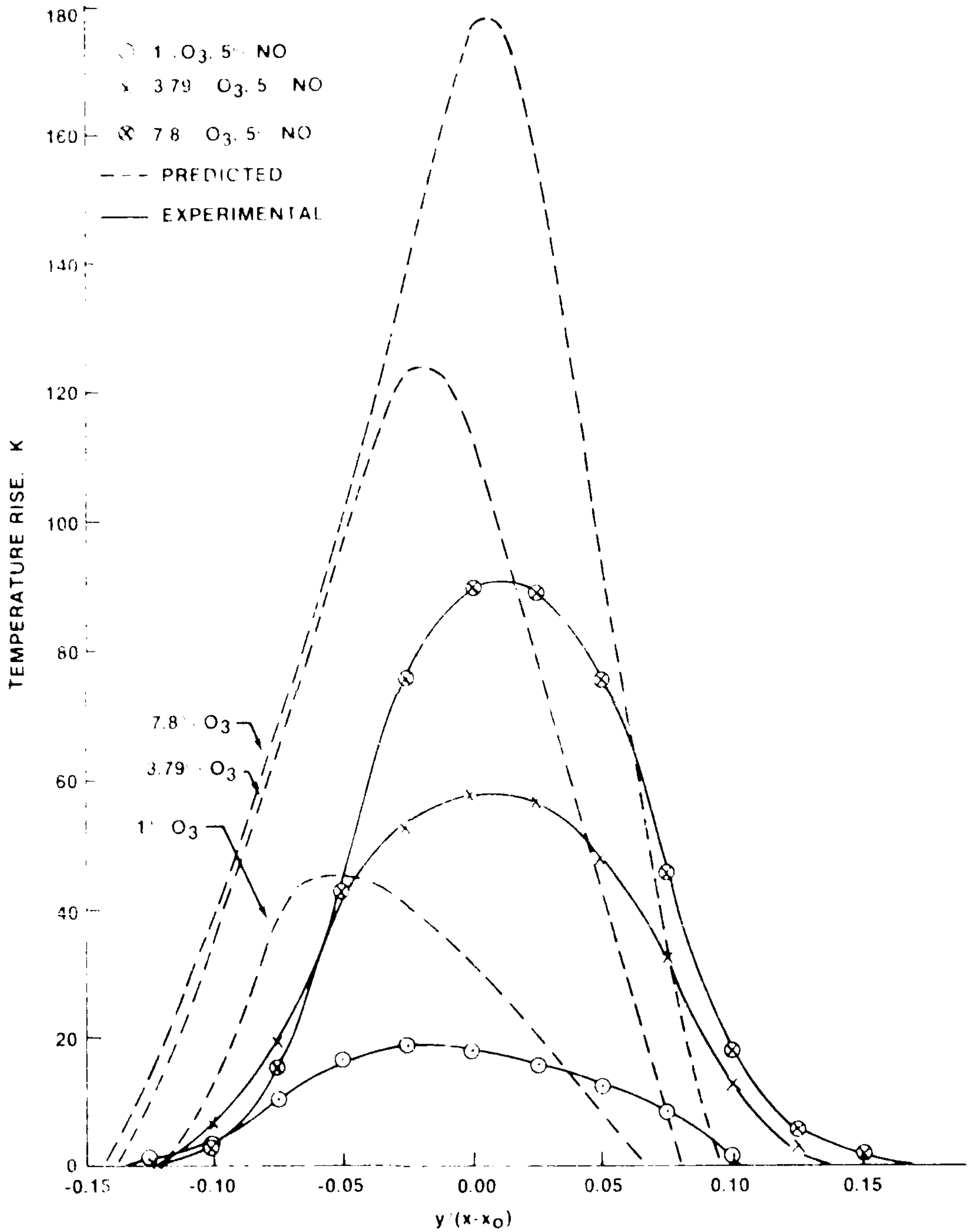

Figure 35. Measured and predicted temperature distribution in shear layers between nitric oxide and ozone.

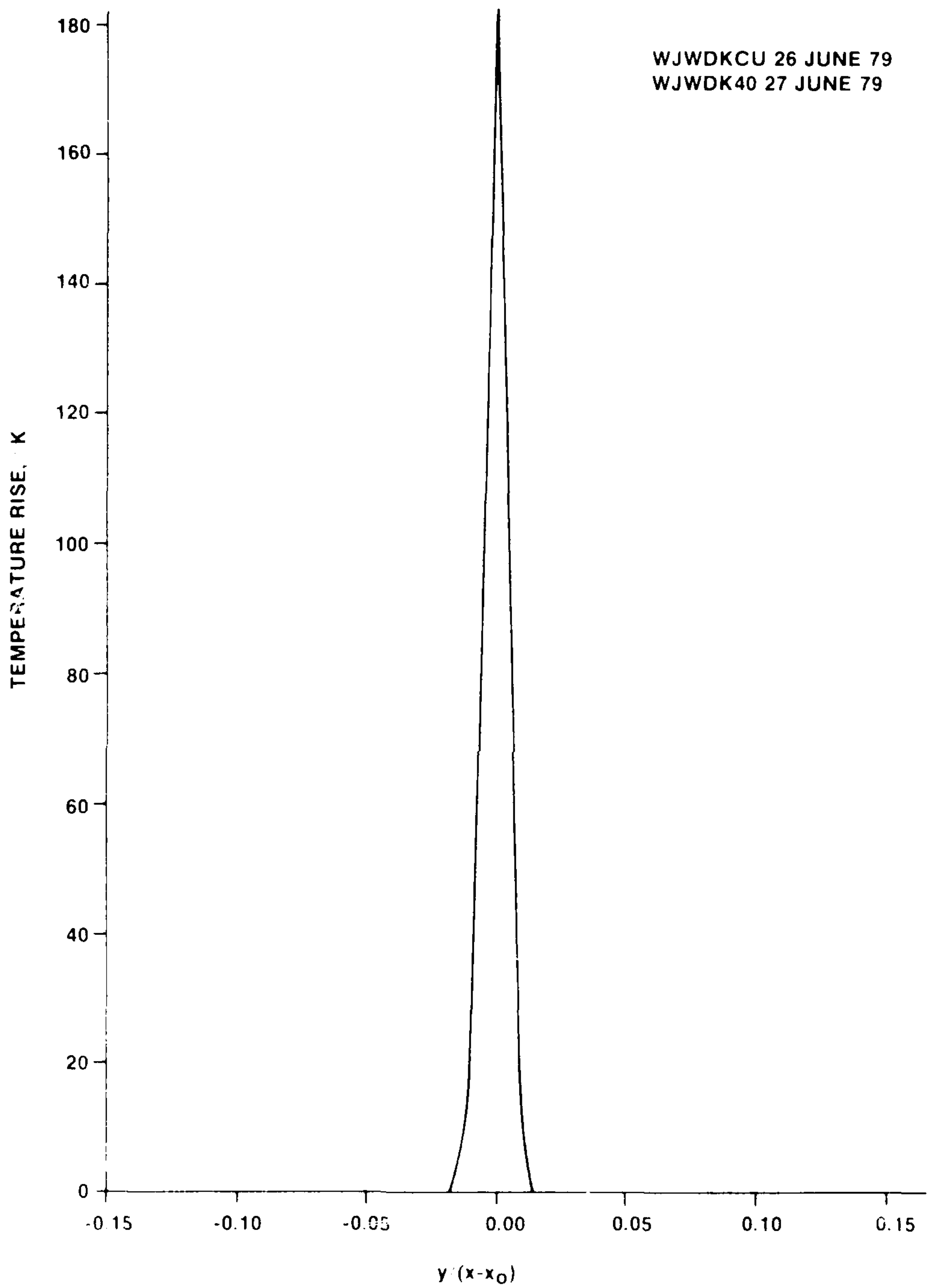

Figure 36. Temperature profile prediction for reacting shear layer using laminar viscosity model - Table 8, case number III.

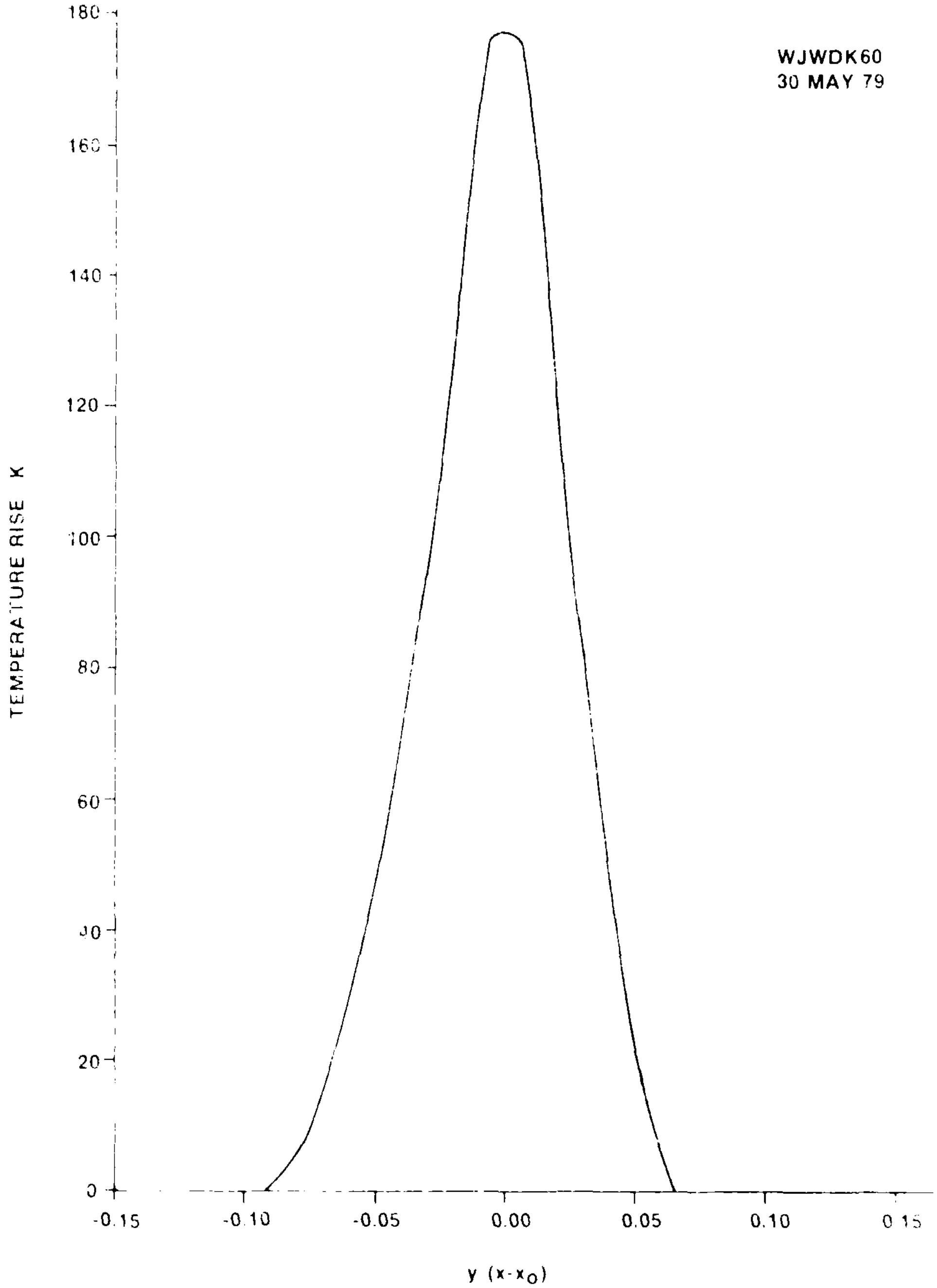

Figure 37. Temperature profile prediction for reacting shear layer using Prandtl mixing length turbulence model. Table 8 case number III.

AD-A094 438 ARMY MISSILE COMMAND REDSTONE ARSENAL AL SYSTEMS SI--ETC F/G 12/1
TURBULENCE MODEL COMPARISONS FOR SHEAR LAYERS AND AXISYMMETRIC --ETC(U)
OCT 79 B J WALKER
UNCLASSIFIED DRSMI/RD-80-1-TR SBIE-AD-E950 074 NL

2 of 2
AD
A094438

END
DATE
FILMED
2 81
DTIC

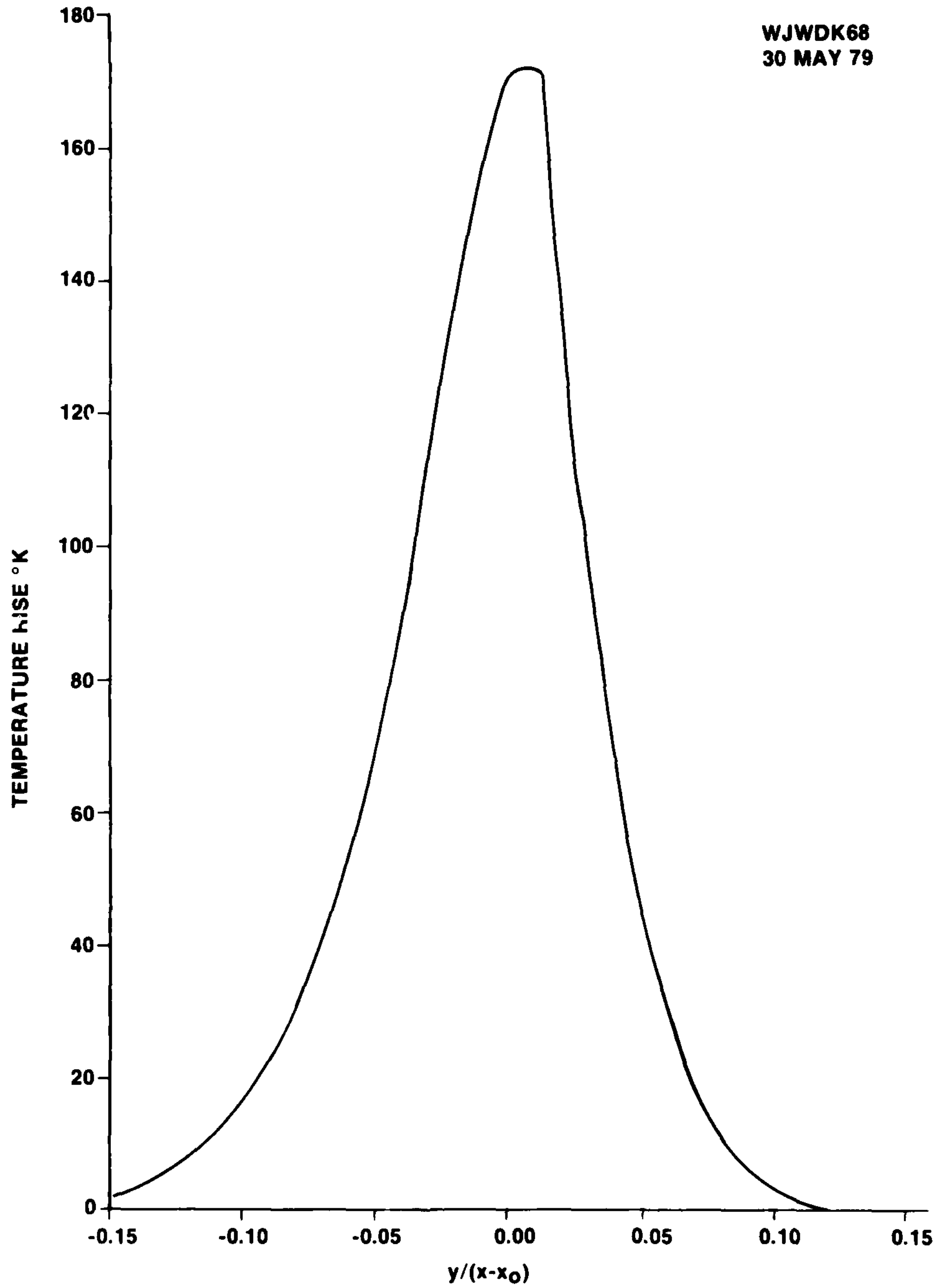

Figure 38. Temperature profile prediction for reacting shear layer using Donaldson-Gray eddy viscosity, turbulence model - Table 8, case number III.

all cases investigated. This was not true, however, for the case where the initial density ratios were significantly greater than one (≈7).

The density profiles across the shear layer were very poorly predicted for all cases examined in this investigation. This was especially true for the case when the high velocity jet fluid was simultaneously the low density fluid in the two-dimensional shear. This is a case that more nearly corresponds to the rocket exhaust plume.

The $k\omega'$ turbulence model gives comparable results with the $k\epsilon 2$ turbulence model. In all cases examined the $k\omega'$ model performed as well as the $k\epsilon 2$ model and in certain instances, it performed much better than the $k\epsilon 2$ model. This was especially true for the M=2.2 air jet exhausting into *still* air.

The temperature profiles that are predicted by the turbulence models are extremely poor. The temperatures are too high by approximately a factor of tw. This indicates that there is a significant large structure in the flows examined. The turbulence models do not account for this structure in any way and hence are all deficient in the basic physics of the flow. *Figure 39* details the structure of a typical non-reacting shear layer and Wallace and Brown [5] have shown similar behavior for the reacting shear layer. Examination of this photograph makes it clear that the vortex structure must be included in the turbulence models in order to obtain reasonable predictions.

Just how much large structure exists in flows more typical of rocket exhaust plumes where the velocities are much higher is not known *a priori*. It is suspected that the large structure will be less evidenced. If this is true, then perhaps the current turbulence models will offer more hope for making reasonable predictions. However, this remains to be seen. Non-reactive flow tests will be run in the near future which will provide the basis for the reasonable assessment of this effect.

APPENDIX A

The comparison of the theory with the experimental data of Brown and Roshko [1] and Wallace and Brown [5] required that the position of the dividing streamline be known. In addition, this information is necessary when determining the amount of mass entrained by the jet or by the shear layer. This was accomplished in the prediction program by utilizing the subroutine DIVSL.

Consider the plane mixing layer shown in *Figure A1*. By taking an element of fluid whose bottom edge is parallel to the dividing streamline, a momentum balance along the fluid element parallel to the dividing streamline as shown in *Figure A2* gives the following

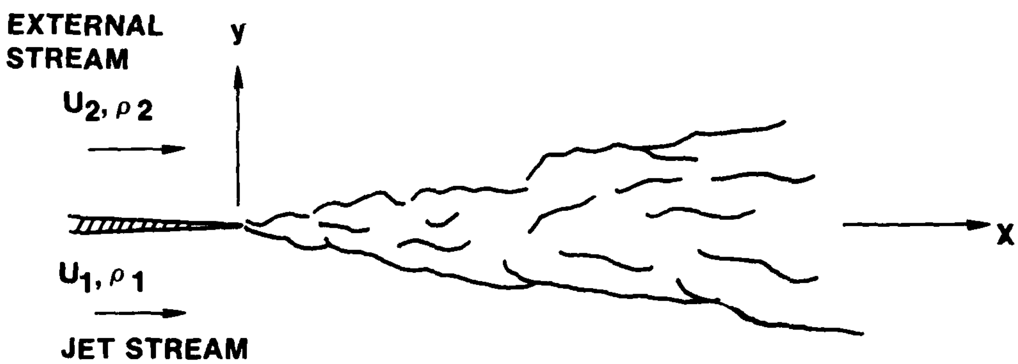

Figure A-1. Plane mixing layer.

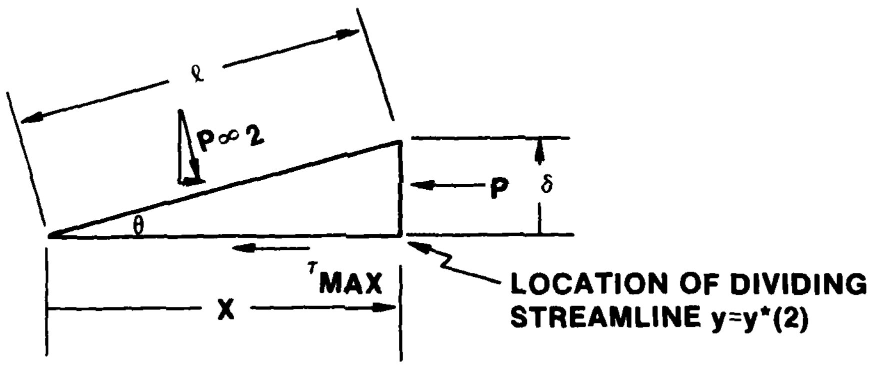

Figure A-2. Plane mixing layer fluid element (top half).

$$- \tau_{max} x + p_{\infty_2} \sin\theta \ \ell - \int_{y^*(x)}^{\delta(x)} p dy$$

$$= \int_{y^*(x)}^{\delta(x)} \rho u^2 dy + \int_{y^*(x)}^{\delta(x)} \rho \overline{u'^2} dy + U_{\infty_2} \int_{y^*(x)}^{\delta(x)} \rho u dy \qquad \text{(A1)}$$

But

$$\ell \sin\theta = \delta$$

Hence

$$- \tau_{max} x + p_{\infty_2} \delta - \int_{y^*}^{\delta} p dy$$

$$= \int_{y^*}^{\delta} \rho u^2 dy + \int_{y^*}^{\delta} \rho \overline{u'^2} dy - U_{\infty_2} \int_{y^*}^{\delta} \rho u dy \qquad \text{(A2)}$$

or rewriting

$$- \tau_{max} x + \int_{y^*}^{\delta} \left(p_{\infty 2} - p\right) dy$$

$$= \int_{y^*}^{\delta} \rho u^2 dy + \int_{y^*}^{\delta} \rho \overline{u'^2} dy - U_{\infty_2} \int_{y^*}^{\delta} \rho u dy \qquad \text{(A3)}$$

But

$$p_{\infty_2} = p + \rho \overline{v'^2} \qquad \text{(A4)}$$

Hence (A3) becomes

$$- \tau_{max}\, x + \int_{y^*}^{\delta} \rho \overline{v'^2} dy$$

$$= \int_{y^*}^{\delta} \rho u^2 dy + \int_{y^*}^{\delta} \rho \overline{u'^2} dy - U_{\infty_2} \int_{y^*}^{\delta} \rho u dy \qquad \text{(A5)}$$

so that

$$\tau_{max}\, x = \int_{y^*}^{\delta} \left(\rho \overline{v'^2} - \rho \overline{u'^2}\right) dy + \int_{y^*}^{\delta} \rho u \left(U_{\infty_2} - u\right) dy \qquad \text{(A6)}$$

Similarly if we consider the bottom half of the fluid element shown in *Figure A3*

$$\tau_{max}\, x + p_{\infty_2} \delta - \int_{-\delta}^{y^*} p dy$$

$$= \int_{-\delta}^{y^*} \rho u^2 dy + \int_{-\delta}^{y^*} \rho \overline{u'^2} dy - U_{\infty_1} \int_{-\delta}^{y^*} \rho u dy \qquad \text{(A7)}$$

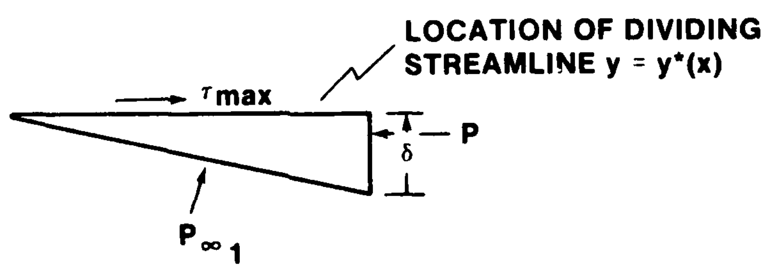

Figure A-3. Plane mixing layer fluid element (bottom half).

and since

$$p_{\infty_1} = p + \rho\overline{v'^2}$$

$$\tau_{max}\ x + \int_{-\delta}^{y^*} \rho\overline{v'^2}dy = \int_{-\delta}^{y^*} \rho u \left(u - U_{\infty_1}\right) dy + \int_{-\delta}^{y^*} \rho\overline{u'^2}\ dy \qquad \text{(A8)}$$

or

$$\tau_{max}\ x = \int_{-\delta}^{y^*} \rho u \left(u - U_{\infty_1}\right) dy + \int_{-\delta}^{y^*} \rho\left(\overline{u'^2} - \overline{v'^2}\right)\ dy \qquad \text{(A9)}$$

Equating (A6) and (A9)

$$\int_{-\delta}^{y^*} \rho u \left(u - u_{\infty_1}\right) dy + \int_{-\delta}^{y^*} \rho\left(\overline{u'^2} - \overline{v'^2}\right) dy$$

$$= \int_{y^*}^{\delta} \rho u \left(U_{\infty_2} - u\right) dy + \int_{y^*}^{\delta} \rho \left(\overline{v'^2} - \overline{u'^2}\right) dy \qquad \text{(A10)}$$

and by assuming $\overline{u'^2} = \overline{v'^2}$, (A10) becomes

$$\int_{y^*(x)}^{\delta(x)} \rho_u \left(U_{\infty_2} - u\right) dy = \int_{-\delta(x)}^{y^*(x)} \rho u \left(u - U_{\infty_1}\right) dy \qquad \text{(A11)}$$

Equation (A11) is utilized to determine the location of the dividing streamline.

Figure A4 illustrates a program that was written to check out the dividing streamline location. Data from a realistic 2-D shear layer in the form of streamwise velocity u and density ρ at normal locations y were input via DATA statements. Utilizing this data the dividing streamline was located utilizing equation (A11) which is coded in subroutine DIVSL. The jet side integral I1 is given by the RHS of equation (A11) and the external side integral I2 is given by the LHS of equation (A11). The trapezoidal rule is utilized for these integrals.

Detailed output for the subroutine DIVSL is given by the namelist OUT2 and for the overall check routine by OUT1. Note the location of the dividing streamline yy given in both namelists. This illustrates a behavior common to the 2-D shear layers studied — a bending of the dividing streamline toward the jet.

Once the dividing streamline has been located, the entrainment can be calculated for both the jet side and the external side. *Figure A5* illustrates some additional calculations which define two integrals utilized in the entrainment calculations. The mass flow integration above and below the dividing streamline is given by I_3 and I_4, respectively. These integrals are defined as

$$I_3 \equiv \int_{-\delta}^{y^*} \rho u dy \tag{A12}$$

$$I_4 = \int_{y^*}^{\delta} \rho u dy \tag{A13}$$

These integrals are utilized to calculate the mass flow changes at streamwise locations and differences in these integrals give the mass flow entrainment. The jet side integral is given by I_3 and the external side integral is given by I_4.

Detailed output for these integrals is given in namelist OUT3. The dividing streamline location is given in namelist OUT1 and OUT2 as before.

```
PROGRAM CHECK       74/74    OPT=1            WJWDKB8          FTN 4.6+439          03/01/79  14.49.17

      PROGRAM CHECK(OUTPUT,TAPE6=OUTPUT)
      DIMENSION U(50),RHO(50),Y(50)
      DATA U/32.81,32.8075,32.7363,32.3921,31.7871,31.0345,30.1917,
     129.2914,28.3548,27.3963,26.4261,25.4519,24.4796,23.5138,
     222.558,21.6152,20.6678,19.7779,18.887,18.0165,17.1676,
     316.3417,15.5394,14.7616,14.0091,13.2827,12.5829,11.9103,
     411.2657,10.6493,10.0619,9.5038,8.9755,8.4774,8.0099,
     57.5732,7.1677,6.7934,6.4504,6.1386,5.8579,5.6079,
     65.3863,5.1985,5.0382,4.9072,4.8058,4.7358,4.6993,4.69/
      DATA Y/9.99802,9.99811,9.99819,9.99827,9.99835,9.99843,
     19.99852,9.99860,9.99868,9.99876,9.99884,9.99892,9.99901,
     29.99909,9.99917,9.99926,9.99935,9.99943,9.99952,
     39.99961,9.9997,9.99978,9.99988,9.99997,10.0001,10.00021,
     410.00027,10.0003,10.0004,10.005,10.0006,10.0007,
     510.0008,10.0009,10.0010,10.0011,10.0013,10.0014,10.0015,
     610.0016,10.0017,10.0018,10.0019,10.0020,10.00211,
     710.00217,10.0022,10.0023,10.0024,10.0025/
      DATA RHO/.113801E-2,.113871E-2,.114292E-2,.116137E-2,
     1.118922E-2,.122133E-2,.125639E-2,.129393E-2,.133360E-2,
     2.137564E-2,.141985E-2,.146636E-2,.151529E-2,.156675E-2,
     3.162090E-2,.167792E-2,.173801E-2,.180138E-2,.186829E-2,
     4.19399E-2,.201363E-2,.209309E-2,.217715E-2,.22664E-2,
     5.236813E-2,.246232E-2,.257E-2,.26849E-2,.280768E-2,
     6.293898E-2,.307959E-2,.32303E-2,.339197E-2,.356551E-2,
     7.375186E-2,.395207E-2,.416708E-2,.439779E-2,.464547E-2,
     8.491064E-2,.51941E-2,.549629E-2,.581726E-2,.615651E-2,
     9.651233E-2,.688088E-2,.725263E-2,.760333E-2,.786663E-2,
     1.796427E-2/
      NAMELIST/OUT1/U,RHO,Y,MPSI,YY
      MPSI=50
      CALL DIVSL(U,RHO,Y,MPSI,YY)
      WRITE(6,OUT1)
      STOP
      END
```

Figure A-4. Checkout program listing for dividing streamline location.

```
SUBROUTINE DIVSL       74/74    OPT=1          WJWDKB8          FTN 4.6+439         03/01/79  14.49.17

                  SUBROUTINE DIVSL(U,RHO,Y,NMAX,YY)
                  DIMENSION U(50),RHO(50),Y(50)
                  NAMELIST/OUT2/UINF1,UINF2,UAVG,RHOAVG,DELY,DXI1,DXI2,XI1,
                 $XI2,DELI,DELIS,SLOPE,YY,N,I,J,TEST,NMAX
                  UINF1=U(1)
                  UINF2=U(NMAX)
                  DO 200 N=2,NMAX
            C  EVALUATION OF THE INTEGRAL I1(THE JET SIDE INTEGRAL)
                  DO 100 I=2,N
                  UAVG=(U(I)+U(I-1))/2.
                  RHOAVG=(RHO(I)+RHO(I-1))/2.
                  DELY=Y(I)-Y(I-1)
                  DXI1=RHOAVG*UAVG*(UINF1-UAVG)*DELY
                  XI1=XI1+DXI1
              100 CONTINUE
            C  EVALUATION OF THE INTEGRAL I2(THE EXTERNAL SIDE INTEGRAL)
                  N1=N+1
                  DO 300 J=N1,NMAX
                  RHOAVG=(RHO(J)+RHO(J-1))/2.
                  UAVG=(U(J)+U(J-1))/2.
                  DELY=Y(J)-Y(J-1)
                  DXI2=RHOAVG*UAVG*(UAVG-UINF2)*DELY
                  XI2=XI2+DXI2
              300 CONTINUE
            C  TEST TO CHECK WHERE INTEGRALI1=INTEGRAL I2
                  IF(XI2.LT.XI1.AND.N.EQ.2)GO TO 900
                  GO TO 400
              900 WRITE(6,600)
              600 FORMAT(1X,*THE DIVIDING STREAMLINE IS BETWEEN THE FIRST TWO GRID P
                 $OINTS*)
                  CALL EXIT
              400 CONTINUE
                  DELI=XI2-XI1
                  IF(N.EQ.2)DELIS=DELI
                  TEST=DELI*DELIS
                  IF(TEST.LT.0.)GO TO 700
                  DELIS=DELI
                  XI1=0.
                  XI2=0.
                  WRITE(6,OUT2)
              200 CONTINUE
              700 CONTINUE
            C  THE INTEGRALS ARE EQUAL BETWEEN N-1 AND N
                  DELY=Y(N)-Y(N-1)
                  SLOPE=(DELI-DELIS)/DELY
                  YY=Y(N-1)-DELIS/SLOPE
                  WRITE(6,OUT2)
                  RETURN
                  END


SYMBOLIC REFERENCE MAP (R=3)
```

Figure A-4. (Continued).

```
$OUT2
UINF1    = .3281E+02,
UINF2    = .469E+01,
UAVG     = .469465E+01,
RHOAVG   = .791555E-02,
DELY     = .79999999996655E-04,
DXI1     = .44190738442919E-04,
DXI2     = .17279742611142E-07,
XI1      = .45976435164897E-03,
XI2      = .43022827818738E-03,
DELI     = -.29536073461593E-04,
DELIS    = .47861884528152E-04,
SLOPE    = -.96747447525215E+00,
YY       = .99997494709532E+01,
N        = 22,
I        = 23,
J        = 51,
TEST     = -.14136521374338E-08,
NMAX     = 50,
$END
```

Figure A-4. (Continued).

```
$OUT1
Q      = .3281E+02, .328075E+02, .327363E+02, .323921E+02, .317871E+02, .310345E+02, .301917E+02, .292914E+02,
         .283548E+02, .273963E+02, .264261E+02, .254519E+02, .244796E+02, .235138E+02, .22558E+02, .216152E+02,
         .206878E+02, .197779E+02, .18887E+02, .180165E+02, .171678E+02, .163417E+02, .155394E+02, .147616E+02,
         .140091E+02, .132827E+02, .125829E+02, .119103E+02, .112657E+02, .106493E+02, .100619E+02, .95038E+01,
         .89755E+01, .84774E+01, .80099E+01, .75732E+01, .71677E+01, .67934E+01, .64504E+01, .61388E+01,
         .58579E+01, .56079E+01, .53883E+01, .51985E+01, .50382E+01, .49072E+01, .48058E+01, .47358E+01,
         .46993E+01, .469E+01,
RHO    = .113861E-02, .113871E-02, .114292E-02, .116137E-02, .11892E-02, .122133E-02, .125639E-02, .12939E-02,
         .133366E-02, .137564E-02, .141985E-02, .146636E-02, .151524E-02, .156675E-02, .16209E-02, .167792E-02,
         .173801E-02, .180138E-02, .186829E-02, .1939E-02, .201383E-02, .209309E-02, .217715E-02, .22664E-02,
         .23613E-02, .246232E-02, .257E-02, .26849E-02, .280766E-02, .293698E-02, .307959E-02, .32303E-02,
         .339197E-02, .356551E-02, .375188E-02, .395207E-02, .416708E-02, .43979E-02, .465347E-02, .491064E-02,
         .51941E-02, .549629E-02, .581728E-02, .615651E-02, .651233E-02, .688088E-02, .725283E-02, .760333E-02,
         .786683E-02, .796427E-02,
Y      = .999802E+01, .999811E+01, .999819E+01, .999827E+01, .999835E+01, .999843E+01, .999852E+01, .99986E+01,
         .999868E+01, .999876E+01, .999884E+01, .999892E+01, .999901E+01, .999909E+01, .999917E+01, .999926E+01,
         .999935E+01, .999943E+01, .999952E+01, .999961E+01, .99997E+01, .999978E+01, .999988E+01, .999997E+01,
         .100001E+02, .1000021E+02, .1000027E+02, .100003E+02, .100004E+02, .100005E+02, .100006E+02, .100007E+02,
         .100008E+02, .100009E+02, .10001E+02, .100011E+02, .100013E+02, .100014E+02, .100015E+02, .100016E+02,
         .100017E+02, .100018E+02, .100019E+02, .10002E+02, .1000211E+02, .1000217E+02, .100022E+02, .100023E+02,
         .100024E+02, .100025E+02,
MPSI   = 50,
YY     = .9999749470953E+01,
$END
```

Figure A-4. (Concluded).

```
PROGRAM CHECK       74/74    OPT=1          [redacted]          FTN 4.6+439          04/19/79  17.14.26

      PROGRAM CHECK(OUTPUT,TAPE6=OUTPUT)
      DIMENSION U(50),RHO(50),Y(50)
      DATA U/32.81,32.8075,32.7363,32.3921,31.7871,31.0345,30.1917,
     129.2914,28.3548,27.3963,26.4261,25.4519,24.4796,23.5138,
     222.558,21.6152,20.6878,19.7779,18.887,18.0165,17.1678,
     316.3417,15.5394,14.7616,14.0091,13.2827,12.5829,11.9103,
     411.2657,10.6493,10.0619,9.5036,8.9755,8.4774,8.0099,
     57.5732,7.1677,6.7934,6.4504,6.1386,5.8579,5.6079,
     65.3883,5.1985,5.0382,4.9072,4.8058,4.7358,4.6993,4.69/
      DATA Y/9.99802,9.99811,9.99819,9.99827,9.99835,9.99843,
     19.99852,9.99860,9.99868,9.99876,9.99884,9.99892,9.99901,
     29.99909,9.99917,9.99926,9.99935,9.99943,9.99952,
     39.99961,9.9997,9.99978,9.99988,9.99997,10.0001,10.00021,
     410.00027,10.0003,10.0004,10.005,10.0006,10.0007,
     510.0008,10.0009,10.0010,10.0011,10.0013,10.0014,10.0015,
     610.0016,10.0017,10.0018,10.0019,10.0020,10.00211,
     710.00217,10.0022,10.0023,10.0024,10.0025/
      DATA RHO/.113861E-2,.113871E-2,.114292E-2,.116137E-2,
     1.11892E-2,.122133E-2,.125639E-2,.12939E-2,.133366E-2,
     2.137564E-2,.141985E-2,.146636E-2,.151529E-2,.156675E-2,
     3.162090E-2,.167792E-2,.173801E-2,.180138E-2,.186824E-2,
     4.1939E-2,.201383E-2,.209309E-2,.217715E-2,.22664E-2,
     5.236133E-2,.246232E-2,.257E-2,.26849E-2,.280766E-2,
     6.293898E-2,.307959E-2,.32303E-2,.339197E-2,.356551E-2,
     7.375188E-2,.395207E-2,.416708E-2,.43979E-2,.464547E-2,
     8.491064E-2,.51941E-2,.549629E-2,.581728E-2,.615651E-2,
     9.651233E-2,.688086E-2,.725283E-2,.760333E-2,.786683E-2,
     1.796427E-2/
      NAMELIST/OUT1/U,RHO,Y,MPSI,YY
      MPSI=50
      CALL DIVSL(U,RHO,Y,MPSI,YY,X13,X14)
      WRITE(6,OUT1)
      STOP
      END
```

Figure A-5. Checkout program listing for dividing streamline location *plus entrainment integrals.*

PRECEDING PAGE BLANK-NOT FILMED

```
      PROGRAM CHECK       74/74    OPT=1          WJWEK98          FTN 4.6+439          04/19/79  17.14.26

              PROGRAM CHECK(OUTPUT,TAPE6=OUTPUT)
              DIMENSION U(50),RHO(50),Y(50)

      SUBROUTINE DIVSL    74/74    OPT=1          WJWEK98          FTN 4.6+439          04/19/79  17.14.26
                                                INPUT      OUTPUT
              SUBROUTINE DIVSL(U,RHO,Y,NMAX,YY,XI3,XI4)
              DIMENSION U(50),RHO(50),Y(50)
              NAMELIST/OUT2/UINF1,UINF2,UAVG,RHOAVG,DELY,DXI1,DXI2,XI1,
             $XI2,DELI,DELIS,SLOPE,YY,N,I,J,TEST,NMAX
              NAMELIST/OUT3/UDSL,RDSL,UAV,RAVG,DELI3,XI3,XI4,VOUJ,VOUE
              UINF1=U(1)
              UINF2=U(NMAX)
              DO 200 N=2,NMAX
        C  EVALUATION OF THE INTEGRAL I1(THE JET SIDE INTEGRAL)
              DO 100 I=2,N
              UAVG=(U(I)+U(I-1))/2.
              RHOAVG=(RHO(I)+RHO(I-1))/2.
              DELY=Y(I)-Y(I-1)
              DXI1=RHOAVG*UAVG*(UINF1-UAVG)*DELY
              DXI3=RHOAVG*UAVG*DELY
              XI3=XI3+DXI3
              XI1=XI1+DXI1
          100 CONTINUE
        C  EVALUATION OF THE INTEGRAL I2(THE EXTERNAL SIDE INTEGRAL)
              N1=N+1
              DO 300 J=N1,NMAX
              RHOAVG=(RHO(J)+RHO(J-1))/2.
              UAVG=(U(J)+U(J-1))/2.
              DELY=Y(J)-Y(J-1)
              DXI2=RHOAVG*UAVG*(UAVG-UINF2)*DELY
              DXI4=RHOAVG*UAVG*DELY
              XI4=XI4+DXI4
              XI2=XI2+DXI2
          300 CONTINUE
        C  TEST TO CHECK WHERE INTEGRALI1=INTEGRAL I2
              IF(XI2.LT.XI1.AND.N.EQ.2)GO TO 900
              GO TO 400
          900 WRITE(6,800)
          800 FORMAT(1X,*THE DIVIDING STREAMLINE IS BETWEEN THE FIRST TWO GRID P
             $OINTS*)
              CALL EXIT
          400 CONTINUE
              DELI=XI2-XI1
              IF(N.EQ.2)DELIS=DELI
              TEST=DELI*DELIS
              IF(TEST.LT.0.)GO TO 700
              DELIS=DELI
              XI1=0.
              XI2=0.
              XI3=0.
              XI4=0.
              WRITE(6,OUT2)
          200 CONTINUE
          700 CONTINUE
        C  THE INTEGRALS ARE EQUAL BETWEEN N-1 AND N
              DELY=Y(N)-Y(N-1)
              SLOPE=(DELI-DELIS)/DELY
              YY=Y(N-1)-DELIS/SLOPE
              WRITE(6,OUT2)
        C  CALCULATE ENTRAINMENT BY INTEGRATION OF M-DOT ABOVE AND BELOW DIVIDING S.L.
        C  INTERPOLATE FOR U AND RHO AT THE DIVIDING STREAMLINE
              CALL BOATLI(YY,UDSL,Y,U,NMAX)
```

Figure A-5. (Continued).

```
SUBROUTINE DIVSL       74/74    OPT=1       WJWDK98              FTN 4.6+439          04/19/79  17.14.26

            CALL BOATLI(YY,RDSL,Y,RHO,NMAX)
      C   EVALUATION OF DELI3=-DELI4
            UAV=(UDSL+U(N))/2.
            RAVG=(RDSL+RHO(N))/2.
            DELI3=UAV*RAVG*(Y(N)-YY)
      C   EVALUATION OF M-DOT ABOVE AND BELOW THE DIVIDING STREAMLINE
            XI3=XI3-DELI3
            XI4=XI4+DELI3
            DX=.5642626E-4
            VOUU=XI3/RHO(1)/DX/U(1)
            VOUF=XI4/RHO(MPSI)/DX/U(1)
            WRITE(6,OUT3)
            RETURN
            END

SUBROUTINE BOATLI      74/74    OPT=1                            FTN 4.6+439          04/19/79  17.14.26
                                  INPUT OUTPUT  INPUT
            SUBROUTINE BOATLI(XIN,YOUT,XXX,YYY,N)
            DIMENSION XXX(50),YYY(50)
            K=2
         20 IF(XIN.LE.XXX(K))GO TO 10
            K=K+1
            IF(K.GT.N)WRITE(6,100)
        100 FORMAT(1X,*$$$$$$$$$$K.GT.N IN BOATLI$$$$$$$$$$*)
            IF(K.GT.N)CALL EXIT
            GO TO 20
         10 RAT=(XIN-XXX(K-1))/(XXX(K)-XXX(K-1))
            YOUT=YYY(K-1)+RAT*(YYY(K)-YYY(K-1))
            RETURN
            END
```

Figure A-5. (Continued).

```
$OUT2
UINF1    = .3281E+02,
UINF2    = .469E+01,
UAVG     = .469465E+01,
RHOAVG   = .791555E-02,
DELY     = .7999999996855E-04,
DXI1     = .44190738442919E-04,
DXI2     = .17279742611142E-07,
XI1      = .45976435164897E-03,
XI2      = .43022827818738E-03,
DELI     = -.29536073461593E-04,
DELIS    = .47861884528152E-04,
SLOPE    = -.96747447525215E+00,
YY       = .99997494709532E+01,
N        = 22,
I        = 23,
J        = 51,
TEST     = -.14136521374338E-08,
NMAX     = 50,
$END

$OUT3
UDSL     = .16656950569018E+02,
RDSL     = .20628433469309E-02,
UAV      = .16499325284509E+02,
RAVG     = .20779666734655E-02,
DELI3    = .10466898351745E-05,
XI3      = .63730432656421E-04,
XI4      = .89289814486664E-04,
VOUJ     = .29198329263413E+02,
VOUE     = .99315082233911E-02,
$END
```

Figure A-5. (Continued).

```
$OUT1

U        = .3281E+02, .328075E+02, .327363E+02, .323921E+02, .317871E+02,      .310345E+02, .301917E+02, .292914E+02,
           .283548E+02, .273963E+02, .264261E+02, .254519E+02, .244796E+02,   .235138E+02, .22558E+02, .216152E+02,
           .206878E+02, .197779E+02, .18887E+02, .180165E+02, .171678E+02,    .163417E+02, .155394E+02, .147616E+02,
           .140091E+02, .132827E+02, .125829E+02, .119103E+02, .112657E+02,   .106493E+02, .100619E+02, .95036E+01,
           .89755E+01, .84774E+01, .80099E+01, .75732E+01, .71677E+01,        .67934E+01, .64504E+01, .61386E+01,
           .58579E+01, .56079E+01, .53883E+01, .51985E+01, .50382E+01,        .49072E+01, .48058E+01, .47358E+01,
           .46993E+01, .469E+01,

RHO      = .113861E-02, .113871E-02, .114292E-02, .116137E-02, .11892E-02,    .122133E-02, .125639E-02, .12939E-02,
           .133366E-02, .137564E-02, .141985E-02, .146636E-02, .151529E-02,   .156675E-02, .16209E-02, .167792E-02,
           .173801E-02, .180138E-02, .186829E-02, .1939E-02, .201383E-02,     .209309E-02, .217715E-02, .22664E-02,
           .23613E-02, .246232E-02, .257E-02, .26849E-02, .280766E-02,        .293898E-02, .307959E-02, .32303E-02,
           .339197E-02, .356551E-02, .375188E-02, .395207E-02, .416708E-02,   .43979E-02, .464547E-02, .491064E-02,
           .51941E-02, .549629E-02, .581728E-02, .615651E-02, .651233E-02,    .688086E-02, .725283E-02, .760333E-02,
           .786683E-02, .796427E-02,

Y        = .999802E+01, .999811E+01, .999819E+01, .999827E+01, .999835E+01,  .999843E+01, .999852E+01, .99986E+01,
           .999868E+01, .999876E+01, .999884E+01, .999892E+01, .999901E+01,   .999909E+01, .999917E+01, .999926E+01,
           .999935E+01, .999943E+01, .999952E+01, .999961E+01, .99997E+01,    .999978E+01, .999986E+01, .999997E+01,
           .100001E+02, .1000021E+02, .1000027E+02, .100003E+02, .100004E+02, .10005E+02, .100006E+02, .100007E+02,
           .100008E+02, .100009E+02, .10001E+02, .100011E+02, .100013E+02,    .100014E+02, .100015E+02, .100016E+02,
           .100017E+02, .100018E+02, .100019E+02, .10002E+02, .1000211E+02,   .1000217E+02, .100022E+02, .100023E+02,
           .100024E+02, .100025E+02,

MPSI     = 50,

YY       = .9999749470953?E+01,

$END
```

Figure A-5. (Concluded).

APPENDIX B

For the reacting shear layer comparison, it became of interest to compare the resulting temperature rise in the shear layer with that predicted by a laminar mixing model. Hence, it was necessary to add this capability to the shear layer program BOAT. The following extension to the code (*Figure B1*) is necessary to accomplish this. The details of the laminar mixing model are given in a separate report [8].

```
SUBROUTINE LAMVISC     74/74    OPT=1      WJWDK4I             FTN 4.6+439          06/26/79

            SUBROUTINE LAMVISC(NS,MPSI,XMUL,T,WTMOLE,ALPHA,WTMIX)                    C18
            DIMENSION XMUL(50),XMF(25,50),T(50),WTMOLE(25),ALPHA(25,50),             C18
           1XMU(5),PHI(25,25),WTMIX(50)                                              C18
            NT=9                                                                     C18
            DO 30 K=1,MPSI                                                           C18
            XMUL(K)=0.                                                               C18
            DO 20 I=1,NS                                                             C18
            DO 40 J=1,NS                                                             C18
         40 XMF(J,K)=ALPHA(J,K)/WTMIX(K)                                             C18
            CALL MUSPEC(NT,NS,T(K),XMU)                                              C18
            SUMD=0.                                                                  C18
            DO 10 J=1,NS                                                             C18
            PHI(I,J)=1./SQRT(8.)*(1.+WTMOLE(I)/WTMOLE(J))**(-.5)*                    C18
           1(1.+SQRT(XMU(I)/XMU(J))*(WTMOLE(J)/WTMOLE(I))**.25)**2                   C18
         10 SUMD=SUMD+XMF(J,K)*PHI(I,J)                                              C18
            XNUM=XMF(I)*XMU(I)/SUMD                                                  C18
         20 XMUL(K)=XMUL(K)+XNUM                                                     C18
         30 CONTINUE                                                                 C18
            RETURN                                                                   C18
            END                                                                      C18
```

```
SUBROUTINE MUSPEC      74/74    OPT=1      WJWDK4I             FTN 4.6+439          06/26/79

            SUBROUTINE MUSPEC(NT,NS,T,XMU)                                           C18
            DIMENSION C(4,9),XI(9),S(2),C1(9,5),FXI(9),C2(4,9,5),XMU(5)              C18
C     THIS DATA HAS BEEN ARRANGED ASSUMING THE SPECIES ARE READ IN THE FOLL          C18
C     ORDER - NO,N2,O3,NO2,O2 - SPECIES DATA INPUT IN ANY OTHER ORDER WILL           C18
C     IN AN ERROR                                                                    C18
            DATA(C1(I,1),I=1,9)/136.5,192.0,239.7,282.0,320.5,356.2,                 C18
           1389.9,421.9,452.4/                                                       C18
            DATA(C1(I,2),I=1,9)/131.3,177.7,217.2,252.7,285.4,315.6,                 C18
           1344.0,371.0,397.1/                                                       C18
            DATA(C1(I,3),I=1,9)/114.7,170.1,220.1,265.0,305.9,343.5,                 C18
           1378.8,412.0,443.6/                                                       C18
            DATA(C1(I,4),I=1,9)/78.9,119.1,158.6,195.9,230.8,263.3,                  C18
           1293.9,322.8,350.1/                                                       C18
            DATA(C1(I,5),I=1,9)/147.9,206.4,256.5,301.0,341.4,379.1,                 C18
```

Figure B-1. Capability of the shear layer program BOAT.

```
      1414.8,446.5,480.6/                                              C18
      DATA NCNT/0/                                                     C18
      IF(NCNT.EQ.1)GO TO 100                                           C18
      N1=NT                                                            C18
      N=N1-1                                                           C18
      XI(1)=200.                                                       C18
      DO 10 I=2,NT                                                     C18
   10 XI(I)=XI(I-1)+100.                                               C18
      DO 20 I=1,NS                                                     C18
      DO 30 J=1,N1                                                     C18
      C(1,J)=C1(J,I)                                                   C18
   30 FXI(J)=C(1,J)                                                    C18
      CALL ENDPTSL(XI,FXI,N1,S)                                        C18
      C(2,1)=S(1)                                                      C18
      C(2,N1)=S(2)                                                     C18
      CALL SPLINE(N,XI,C)                                              C18
      CALL CALCCF(N,XI,C)                                              C18
      DO 40 L=1,4                                                      C18
      DO 40 J=1,9                                                      C18
   40 C2(L,J,I)=C(L,J)                                                 C18
   20 CONTINUE                                                         C18
      NCNT=1                                                           C18
  100 CONTINUE                                                         C18
      DO 60 K=1,NS                                                     C18
      DO 60 I=1,4                                                      C18
      DO 60 J=1,NT                                                     C18
      C(I,J)=C2(I,J,K)                                                 C18
   60 XMU(K)=PCUBIC(T,N,XI,C)                                          C18
      RETURN                                                           C18
      END                                                              C18
```

SUBROUTINE CALCCF 74/74 OPT=1 WJWDK4I FTN 4.6+439 06/26/79

```
      SUBROUTINE CALCCF(N,XI,C)                                        C18
      DIMENSION XI(100),C(4,100)                                       C18
      DO 10 I=1,N                                                      C18
      DX=XI(I+1)-XI(I)                                                 C18
      DIVDF1=(C(1,I+1)-C(1,I))/DX                                      C18
      DIVDF3=C(2,I)+C(2,I+1)-2.*DIVDF1                                 C18
      C(3,I)=(DIVDF1-C(2,I)-DIVDF3)/DX                                 C18
   10 C(4,I)=DIVDF3/DX/DX                                              C18
      RETURN                                                           C18
      END                                                              C18
```

Figure B-1. (Continued).

```
SUBROUTINE FNDPTSL     74/74    OPT=1       WJWDK4I            FTN 4.6+439        06/26/79

      SUBROUTINE FNDPTSL(XI,FXI,NK,S)                                            C18
C     CALCULATION OF SLOPE AT FIRST AND LAST POINT FOR SPLINE FIT USING LAG     C18
C     POLYNOMIALS                                                                C18
      DIMENSION XI(100),FXI(100),S(2)                                            C18
      DO 30 I=1,2                                                                C18
      IF(I.NE.1)GO TO 10                                                         C18
      X=XI(1)                                                                    C18
      K=4                                                                        C18
      GO TO 20                                                                   C18
   10 X=XI(NK)                                                                   C18
      K=NK                                                                       C18
   20 A0=X-XI(K-3)                                                               C18
      A1=X-XI(K-2)                                                               C18
      A2=X-XI(K-1)                                                               C18
      A3=X-XI(K)                                                                 C18
      B0=XI(K-3)-XI(K-2)                                                         C18
      B1=XI(K-3)-XI(K-1)                                                         C18
      B2=XI(K-3)-XI(K)                                                           C18
      C1=XI(K-2)-XI(K-1)                                                         C18
      C2=XI(K-2)-XI(K)                                                           C18
      D1=XI(K-1)-XI(K)                                                           C18
      XLPR1=(A1*(A2+A3)+A2*A3)/(B0*B1*B2)                                        C18
      XLPR2=(A0*(A2+A3)+A2*A3)/(-1.*B0*C1*C2)                                    C18
      XLPR3=(A0*(A1+A3)+A1*A3)/(B1*C1*D1)                                        C18
      XLPR4=(A0*(A1+A2)+A1*A2)/(-1.*B2*C2*D1)                                    C18
   30 S(I)=FXI(K-3)*XLPR1+FXI(K-2)*XLPR2+FXI(K-1)*XLPR3+FXI(K)*XLPR4             C18
      RETURN                                                                     C18
      END                                                                        C18

FUNCTION PCUBIC        74/74    OPT=1       WJWDK4I            FTN 4.6+439        06/26/79

      FUNCTION PCUBIC(XBAR,N,XI,C)                                               C18
      DIMENSION XI(100),C(4,100)                                                 C18
      DATA I/1/                                                                  C18
      DX=XBAR-XI(I)                                                              C18
      IF(DX)10,30,20                                                             C18
   10 IF(I.EQ.1)GO TO 30                                                         C18
      I=I-1                                                                      C18
      DX=XBAR-XI(I)                                                              C18
      IF(DX)10,30,30                                                             C18
```

Figure B-1. (Continued).

```
19 I=I+1                                                      C18
   DX=DDX                                                     C18
20 IF(I.EQ.N)GO TO 30                                         C18
   DDX=XBAR-XI(I+1)                                           C18
   IF(DDX)30,19,19                                            C18
30 PCUBIC=C(1,I)+DX*(C(2,I)+DX*(C(3,I)+DX*C(4,I)))           C18
   RETURN                                                     C18
   END                                                        C18
```

```
SUBROUTINE SPLINE      74/74    OPT=1       WJWDK4I           FTN 4.6+439       06/26/79

   SUBROUTINE SPLINE(N,XI,C)                                  C18
   DIMENSION XI(100),C(4,100),D(100),DIAG(100)                C18
   DATA DIAG(1),D(1)/1.,0./                                   C18
   NP1=N+1                                                    C18
   DO 10 M=2,NP1                                              C18
   D(M)=XI(M)-XI(M-1)                                         C18
10 DIAG(M)=(C(1,M)-C(1,M-1))/D(M)                             C18
   DO 20 M=2,N                                                C18
   C(2,M)=3.*(D(M)*DIAG(M+1)+D(M+1)*DIAG(M))                  C18
20 DIAG(M)=2.*(D(M)+D(M+1))                                   C18
   DO 30 M=2,N                                                C18
   G=-D(M+1)/DIAG(M-1)                                        C18
   DIAG(M)=DIAG(M)+G*D(M-1)                                   C18
30 C(2,M)=C(2,M)+G*C(2,M-1)                                   C18
   NJ=NP1                                                     C18
   DO 40 M=2,N                                                C18
   NJ=NJ-1                                                    C18
40 C(2,NJ)=(C(2,NJ)-D(NJ)*C(2,NJ+1))/DIAG(NJ)                 C18
   RETURN                                                     C18
   END                                                        C18
```

Figure B-1. (Concluded).

REFERENCES

1. Brown, G. L. and Roshko, A., "On Density Effects and Large Structure in Turbulent Mixing Layers," *Journal of Fluid Mechanics*, Vol. 64, 1974, pp. 775-816.

2. Roshko, A., "Structure of Turbulent Flows: A New Look," *AIAA Journal*, Vol. XIV, No. 10, October 1976, pp. 1349-1357.

3. Klebanoff, P. S., "Characteristics of Turbulence in a Boundary Layer with Zero Pressure Gradient," NACA Report 1247, 1955.

4. Milinazzo, F. and Saffman, P. G., "Turbulence Predictions for the Inhomogeneous Mixing Layer," *Studies in Applied Mathematics*, Vol. 55, 1976, pp. 45-63.

5. Wallace, A. K. and Brown, G. L., "A Reacting Shear Layer with Significant Heat Release: An Experiment," Second Symposium on Turbulent Shear Flows, Imperial College, London, July 1979.

6. Brown, G. L., "The Entrainmental Large Structure in Turbulent Mixing Layers," 5th Australasian Conference on Hydraulics and Fluid Mechanics, University of Canterbury, Christ-Church, New Zealand, 9-13 December 1974.

7. *Anon., Free Turbulent Shear Flows*, Volumes I & II, NASA SP-321, Langley Research Center, July 1972.

8. Walker, B. J., "Calculation of the Laminar Viscosity of a Gaseous Mixture for Gas Dynamic Mixing Comparisons for a Reacting Shear Layer," US Army MICOM Report TR-RD-80-2, Redstone Arsenal, Alabama, October 1979.

9. Dash, S. M. and Pergament, H. S., "A Computational Model for the Prediction of Jet Entrainment in the Vicinity of Nozzle Boattails (The BOAT Code)," NASA Contractor Report 159001, Langley Research Center, Hampton, Virginia, November 1978.

REFERENCES (CONCLUDED)

10. Mikatarian, R. R., Kau, C. J. and Pergament, H. S., "A Fast Computer Program for Nonequilibrium Rocket Plume Predictions," Air Force Rocket Propulsion Laboratory Report No. AFRPL-TR-72-94, August 1972.

11. Dash, S., Weilerstein, G., and Vaglio-Laurin, R., "Compressibility Effects in Free Turbulent Shear Flows," AFOSR Report TR-75-1436, August 1975.

12. Dash, S. M., Pergament, H. S., and Thorpe, R. O., "A Modular Approach for the Coupling of Viscous and Inviscid Processes in Exhaust Plume Flows," AIAA Paper 79-0150, 17th Aerospace Sciences Meeting, New Orleans, Louisiana, January 15-17, 1979.

SYMBOLS

x	Axial Coordinate
r	Radial Coordinate
u	Axial Velocity
v	Radial Velocity
ρ	Density
Pr	Turbulent Prandtl Number, $\frac{\mu C p}{K}$
Sc	Turbulent Schmidt Number, $\mu / \rho D$
Le	Turbulent Lewis Number, Pr/Sc
p	Pressure
μ	Viscosity
F	X/MW
X	Mole Fraction of i^{th} Specie
W	Mixture Molecular Weight
h	Enthalpy of i^{th} Specie
T	Static Temperature
h_i	Heat of Formation of i^{th} Specie
k	Thermal conductivity

SYMBOLS (Continued)

w_i	Net Rate of Chemical Production of i^{th} Specie
ψ	Stream Function (Equation 6)
MW	Molecular Weight
k	Turbulent Kinetic Energy, $\frac{1}{2}(u'^2+v'^2)$
σ_k	Prandtl Number for Turbulent Kinetic Energy
σ_ϵ	Prandtl Number for Turbulent Dissipation
ϵ, ε (same throughout report)	Turbulent Dissipation Rate
δ	Shear Layer Thickness
M	Mach Number
a	Sonic Velocity
$\overline{k}$	Compressibility Factor
ω	Pseudo-Vorticity
Cp	Heat Capacity at Constant Pressure
u_τ	Wall Shear Stress Velocity, $\sqrt{\tau w}$
δ^*	Boundary Layer Displacement Thickness
θ^*	Momentum Thickness
γ	Ratio of Specific Heats
$\overline{R}$	Universal Gas Constant
R	$\overline{R}$/MW
Λ	Defined in Equation [illegible]
H	Enthalpy

SYMBOLS (Continued)

$C_{\epsilon 1}$, $C_{\epsilon 2}$, C_{μ}, σ_k, σ_ϵ	$k\epsilon 2$ Turbulence model constants (Equations 10 and 11)
$C_{\omega 2}$, $C_{\omega 3}$, $C_{\omega 4}$, $C_{\omega 5}$, C_{k1}, $C_{k\sigma}$	$k\omega^2$ Turbulence model constants (Equations 18–20)
C_{μ}, $C_{\epsilon 1}$, $C_{\epsilon 2}$	Empirical constants in $k\epsilon 2$ formulation
$\overline{P}/\epsilon$, F	Functional corrections for weak shear flows in $k\epsilon 2$ formulation (Ref. 7)
e	Specific turbulent kinetic energy
P	Defined by Equation 25
ω	Cole's Universal Wave Function (Equation 29)
τ_ω	Wall shear stress
δ^*	Displacement thickness
η	Non-dimensional radial coordinate, $\frac{r - r_j}{r_e - r_j}$
θ	Momentum thickness
y	Cross stream distance from dividing streamline

SYMBOLS (Concluded)

β', α', α'', C_1, C_2, C_3, C_4, C_5, C_6	Constants in $k\omega'$ formulation
U	Mean axial velocity
V	Mean radial velocity
z	ω^2
ν	μ/ρ

Subscripts

max	Maximum
o	Initial value
C	Centerline
e	External stream
j	Jet stream
∞	Free stream
t	Turbulent

DISTRIBUTION

	No. of Copies
University of Illinois Dr. A. L. Addy 208 Mechanical Engineering Laboratory Urbana, IL 61801	 1
BMDATC ATC-14, Dr. Larry C. Atha PO Box 1500 Huntsville, AL 35807	 1
Rockwell/Downey Mr. Harold J. Babrov Space Information Systems Division 12214 Lakewood Blvd Downey, CA 90241	 1
Bell Aerospace Corporation Mr. Arthur H. Blessing PO Box 1 Buffalo, NY 14240	 1
Calspan Corporation Attn: Dr. Donald W. Boyer Dr. Paul V. Marrone Dr. Walter H. Wurster PO Box 400 Buffalo, NY 14221	 1 1 1
Physics Dynamics/La Jolla Dr. Frederick P. Boynton PO Box 556 La Jolla, CA 92038	 1
Naval Weapons Center Attn: Code 3245, Mr. S. Breil Code 3241, Mr. A. Victor China Lake, CA 93555	 1 1
Naval Ordnance Station Attn: Code 5252E, Mr. G. Buckle Code 5233D, Mr. H. Hodgkins Indian Head, MD 20640	 1 1
Spectron/Costa Mesa Dr. C. W. Busch 3303 Harbor Blvd Costa Mesa, CA 92626	 1
AFRPL/PACP Attn: Dr. David Mann Dr. T. D. McCay Edwards AFB, CA 93523	 1 1
Aerochem Research/Princeton Dr. Hartwell Calcote PO Box 12 Princeton, NJ 08540	 1
Rockwell International Rocketdyne Division Code D/536, Mr. R. Campbell 6633 Canoga Avenue Canoga Park, CA 91304	 1
Aerojet Solid Propulsion Company Attn: Mr. James P. Coughlin Mr. A. W. McPeak PO Box 13400 Sacramento, CA 95813	 1 1
SAI/Princeton Attn: Dr. Sanford M. Dash Dr. E. S. Fishburne 1101 State Road, Bldg H Princeton, NJ 08540	 1 1
Grumman/Bethpage Grumman Aerospace, Inc. Attn: Dr. Paul D. Del Guidice Dr. Stanley Rudman S. Oyster Bay Road Bethpage, LI, NY 11714	 1 1
ARC/Alexandria Dr. Mark Director 5390 Cherokee Avenue Alexandria, VA 22314	 1
Hercules/Cumberland Aerospace Division-Allegany Ballistics Laboratory Attn: Mr. Thomas E. Durney Mr. Robert C. Foster PO Box 210 Cumberland, MD 21502	 1 1
AFATL/DLMQ Dr. D. E. Ebeoglu Eglin AFB, FL 32542	 1
University of Tennessee Space Institute Attn: Dr. W. Michael Farmer Dr. James M. Wu Dr. Kenneth E. Harwell Tullahoma, TN 37388	 1 1 1

DISTRIBUTION (Continued)

United Technologies Corporation
Chemical Systems Division
Mr. B. R. Felix 1
PO Box 358
Sunnyvale, CA 94088

Ford Aerospace & Commercial Corporation
Aeronautic Division
Attn: Mr. Alson C. Frazer 1
Mr. L. E. Horowitz 1
Ford & Jamboree Roads
Newport Beach, CA 92663

Photon Research Associates, Inc.
Attn: Dr. G. Newton Freeman 1
Dr. Claus B. Ludwig 1
PO Box 1318
La Jolla, CA 92038

Aerodyne Research, Inc.
Attn: Dr. Michael E. Gersh 1
Dr. James S. Draper 1
Crosby Drive
Bedford Research Park
Bedford, MA 01730

Johns Hopkins University
Applied Physics Laboratory-Chemical Propulsion Information Agency
Attn: Mr. Theodore M. Gilliland 1
Mr. Andreas V. Jensen 1
Johns Hopkins Road
Laurel, MD 20810

NASA-Marshall Space Flight Center
Attn: Code ED-33, Dr. T. Greenwood 1
Technical Library 1
Mr. Joseph L. Sims 1
Huntsville, AL 35812

United Technologies Corporation
Research Center
Dr. Roy N. Guile 1
400 Main Street
East Hartford, CT 06108

McDAC/Huntington Beach
Attn: Dr. Donald W. Harvey 1
A3-328, Library 1
Dept 204/13-3,
Mr. G. F. Greenwald 1
5301 Bolsa Avenue
Huntington Beach, CA 92647

Martin-Marietta Corporation
Mr. Larry B[illegible]low 1
Mail Stop 0482
PO Box 179
Denver, CO 80201

AFAPL/RJA
Mr. Norman A. Hirsch 1
Wright-Patterson AFB, OH 45433

Naval International Interpretational Service Center (NISC)
Code 452, Mr. James Hyland 1
4301 Suitland Road
Washington, DC 20390

Thiokol Chemical Corporation
Wasatch Division
Mr. M. J. Janis 1
Brigham City, UT 84302

Aerospace Corporation
Attn: Dr. Richard H. Lee 1
Dr. Duane Nelson 1
Dr. Ronald R. Herm 1
PO Box 92957
Los Angeles, CA 90009

Lincoln Laboratory/MIT
Dr. J. Lowder 1
PO Box 73
Lexington, MA 02173

AFSC/FTD
Attn: Mr. S. Marusa 1
Mr. R. Fargnoli 1
Wright-Patterson AFB, OH 45433

Naval Missile Center
Mr. D. E. Papche 1
Code 5351
Point Mugu, CA 93042

Lockheed Missile & Space Company
Attn: Mr. Morris M. Penny 1
Ms. Beverley J. Audeh 1
Mr. L. Ring 1
PO Box 1103
Huntsville, AL 35802

AFGL (OPR)
Mr. B. P. Sandford 1
Hanscom AFB, ME 01731

Environmental Research Institute
of Michigan
Dr. L. M. Peterson 1
PO Box 8618
Ann Arbor, MI 48107

General Dynamics-Pomona Division
Attn: Mr. E. T. Piesik 1
Technical Library 1
PO Box 2507
Pomona, CA 91766

Chrysler Corporation Michoud
Defense Space Division
Mr. E. A. Rawls 1
PO Box 29200
New Orleans, LA 70189

Physical Sciences, Inc.
Mr. Curt Ray 1
30 Commerce Way
Woburn, MA 01801

Remtech, Inc.
Dr. John S. Reardon 1
2603 Arties Street
Huntsville, AL 35805

ARO, Inc.
Arnold Engineering Development Center
Attn: Mr. Robert P. Rhodes 1
Dr. Wheeler K. McGregor 1
Dr. Charles C. Limbaugh 1
Mr. W. D. Williams 1
Mr. R. C. Bauer 1
Dr. C. E. Peters 1
Technical Library 1
Arnold AFS, TN 37389

NASA/JSC
Code EX-3, Mr. B. B. Roberts 1
Houston, TX 77058

ARDC
CPT William E. Rothschild 1
Code XRB
Eglin AFB, FL 32542

Army Ballistic Research Laboratories
Attn: DRDAR-ELL, Mr. E. Schmidt 1
Aberdeen Proving Ground, MD 21005

AEDC/DOT
Attn: Mr. E. Thompson 1
Dr. Herman E. Scott 1
Arnold AFS, TN 37389

AFOSR
LT Robert F. Sperlein 1
Bldg 40
Bolling AFB
Washington, DC 20332

Naval Weapon Space Center
Code 5042, Dr. J. E. Tanner 1
Crane, IN 47522

Armament R&D Command
Attn: DRDAR-IC, Mr. J. Tyroler 1
Dover, NJ 07801

Thiokol Chemical Corporation
Dr. C. Mikkelsen 1
Huntsville, AL 35807

TRW, Inc.
Attn: Mr. Orvil E. Witte 1
Dr. John T. Ohrenberger 1
One Space Park
Redondo Beach, CA 90278

Institute of Defense Analysis
Dr. Hans G. Wolfhard 1
400 Army-Navy Drive
Arlington, VA 22202

Defense Advanced Research
Projects Agency
Dr. Stephen Zakanycz 1
1400 Wilson Blvd
Arlington, VA 22209

Commander
Air Force Armament Laboratory
Mr. C. Butler 1
Eglin AFB, FL 32542

Air Force Flight Dynamics Laboratory
Attn: FDMM, Mr. Gene Fleeman 1
Wright-Patterson AFB, OH 45433

US Air Force Academy
CAPT Brilliant, DFAN 1
USAF Academy, CO 80840

DISTRIBUTION (Continued)

Commander
Naval Surface Weapons Center
White Oak Laboratory
Attn: Code WA-41, Dr. W. Yanta 1
Code WO, Mr. E. Elzufon 1
Silver Springs, MD 20910

NASA-Langley Research Center
Attn: Code MS423, Mr. R. Wilmoth 1
Mr. Charles Jackson 1
Technical Library 1
Hampton, VA 23665

Commanding Officer and Director
Naval Ship Research and
Development Center
Attn: Aerodynamic Laboratory 1
Craderock, MD 20007

NASA-Ames Research Center
Attn: Mr. G. S. Deiwert 202A-1 1
Technical Library 1
Moffet Field, CA 94035

NASA-Lewis Research Center
Attn: Mr. M. A. Beheim 1
Technical Library 1
Cleveland, OH 44315

Sandia Corporation
Sandia Base Division 9322
Mr. W. Curry 1
Box 5800
Albuquerque, NM 87115

University of Notre Dame
Department of Aerospace Engineering
Dr. T. J. Mueller 1
Notre Dame, IN 46556

Naval Air Systems Command
Mr. William Volz 1
Air 320-C, JP-1
Washington, DC 20361

Nielsen Engineering & Research, Inc.
Dr. Jack N. Nielsen 1
850 Maude Avenue
Mountain View, CA 94040

Director of Defense Rsch & Engng
Room 3C128, Technical Library 1
The Pentagon
Washington, DC 20301

Jet Propulsion Laboratory
California Institute of Technology
Attn: Mr. R. Martin 1
Mr. R. Kenneth Baerwald 1
4800 Oak Grove Drive
Pasadena, CA 91109

Boeing Company
Attn: Library Unit Chief 1
Mr. R. J. Dixon 1
Mr. H. L. Giles 1
Mr. J. M. Barton 1
PO Box 3707
Seattle, WA 98124

Vought Corporation
Attn: Mr. C. R. James 1
Mr. D. B. Schoelerman 1
Mr. Richard Summerhays 1
Box 5907
Dallas, TX 75222

Lockheed Aircraft Corporation
Missile and Space Division
Attn: Technical Info Center 1
Dr. Dwayne A. Sheets, 1
Org 62-13, B-104
PO Box 504
Sunnyvale, CA 94086

Martin-Marietta Corporation
Orlando Division
Attn: J. Burns 1
L. Gilbert 1
Dr. L. Sakell 1
PO Box 5837
Orlando, FL 32804

McDonnell-Douglas Corporation
Attn: Technical Library 1
PO Box 516
St. Louis, MO 63166

Northrop Corporation
Electro-Mechanical Division
Mr. E. Clark 1
500 East Orangethorpe Y20
Anaheim, CA 92801

Rockwell International
Columbus Aircraft Division
Mr. Fred Hessman 1
4300 East Fifth Avenue
Columbus, OH 43216

DISTRIBUTION (Concluded)

Hughes Aircraft Company Missile Systems Division Mr. J. B. Harrisberger Canoga Park, CA 91304	1	DRSMI-LP, Mr. Voigt	1
		DRSMI-R, Dr. McCorkle	1
		-RK	1
		-RL	1
US Army Materiel Systems Analysis Activity Attn: DRXSY-MP Aberdeen Proving Ground, MD 21005	1	-RR	1
		-RN	1
		-RS	1
		-RDK	1
		-RDK, Dr. Walker	20
		-RPR	15
		-RPT (Reference Copy)	1
		(Record Copy)	1

DATE
ILMED

8